Aramco Journal of Technology

WINTER 2019

Aramco
Journal
of Technology

The *Aramco Journal of Technology* is published quarterly by the Saudi Arabian Oil Company, Dhahran, Saudi Arabia, to provide the company's scientific and engineering communities a forum for the exchange of ideas through the presentation of technical information aimed at advancing knowledge in the hydrocarbon industry.

Editor

William E. Bradshaw
william.bradshaw.1@aramco.com.sa
tel: +966-013-876-0498

Production Coordination

Richard E. Doughty

Design

Graphic Engine Design Studio
Austin, Texas, U.S.A.

The *Aramco Journal of Technology* gratefully acknowledges the assistance, contribution and cooperation of numerous operating organizations throughout the company.

ISSN 1319-2388

Contents

New Hydrocarbon Reservoir Sweet Spot Identifier Enabling Optimal Field Development Plans

Dr. Ghazi D. Al-Qahtani, Menhal A. Al-Ismael, Abdulhamed A. Al-Faleh, Basharat Ali, and Fouad F. Abouheit

Abstract /

To attain an optimum field development plan in hydrocarbon reservoirs, well placement can be a cumbersome and time-consuming task. A major reason for this is the lack of a sweet spot identification system to direct the process of placing wells in optimum locations. In this article, a novel method is presented for identifying sweet spots in hydrocarbon reservoirs. A new tool devised from this method is able to identify potential well locations, thereby enhancing optimum field development and maximizing field economic recovery.

The developed tool, the optimal reservoir productivity index (OPTIMA — two patents; one granted[1] and one pending[2]), is an innovative parallel simulation-based algorithm for generating an accurate reservoir dynamic productivity index (PI) with efficient high performance computation utilization, which guides decision making in well placement, and field development and management. OPTIMA reduces the computational expense of reservoir simulation, especially for large models by targeting only specific grid cells based on cutoffs of porosity, permeability, and fluid saturations. The tool runs the evaluation based on a set of production control constraints and the duration of the well productivity evaluation. It generates several simulation runs and calculates a time-dependent 4-dimensional array of layer productivity indices for each grid cell in the model. OPTIMA combines the results of the different simulation cases into a 3-dimensional (3D) property array based on calculated values of the total dynamic PI. The 3D property, once loaded into a post-processor, can be used to define an area of interest to evaluate different well types and configurations.

To optimize well placement, the use of static parameters utilization alone is not sufficient since the reservoir reaction is dynamic once the wells start producing. OPTIMA enables robust and speedy evaluation of sweet spots in hydrocarbon reservoirs while capturing reservoir complexity and heterogeneity. The main advantage of OPTIMA is that it calculates the contribution of each grid cell to the well PI based on dynamic parameters that implicitly combine fluid and rock properties with pressure and saturation as they change with time. This ensures that both static and dynamic reservoir parameters are considered in the process of identifying sweet spots. When compared with conventional methods, OPTIMA surpasses in terms of extending the production plateau and maximizing recovery on a field level performance.

This article introduces OPTIMA to identify sweet spots in green and brown fields, which can be used to generate sweet spot maps in a very short time. In fact, the integration of OPTIMA with a reservoir simulator provides a unique opportunity for reservoir engineers to quickly analyze their fields, evaluate the sweet spots, and optimize a field development plan to maximize ultimate recovery of hydrocarbons.

Introduction

Identifying the optimum production strategy for a field development plan is usually the most critical decision to be made. Once wells are drilled, there is no flexibility in changing their surface locations later. The only alteration that can be done is to use workover rigs to sidetrack or recomplete the wells, but the surface locations will remain unchanged. Classically, the selection process for locating wells utilizes available technology, i.e., saturation maps, pressure distribution maps, isopach maps, rock quality maps, etc., and some degree of experience and intuition. The current global decline in new hydrocarbon reservoir discoveries dictates that locating and placing wells needs to be justified much stronger technically than intuitively, and include robust optimization processes to improve the quality of well placement.

To assess the placement of wells using optimization techniques, two major parts have to be established. The first part of the process is how to identify sweet spots in a reservoir. The other part includes the optimization formulation or method to be used[3, 4]. Several methods have been published and used to identify sweet spots in a reservoir. A genetic unit term was introduced in 1996 to designate the distinctive part of the reservoir rock

based on static properties such as geometrical, petrophysical, and spatial properties[5]. The objective was to optimize horizontal or high angle well trajectories, which are defined by azimuth, location, inclination, and length, to maximize productivity and drainage by intersecting with high permeability genetic units. The ultimate goal, therefore, was to come up with the trajectories that interconnect with a larger number of productive genetic units and rank them based on their values and the associated risk with each trajectory. This method utilized static data solely, and the ranking criterion was subjective.

In 1998, computer programs that leveraged on a geo-object concept was introduced[6] to calculate the connected 3-dimensional (3D) bodies, which are referred to as geo-objects, from reservoir properties such as porosity, permeability, and lithofacies[7]. One of the parameters mentioned can be used as the net indicator to represent each cell in a model, which can be ranked according to its connectivity, and then used to place wells. The work was extended[8] by incorporating geologic uncertainty with an optimization set up, where the objective was to maximize the connected geo-objects that are meant to intersect with the minimum number of planned wells. For the optimization loop, a simulated annealing algorithm was used to find the best locations to place the various vertical, deviated, and horizontal wells.

Another approach was defined[9] by computing a 2-dimensional (2D) indicator, referred to as reservoir quality, for each cell in a reservoir model. The quality term represented connected net pay modified by tortuosity. Binary integer programming was used to find the best well sites with the goal of maximizing reservoir quality and incorporating minimum spacing between the wells. This work was extended[10] to 3D models in which the combination of quality indicators and geo-objects are used to identify optimum completions.

Another method[11, 12] was suggested in which a productivity proxy function was created; attempting to account for the possible attributes impacting grid blocks in a reservoir model. The productivity potential map is sought by a collective term that includes porosity, permeability, and oil saturation. An addition to this work was done later[13] by joining preferred phase pressure and distance to the nearest boundary to the productivity proxy function, which was used to guide the well placement strategy in bottom water drive reservoirs.

Cullick et al. (2005)[14] identified multiple well targets that need to be maximized by honoring two categories of filters. The first is the contact between the wells and the ranked pore volume measures in a certain drainage radius. The other data that must be accounted for to maximize the well targets are permeability, distance from fluid contacts, and saturation. The resultant targets should accommodate spacing constraints before establishing well paths or plans that follow certain designs for different types of wells. The goal was to find the optimum location and type for production or injection wells by maximizing total hydrocarbon production or net present value. They linked the optimization scheme with a reservoir simulator and allowed limited movements for each well type to find the highest objective function.

These methods mainly use static parameters to identify sweet spots, which used a method that can be considered as semi-dynamic for the inclusion of net to gross or a permeability thickness parameter that indicates the possibility of fluid movement. Static parameter utilization, however, is not sufficient to find the optimum location of wells. In fact, once the field starts producing, some static parameters will change due to fluid flow, change in fluid saturation, etc. Therefore, it is accepted by the industry that dynamic maps generated from dynamic parameters are more relevant in presenting more accurate images about the quality of a reservoir rock in relation to the active forces within.

The other category of sweet spot delineation is based on dynamic measures. A quality map term was introduced in 1999 in which a single vertical well was placed in different areal grid locations in a model to create 2D cumulative oil maps[15]. The model would ideally run for every well in several grid locations for a long enough time to apprehend assorted trends in the collective oil volume produced. This approach was used to locate wells with an optimization algorithm under geological uncertainty. Later, the quality map approach was used[16] to generate quality maps for oil, gas, and water production to improve the initial population in the well placement optimization process using a genetic algorithm. The best producer locations were identified, using oil and gas quality maps, and the best injector locations were determined using water quality maps, with yields in the maximization of either cumulative hydrocarbon or net present value. Guiding the initial population selection in the genetic algorithm improved the objective function significantly after using quality maps, which was highlighted as one of the main findings.

Ding (2008)[17] used the productivity index (PI) as an objective function to be maximized by optimum well locations in 2008. A numerical PI and field PI were suggested as two different attributes to be maximized. The summation of the numerical PI was the attribute to be maximized. The values of the numerical PI were obtained from the production of horizontal wells in a reservoir model. A field PI was obtained by the calculation of flow rate over total drawdown for one large time step. These attributes were used with a covariance matrix adaptation algorithm to find the optimum well placement.

The quality maps approach has enticed many researchers, and has been used more often when compared with other methods[18, 19]. The long simulation runs required to obtain one map, especially in large models, could cause a reluctance to implement this approach in actual reservoirs. The PI method previously discussed is preliminary and not precise since Peaceman's[20-22] PI calculation method is intended for vertical wells, while the production used[17] to calculate

PI values was from horizontal wells, which could result in erroneous answers[23].

The traditional aforementioned methods of cumulative oil or the reservoir quality index based on simulation history provides a rudimentary means for the determination of effective sweet spot regions throughout the reservoir. An intelligent solution must be introduced that is comprehensive, efficient, simulation-based, and utilizing reservoir engineering best practices, which is conceptually depicted in Fig. 1. The new solution must be intelligent enough to optimize high performance computation resources. In this article, we will introduce a novel approach to identify sweet spots in a reservoir utilizing total PI calculations.

To achieve an efficient sweet spot identification, the optimal reservoir PI (OPTIMA) engine goes beyond reservoir history by evaluating the dynamic PI of every well location for optimal well placement. OPTIMA intelligently evaluates the productivity potential for each spot in a reservoir simulation model in prediction, and optimizes the target regions for well placement.

Fig. 1 *OPTIMA developed property.*

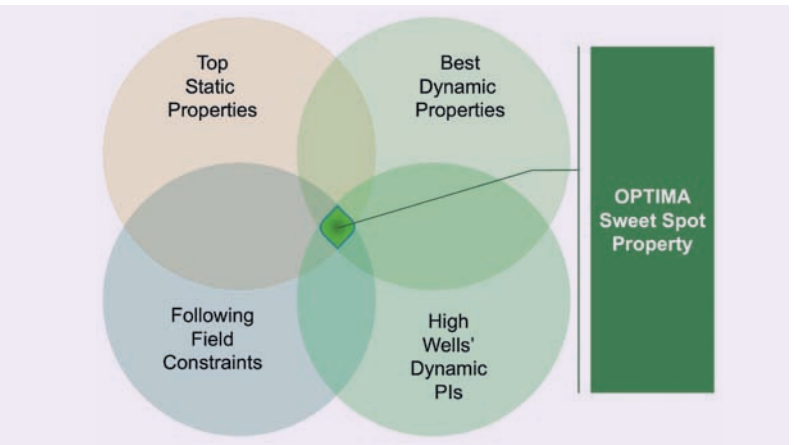

Fig. 2 *Multiple simulation cases with different assessment well locations.*

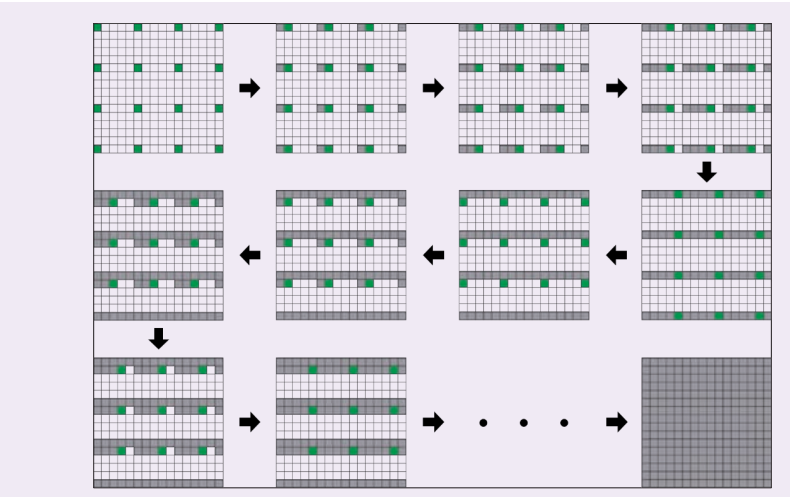

Methodology

The optimal reservoir productivity workflow identifies the high potential regions that can be used for drilling wells in an oil reservoir by assessing well productivity. Numerical simulation is utilized to generate the sweet spots and extrapolate performance domains reflecting reservoir energy and dynamicity. The PI at each grid cell in the simulation model is calculated at each time step within a period of prediction. The PI is a measure of well potential or ability to produce a number of barrels per day for every psi of pressure. Therefore, all grid cells have to be penetrated by assessment wells for the simulator to compute the productivity at each grid cell.

At the initial stage, the workflow shuts in all existing wells in the simulation model and places one assessment well that penetrates all the layers. Multiple prediction scenarios are simulated in which each scenario has one assessment well in a different location. Therefore, the number of simulation scenarios required will be equal to the number of grid cells in one layer in the simulation model. This is done to assess the PI in each grid column. Combining the results from all the scenarios provides a complete picture of the productivity in each area in the reservoir.

This process would require thousands or more of simulation cases in which each case is used for assessing one column of grid cells only. This would consume a huge amount of time and resources, especially for huge simulation models with multimillion grid cells in size. For this reason, the workflow introduces well spacing as an important element that accommodates well interference in the process. Instead of placing one assessment well in each simulation case, multiple assessment wells are placed taking into consideration the reservoir connectivity and permeability, which determines a suitable spacing between the assessment wells, Fig. 2.

For high permeability reservoirs, spacing between the assessment wells is increased to avoid interference that could lead to misleading results, and may not reflect the actual productivity potential. Placing multiple assessment wells improved the performance of running the workflow where it reduced the number of simulation cases by more than two orders of magnitude. The number of simulation cases required to run the workflow depends on the chosen well spacing, which can be calculated using the formula $N = (x+1)^2$, where N is the number of simulation cases with different layouts of well locations and x is the spacing between the assessment wells in terms of the number of grid cells.

Another feature that improved the overall performance of the workflow is the filtering capability. Wells are placed in high potential zones only. Depending on the nature of the reservoir and the objective of the study, cutoffs can be applied on the oil saturation,

Fig. 3 *The number of assessment wells placed by OPTIMA in two different cases.*

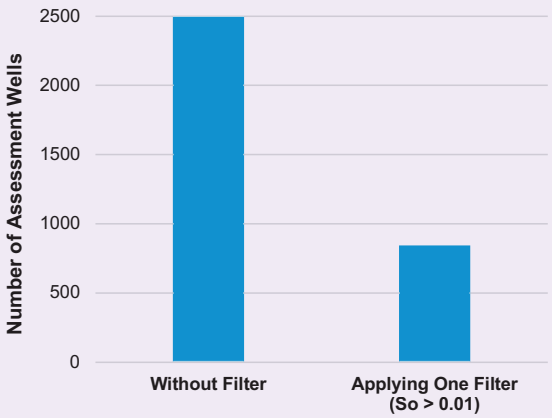

Fig. 5 *The integration of PI over time (TDPI) of one grid cell.*

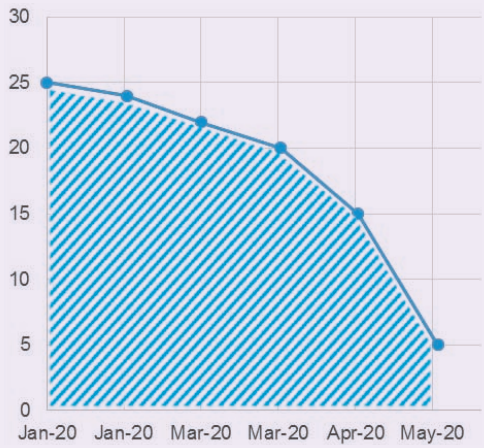

the permeability, or any reservoir static or dynamic property. Assessment wells are placed to penetrate only the potential zones after filtering out unnecessary grid cells. As a result, this step reduces the size of the investigated solution space, and thereby speeds up well calculations in the simulation runs.

Figure 3 compares two different OPTIMA cases, one without applying filters and another applying a filter on oil saturation (So > 0.01). The number of assessment wells was reduced from 2,500 to 845. The assessment wells are a plurality of single lateral pseudo wells placed vertically to calculate the PI at each grid cell. These wells exhibit certain spacing and production constraints that can result in unleashed reservoir productivity potential from every spot. The production rate can be controlled and usually set to very high values for the assessment wells to produce with their full potential and for OPTIMA to calculate the potential productivity. Similarly, bottom-hole pressure (BHP) is set to minimum — above bubble point pressure — to assess the well's potential.

OPTIMA analyzes oil PI results from the simulation output and creates a new sweet spot identifier: Total Dynamic PI (TDPI). TDPI is the integration of PI values with respect to time, and it describes how productive each grid cell is if the reservoir pressure changes per psi. Figure 4 shows the PI values vs. time for one grid cell generated by the simulator. Figure 5 shows how the TDPI is calculated.

OPTIMA generates a 3D reservoir property of normalized TDPI values ranging between 0 and 1. The normalization is performed to simplify understanding the result, and to streamline post-processing and analysis.

The workflow is integrated within a simulation environment, which automates creating the multiple simulation cases with different well locations, running simulation, analyzing results and generating the TDPI 3D

Fig. 4 *The PI of one grid cell at different simulation time steps.*

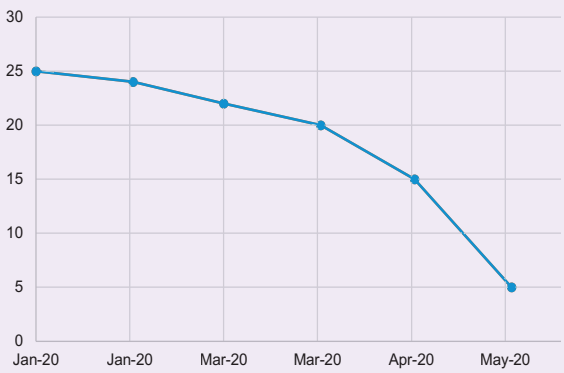

Fig. 6 *An average 2D map of the TDPI array.*

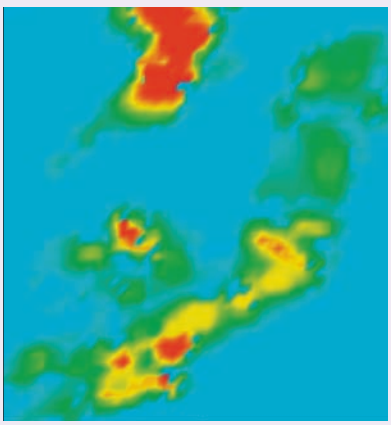

Fig. 7 *The TDPI distribution in one layer (J direction slice).*

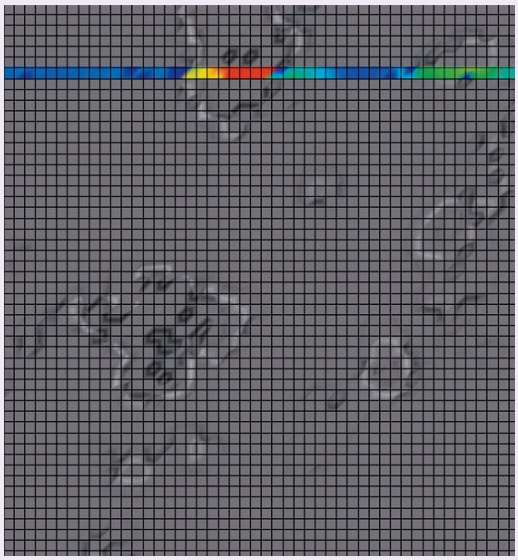

Fig. 9 *Histogram of TDPI array in a logarithmic scale.*

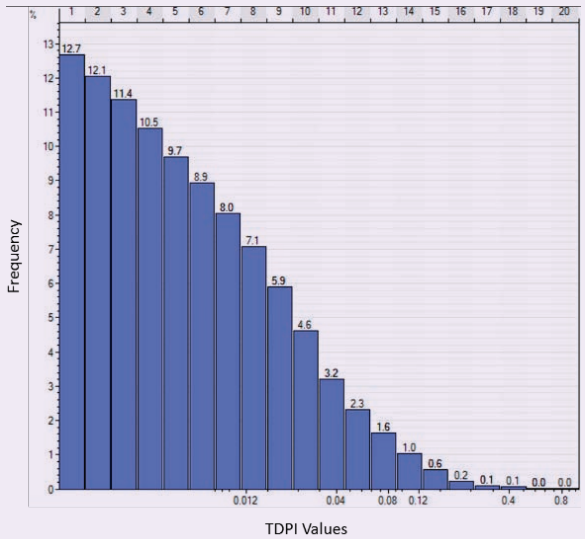

array. It capitalizes on efficient hyper performance computing clusters to run the multiple simulation jobs of millions of grid cell size models.

Results and Discussions

OPTIMA was used to generate sweet spots for multiple simulation cases for different fields. The results discussed in this article are based on a synthetic reservoir model, which exemplifies the procedure applied on actual studies. Different sensitivities were generated and analyzed to measure the impact of changing the different input parameters to the workflow. This includes analyzing the influence of the assessment well spacing and the production rate, although this article focuses more on the established workflow for OPTIMA.

Comparisons between the different sensitivities and optimization of input parameters will be presented in a future article. In general, the results of the analyses indicate that a safe distance must be chosen carefully to avoid interference between the assessment wells. The reservoir model presented in this study has a low permeability and it was chosen to use 1.0 km spacing between the assessment wells. The dimensions of the model are 100*100*20 in x-y-z grid cells, and therefore, 1.0 km corresponds to 10 grid cells. Consequently, a value of 10 grid cells was used as an input to OPTIMA

Fig. 8 *The PI profiles of multiple grid cells at different simulation time steps.*

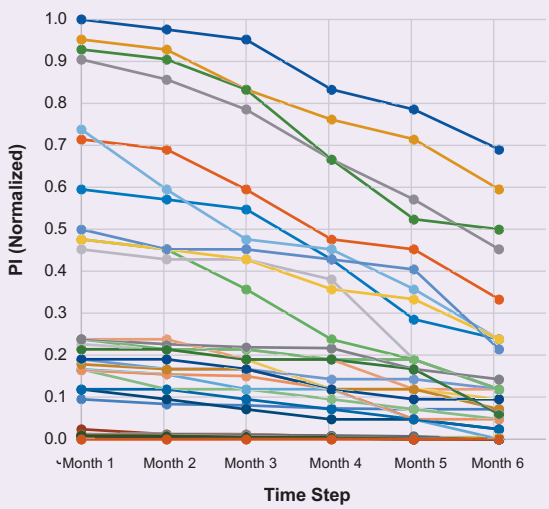

Fig. 10 *Histogram of a filtered TDPI array (> 0.1) in a linear scale.*

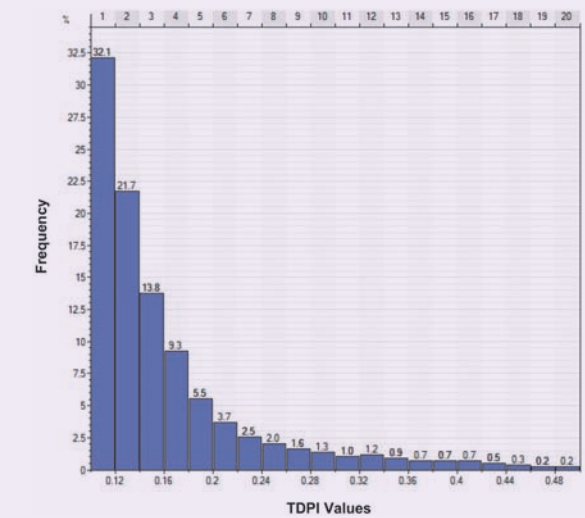

in this study. In addition, the oil production rate of 20,000 barrels per day and BHP of 1,200 psi — just above the bubble point pressure — were used for each of the assessment wells to ensure that they produce with their full potential. As a result of these parameter inputs, 121 simulation runs were required to generate the TDPI 3D array.

After the completion of all simulation runs, OPTIMA generated the TDPI 3D array that was visualized using a post-processing tool. An average 2D map of the TDPI array for a selected region was generated, Fig. 6. Blue areas in the average map represent non-productive areas, whereas the red indicates areas with the highest values of TDPI.

Figure 7 shows the TDPI distribution in one layer in grayscale, but highlighting one row of grid cells in the J direction. The highlighted grid cells show the variation of the TDPI values. Figure 8 shows the PI profiles over time for these grid cells.

Due to the large size of the reservoir, the majority of the grid cells have very small TDPI values — low productivity energy — representing poor quality oil zones. Only a small portion of the reservoir representing good energetic productive zones show relatively high TDPI values. This causes the normalized TDPI array to show very small values for the majority of the

Fig. 11 *An average 2D map of filtered the TDPI array (> 0.1).*

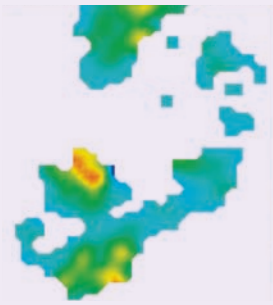

Fig. 12 *Polygons representing sweet spots.*

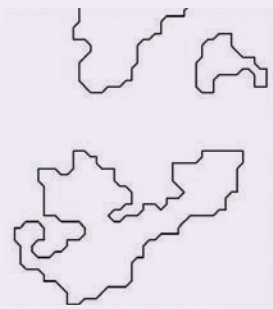

Fig. 13 *The permeability average map and sweet spot polygons.*

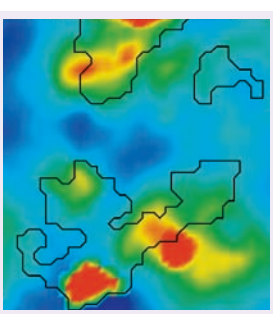

Fig. 14 *The porosity average map and sweet spot polygons.*

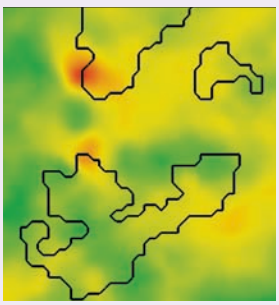

Fig. 15 *The oil saturation average map and sweet spot polygons.*

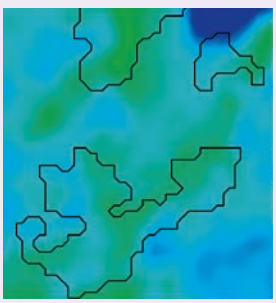

Fig. 16 *The comparison between the TDPI and ROI results.*

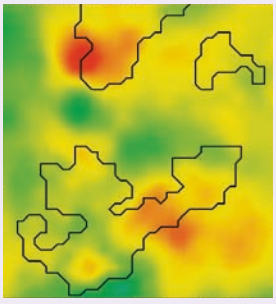

Fig. 17 *The prediction scenario showing the four wells placed in sweet spots.*

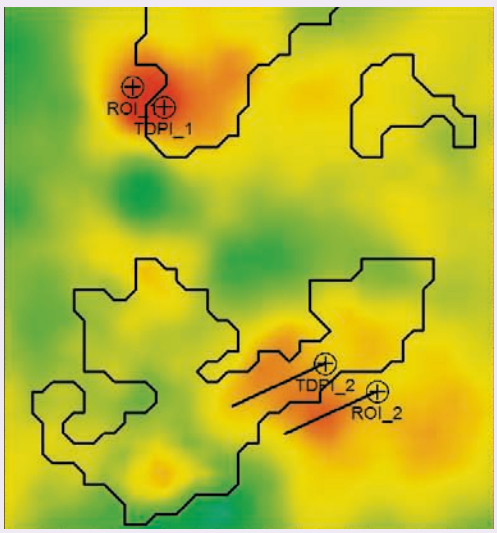

Fig. 19 *Production performance ratio for the vertical wells placed using TDPI and ROI methods.*

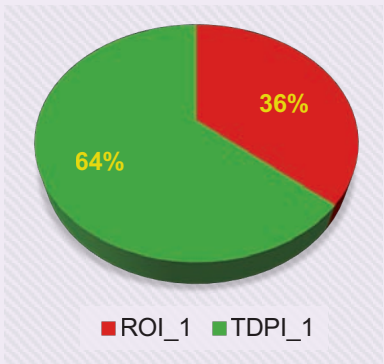

array, and makes it difficult to analyze in a linear scale. Therefore, one way to analyze the TDPI distribution is to plot in a logarithmic scale, Fig. 9.

The analysis is focused on regions with TDPI values greater than 0.1, which represents the highly energetic productive oil zones. As a result, the TDPI array was filtered and plotted in a histogram using a linear scale, Fig. 10.

After filtering out poor quality areas, another average 2D map of the new filtered TDPI array of the same selected region was generated. Figure 11 shows the filtered TDPI average map, in which the color scale is different than the one used in Fig. 6, due to a different range of values.

The filtered TDPI average map presented in Fig. 11 shows connected volumes for high energetic oil productive zones. Small connected volumes are filtered out to put more focus on analyzing the potential areas for drilling new wells. Polygons were created around the new filtered regions to represent the sweet spots, Fig. 12.

The sweet spots presented in Fig. 12 were validated by comparing them with permeability, porosity, and oil saturation maps, Figs. 13 to 15. Figure 13 shows how the sweet spot polygons conform to most of the high permeable areas, except small portions where they have low oil saturation.

Fig. 18 *Normalized cumulative oil production of two prediction vertical wells.*

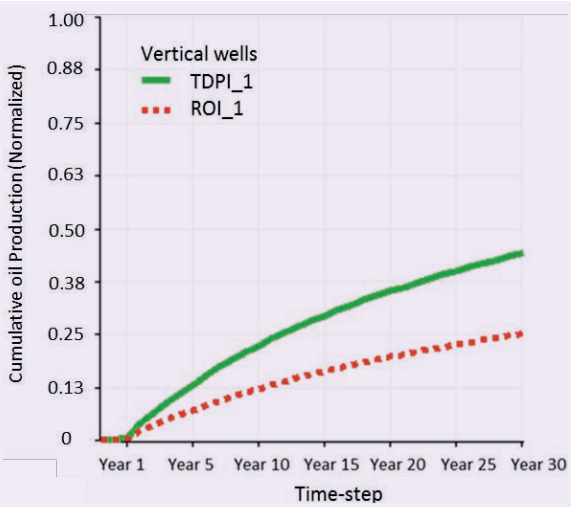

Fig. 20 *Normalized cumulative oil production of two prediction slanted wells.*

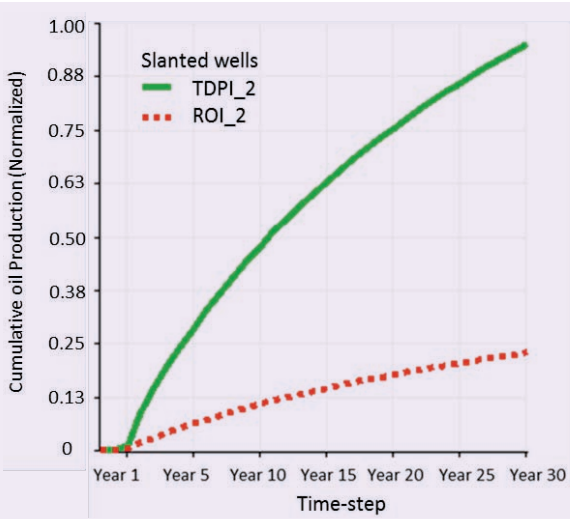

Fig. 21 *Production performance ratio for the slanted wells placed using TDPI and ROI methods.*

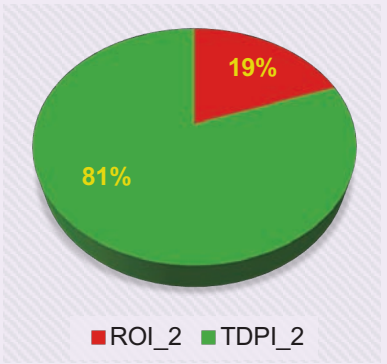

The TDPI-based sweet spots were also compared to the Reservoir Opportunity Index (ROI) map. ROI is a computation of the hydrocarbon pore volume, reservoir pressure, and permeability, and similar to TDPI, is normalized from 0 up to 1[24]. Figure 16 shows the comparison between the TDPI and ROI results.

Prediction wells were placed in the identified sweet spots in the simulation model to assess well performance and evaluate the difference between TDPI and ROI. One vertical well, Well-TDPI_1, was placed inside one of the TDPI sweet spots polygons. The well was placed and perforated crossing all the layers. Also, a slanted well, Well-TDPI_2, was placed inside another TDPI sweet spot polygon. TDPI_2 was also placed and perforated crossing all the layers with a length of 1,000 m.

Another prediction scenario was created by placing two wells, Well-ROI_1 and Well-ROI_2, with similar lengths and configurations to Well-TDPI_1 and Well-TDPI_2. Well-ROI_1 and Well-ROI_2 were placed in areas with high ROI values, but outside the TDPI polygons. Figure 17 shows the location of these four wells. Note that the TDPI wells were placed in a different simulation case than the ROI wells.

The two simulation cases were run for 30 years of prediction, and the results of the well's performance are presented in Figs. 18, 19, 20, and 21. Cumulative oil production, normalized for both the TDPI and ROI wells, were compared for both the vertical and horizontal cases. For the vertical wells, the production performance for the well placed based on the TDPI sweet spot method was almost double that for the well placed using the ROI. For the slanted wells, the TDPI method showed a superior performance of four times over the well placed using the ROI.

The sweet spots calculated using the TDPI and ROI are 3D properties. In this study, prediction wells were placed based on average maps of sweet spots. The wells penetrated all layers of the simulation model. This was done to simplify the analysis, and to focus more on the main technique behind OPTIMA. In reality, wells are optimally digitized to follow the sweet spots in 3D space to ensure they passed through high potential zones only. The average map technique used in this study is useful for quick assessments to guide field development planning and optimization. Such an assessment gives an indication for the potential of utilizing efficient sweet spot systems that can point to energetic oil-rich pockets in reservoirs, and thereby steer adequate development decisions in due course.

It is understood that field level comparison with actual wells drilled on spots identified by the sweet spot methods are the determining evidence of the technique described in this article. Future work can aid in accelerating and obtaining results from the sweet spot methods for other types of reservoirs not currently considered in OPTIMA.

Conclusions

In this article, we introduced OPTIMA to identify sweet spots in hydrocarbon reservoirs. The developed dynamic approach is found to be superior to previous published techniques in identifying sweet spots in oil reservoirs since it comprises both static and dynamic reservoir information, and can be generated with a minimum computational expense. The filtering feature can significantly reduce simulation run time after excluding poor quality regions.

The number of simulation jobs to generate an OPTIMA map is reduced by more than two orders of magnitude with the utilization of a filtering option. One of the direct applications for OPTIMA is in optimizing the location of wells in hydrocarbon reservoirs. The results discussed in this article showed OPTIMA's great potential in this area.

OPTIMA maps can be used for reservoir management decisions in contrasting, characterizing reservoirs, and identifying high and low productive areas. These maps can highlight devastated regions required for pressure support or other actions, unleashing the reservoir response to any dynamic change that occurred in the reservoir vicinity, which opens the floor to use OPTIMA maps in intelligent field systems.

Acknowledgments

The authors would like to thank the management of Saudi Aramco for their support and permission to publish this article.

This article was presented at the SPE Kingdom of Saudi Arabia Annual Technical Symposium and Exhibition, Dammam, Saudi Arabia, April 16-18, 2019.

References

1. Al-Qahtani, G.D., Soliman, M.Y. and de Farias Jr., I.R.: "Methods, Systems, and Computer Medium having Computer Programs Stored thereon to Optimize Reservoir Management Decisions," U.S. Patent No. 9,816,366, April 2017.

2. Al-Qahtani, G.D., Al-Faleh, A.A., Nasser, K.A., Abouheit, F.F., et al.: "Methods, Systems, and Computer Medium having Computer Programs Stored thereon to Optimize Reservoir Management Decisions based on Reservoir Properties," U.S. Patent No. 20,180,258,748 A1, submitted November 2017.

3. Al-Qahtani, G.D., Alzahabi, A., Kozyreff, E., de Farias Jr., I.R., et al.: "A Comparison between Evolutionary Metaheuristics and Mathematical Optimization to Solve the Wells Placement Problem," *Advances in Chemical Engineering and Science*, Vol. 3, Issue 4, October 2013, pp. 30-36.

4. Al-Qahtani, G.D., Alzahabi, A., Spinner, T. and Soliman, M.Y.: "A Computational Comparison between Optimization Techniques for Wells Placement Problem: Mathematical Formulations, Genetic Algorithms and Very Fast Simulated Annealing," *Journal of Materials Science and Chemical Engineering*, Vol. 2, Issue 10, October 2014, pp. 59-73.

5. Seifert, D., Lewis, J.J.M., Hern, C.Y. and Steel, N.C.T.: "Well Placement Optimization and Risking Using 3D Stochastic Reservoir Modeling Techniques," SPE paper 35520, presented at the European 3D Reservoir Modeling Conference, Stavanger, Norway, April 16-17, 1996.

6. Gutteridge, P.A. and Gawith, D.E.: "Connected Volume Calibration for Well Path Ranking," SPE paper 35503, presented at the European 3D Reservoir Modeling Conference, Stavanger, Norway, April 16-17, 1996.

7. Deutsch, C.V.: "Fortran Programs for Calculating Connectivity of Three-Dimensional Numerical Models and for Ranking Multiple Realizations," *Computers & Geosciences*, Vol. 24, Issue 1, January 1998, pp. 69-76.

8. Wang, B.: "Well Site Selection Algorithm Considering Geological, Economical and Engineering Constraints," M.S. Thesis, University of Alberta, 2001, 66 p.

9. Vasantharajan, S. and Cullick, A.S.: "Well Site Selection Using Integer Programming Optimization," *Proceedings of International Association for Mathematical Geosciences*, Vol. 1, 1997, pp. 421-426.

10. Ierapetritou, M.G., Floudas, C.A., Vasantharajan, S. and Cullick, A.S.: "Optimal Location of Vertical Wells: Decomposition Approach," *AIChE Journal*, Vol. 45, Issue 4, April 1999, pp. 844-859.

11. Kharghoria, A., Cakici, M., Narayanasamy, R., Sinha, S., et al.: "Productivity-based Method for Selection of Reservoir Drilling Target and Steering Strategy," SPE paper 85341, presented at the SPE/IADC Middle East Drilling Technology Conference and Exhibition, Abu Dhabi, UAE, October 20-22, 2003.

12. Narayanasamy, R., Davies, D.R. and Somerville, J.M.: "Well Location Selection from a Static Model and Multiple Realizations of a Geomodel Using Productivity Potential Map Technique," SPE paper 99877, presented at the SPE EUROPEC/EAGE Annual Conference and Exhibition, Vienna, Austria, June 12-15, 2006.

13. Liu, N. and Jalali, Y.: "Closing the Loop between Reservoir Modeling and Well Placement and Positioning," SPE paper 98198, presented at the Intelligent Energy Conference and Exhibition, Amsterdam, the Netherlands, April 11-13, 2006.

14. Cullick, A.S., Narayanan, K. and Gorell, S.B.: "Optimal Field Development Planning of Well Locations with Reservoir Uncertainty," SPE paper 96986, presented at the SPE Annual Technical Conference and Exhibition, Dallas, Texas, October 9-12, 2005.

15. Da Cruz, P.S., Horne, R.N. and Deutsch, C.V.: "The Quality Map: A Tool for Reservoir Uncertainty Quantification and Decision Making," SPE paper 56578, presented at the SPE Annual Technical Conference and Exhibition, Houston, Texas, October 3-6, 1999.

About the Authors

Dr. Ghazi D. Al-Qahtani

Ph.D. in Petroleum Engineering, Texas Tech University

Dr. Ghazi D. Al-Qahtani is a Petroleum Engineering Specialist currently leading the Advance Simulation Modeling Group in Saudi Aramco's Reservoir Description and Simulation Department. Previously, he led several integrated reservoir study projects and supervised gas and oil reservoir management and simulation units under the Upstream business line.

In 2018, after graduating from the company's Technical Development Program, the Petroleum Engineering & Development Admin Area named Ghazi a Specialist in Complex Well Modeling and Optimization. He initiated and co-developed "OPTIMA," a unique Saudi Aramco patented integrated simulation-based solution to assess reservoir productivity by nominating sweet spots for optimal oil field development. Ghazi also initiated and co-developed "WePO," an innovative well placement optimization algorithm to find optimum locations and trajectories for hydrocarbon wells in large-scale reservoirs using transshipment network formulations and graph theory principles.

He has authored four U.S. patent applications, with two granted and two pending. Ghazi has also coauthored a book entitled *Fundamentals of Corrosion and Scaling for Petroleum and Environmental Engineers.* He has authored and coauthored more than 20 journal and conference papers on areas covering reservoir simulation technologies, field development plans, well placement optimization in conventional/unconventional reservoirs, and accelerating the development of integrated professionals.

Ghazi acted as a Ph.D. committee member and participated in several geoscience and petroleum related conferences, workshops, and symposiums as chairman, keynote speaker, steering committee member, and presenter.

He is a founding member of the Digital Technology Governance Association and a member of the Society of Petroleum Engineers (SPE), and the Saudi Council of Engineers.

Ghazi received his B.S. degree in Petroleum Engineering from King Fahd University of Petroleum and Minerals (KFUPM), Dhahran, Saudi Arabia, his M.S. degree in Petroleum Engineering from the University of Southern California, Los Angeles, CA, and his Ph.D. degree in Petroleum Engineering with a minor in Industrial Engineering from Texas Tech University, Lubbock, TX.

16. Túpac, Y.J., Almeida, L.F., Pacheco, M.A.C. and Vellasco, M.M.B.R.: "Evolutionary Optimization of Oil Field Development," SPE paper 107552, presented at the Digital Energy Conference and Exhibition, Houston, Texas, April 11-12, 2007.

17. Ding, D.Y.: "Optimization of Well Placement Using Evolutionary Methods," SPE paper 113525, presented at the EUROPEC/EAGE Conference and Exhibition, Rome, Italy, June 9-12, 2008.

18. Cottini-Loureiro, A. and Araujo-Fresky, M.G.: "Optimized Well Location by Combination of Multiple Realization Approach and Quality Map Methods," SPE paper 95413, presented at the SPE Annual Technical Conference and Exhibition, Dallas, Texas, October 9-12, 2005.

19. Le Ravalec-Dupin, M.: "Optimizing Well Placement with Quality Maps Derived from Multi-fidelity Meta-Models," SPE paper 154416, presented at the SPE EUROPEC/EAGE Annual Conference and Exhibition, Copenhagen, Denmark, June 4-7, 2012.

20. Peaceman, D.W.: "Interpretation of Well Block Pressures in Numerical Reservoir Simulation," *Society of Petroleum Engineers Journal*, Vol. 18, Issue 3, June 1978, pp. 183-194.

21. Peaceman, D.W.: "Interpretation of Well Block Pressures in Numerical Reservoir Simulation — Part 3: Off-Center and Multiple Wells within a Well Block," SPE paper 16976, presented at the SPE Annual Technical Conference and Exhibition, Dallas, Texas, September 27-30, 1987.

22. Peaceman, D.W.: "Interpretation of Well Block Pressures in Numerical Reservoir Simulation with Nonsquare Grid Blocks and Anisotropic Penneability," *Society of Petroleum Engineers Journal*, Vol. 23, Issue 3, June 1983, pp. 531-543.

23. Shu, J.: "Comparison of Various Techniques for Computing Well Index," M.S. Thesis, Stanford University, 2005, 35 p.

24. Al-Baqawi, A.M., Al-Naim, H.A., Araque, A.J., Habbtar, A.H., et al.: "Effective Well Placement and Trajectory Planning Approach through Collaboration Environment Tools," SPE paper 143071, presented at the SPE EUROPEC/EAGE Annual Conference and Exhibition, Vienna, Austria, May 23-26, 2011.

Menhal A. Al-Ismael

M.S. in Petroleum Engineering, King Fahd University of Petroleum and Minerals

Menhal A. Al-Ismael is a Petroleum Engineering Systems Analyst working in the Simulation Systems Division of Saudi Aramco's Petroleum Engineering Applications Services Department, where he provides solutions and system support to reservoir simulation studies.

Menhal has more than 10 years of experience in petroleum engineering systems support working on many projects in the area of field development planning and optimization.

He is a Society of Petroleum Engineers (SPE) certified petroleum engineer.

Menhal received his B.S. degree in Information and Computer Science, and his M.S. degree in Petroleum Engineering, both from King Fahd University of Petroleum and Minerals (KFUPM), Dhahran, Saudi Arabia.

Abdulhamed A. Al-Faleh

M.S. in Petroleum Engineering, Texas A&M University

Abdulhamed A. Al-Faleh is a Petroleum Engineer System Analyst, working as the Reservoir Engineering Systems Development Team Lead in Saudi Aramco's Petroleum Engineering Applications Services Department of the Exploration and Petroleum Engineering Center – Computer Center (ECC). He has more than 10 years of experience in the oil and gas industry.

During Abdulhamed's career, he has played a key role in the development of several systems in the areas of reservoir simulation, reservoir management and reserves.

Abdulhamed received his B.S. degree in Software Engineering from King Fahd University of Petroleum and Minerals (KFUPM), Dhahran, Saudi Arabia. He also received an M.S. degree in Petroleum Engineering from Texas A&M University, College Station, TX.

Basharat Ali

M.S. in Petroleum Engineering, Imperial College London

Basharat Ali is a Senior Petroleum Engineer working with the Northern Area Offshore Team in Saudi Aramco's Reservoir Description & Simulation Department. He joined Saudi Aramco in May 2013.

Prior to this, Basharat worked as a Principle Reservoir Engineer with the Eni U.K. Ltd., and as a Reservoir Engineering Workflow Consultant with Schlumberger, U.K. He has 15 years of experience in the oil and gas industry in areas covering reservoir simulation, well testing, production optimization, and field development planning. Basharat's main focus area is assisted field development planning using IR 4.0.

He received his B.E. degree in Mechanical Engineering from UET Peshawar, Pakistan, and in 2004, Basharat received his M.S. degree in Petroleum Engineering from Imperial College London, London, U.K.

Fouad F. Abouheit

B.S. in Mathematics, University of Houston

Fouad F. Abouheit is a Petroleum Engineer System Analyst working with the Simulation Systems Division of Saudi Aramco's Petroleum Engineering Application Services Department. He provides upstream consultation and software development in reservoir simulation workflows related to developing solutions for full field well planning and development, efficient grid and complex well data exchange with corporate flow simulators, and enabling an optimal reservoir sweet spot identifier application.

Fouad has more than 25 years of oil and gas industry experience, obtained through a variety of international research and development positions.

He received his B.S. degree in Mathematics from the University of Houston, Houston, TX.

Experimental and Simulation Approaches on Evaluating an Improved Hydraulic Fracturing Treatment for Stimulating Tight Carbonate Reservoirs

Dr. Feng Liang, Dr. Yanhui Han, Dr. Hui-Hai Liu, Dr. Rajesh K. Saini, and Dr. Jose I. Rueda

Abstract /

Hydraulic fracturing has been widely used in stimulating tight carbonate reservoirs to improve oil and gas production. Improving and maintaining the connectivity between the natural and induced microfractures in the far-field and the primary fracture networks are essential to enhance the well production rate since these natural and induced unpropped microfractures tend to close after the release of hydraulic pressure during production. This article provides a conceptual approach of an improved hydraulic fracturing treatment to enhance the well's productivity by minimizing the closure of the microfractures in tight carbonate reservoirs and enlarging the fracture aperture.

The proposed improved fracturing treatment was to use the mixture of the delayed acid generating materials along with microproppants in the pad/pre-pad fluids during the engineering process. The proof-of-concept laboratory coreflood experiments were conducted under elevated temperature on a core plug assembly, which was comprised of a one-half core Eagle Ford sample, another half core of hastelloy core plug, and a mixture of delayed acid generating materials along with small-sized proppants sandwiched by two half cores. Simulations using the discrete element method (DEM) and the lattice Boltzmann method (LBM) for three different scenarios — 14 cases in total — were conducted to further demonstrate the feasibility of the concept.

The delayed acid generating materials used in this strategy not only create voids to enlarge the aperture in flow pathways within microfractures owing to degradation introduced by elevated temperatures and the interaction with the treatment fluids, but also generate more microfractures through the fluid's chemical reaction with the calcite formation. The microproppants were used to support the opening of natural or newly induced microfractures. A surface profilometer was used to quantify the surface etched profile before and after coreflood experiments.

Simulations of fluid flow through proppant assembly (inside of the microfractures) were conducted to estimate the permeability of the fractures under three different scenarios: (1) fluid flow in a microfracture without proppant, (2) fluid flow in a microfracture with small-sized proppants, and (3) fluid flow in a microfracture supported by small-sized proppants and generated voids on the fracture walls. The simulation results show that with proppant support (Scenario 2), the microfracture permeability can be increased by tens to hundreds of times in comparison to Scenario 1, depending on the gaps between proppant particles. The permeability of the proppant supported microfracture (Scenario 3) can be further enhanced by the cavities created by the reactions between the generated acid and calcite formation.

This work provides experimental evidence that the use of the mixture of the delayed acid generating materials along with microproppants or small-sized proppants in stimulating tight carbonate reservoirs in the pad/pre-pad fluids during the engineering process might be able to effectively improve and sustain permeability of flow pathways from microfractures — either natural or induced. These findings will be beneficial to the development of an improved hydraulic fracturing treatment for stimulating carbonate-rich tight gas reservoirs.

Introduction

While acid fracturing and matrix acidizing have proved to be effective in stimulating conventional carbonate reservoirs because of carbonate reactivity with acids[1-4], it is well-known that the combination of horizontal drilling and hydraulic fracturing has been the most effective stimulation technique to produce natural gas from carbonate-rich tight gas or shale formations due to much lower permeability — nd to µd range — and different pore structures[5-7]. Because the low permeability of rock matrix bottlenecks the flow of hydrocarbon

fluids, creating complex fractures in the rock matrix is highly desired to improve and maintain conductive flow paths for enhancing the production.

Baihly et al. (2010)[8] has compared the production trends of horizontal wells in different shale gas basins, including Barnett Shale, Fayetteville Shale, Woodford Shale, Haynesville Shale, and Eagle Ford Shale plays, and observed that the gas production rate declines rapidly within the first few months of production. They also noted that the production rate does not reach its peak in the first few months, which might be due to the fact that the early production rate is affected by the wellbore cleanup conditions in that the gas is produced along with water and the residual fracturing fluids.

Wang (2017)[9] has studied the factors controlling the shale gas production and production decline trend in fractured systems. These include effects of the existence of adsorption gas, matrix permeability, rock mechanics properties like creep and viscoelastic behaviors, clay content, organic content and maturity, evolution of shale matrix apparent permeability, non-stimulated reservoir volume, and the density, conductivity, and connectivity of fracture networks. He concluded that regardless of the matrix permeability, the denser fracture networks and larger fracture surface areas inside the stimulated reservoir volume always led to higher production. Enhancing the connectivity of natural or induced microfractures in the far-field to the primary fracture branches is essential to enhance well production in unconventional fields.

These microfractures, besides the primary fracture networks generated by hydraulic fracturing, should be an important contributor to the high production rate at the initial production stage. The commonly observed quick production rate decline at least partially results from the closure of these microfractures. During hydrocarbon production, the pore pressure declines and accordingly the effective stress increases, resulting in the closure of these non-proppant supported microfractures with production. Note that due to the size constraints, conventional proppants are too big to be applied into these microfractures and transportation characteristics of the proppants further limit how far they can travel into stimulated areas.

Recently, introducing microproppants into the pad fluids has been shown to be able to enhance well production in unconventional gas and condensate-rich fields[10, 11], because microproppants can migrate into the microfractures and keep them open during production.

Also, in a typical hydraulic fracturing process, millions of gallons of water-based fracturing fluids are generally used as the carrying fluids to transport proppants into the fractures. Subsequently, it has been commonly observed that only 10% to 35% of the fracturing fluid flows back to the well, and the rest is retained in the formation[12-14]. The imbibition of fracturing fluid into the rock matrix is considered one of the main mechanisms that cause fracturing fluid loss and reservoir damage, which reduces the permeability of the gas-oil phase, and thereby decreases the productivity[12, 15, 16].

Most recently, Liang et al. (2018 and 2019)[17, 18] reported that a considerable amount of dissolution and precipitation has been observed in imbibition tests of rock samples from an organic-rich tight carbonate formation in neutral pH fracturing fluid lab experiments. The dissolution of the sulfate and carbonate minerals results in a potential increase of the absolute permeability of the reservoir rocks. Therefore, diluted acids can be used while fracturing to maintain the conductivity of the generated microfractures by nonuniformly etching the fracture surfaces in carbonate-rich shales.

Wu and Sharma (2017)[19] have demonstrated the in situ changes of microstructures and pore structures for high carbonate Bakken Shale that was treated with 3% hydrochloric acid. Channels in carbonate-rich regions, cavities or grooves in carbonate islands or carbonate rings, and roughness in areas of scattered carbonate were observed after acid treatment, caused by the reactive nature of carbonates with dilute acids.

To increase the matrix permeability by improving the mineral dissolution ability of the imbibed fluid to the formation, while minimizing the softening effect of a calcite-rich shale surface, we propose to apply a mixture of the delayed acid generating materials along with microproppants in the pad/pre-pad fluids in the engineering process of the hydraulic fracturing stimulation process. The delayed acid generating chemicals could help generate more fractures/or microfractures due to the chemical reactions with the calcite formation, giving the microproppants a better chance at being transported into these induced microfractures, or the connected natural microfractures.

The major objective of this work is to develop a conceptual approach of improved hydraulic fracturing treatments to enhance the well productivity by combining advantages of the two key elements: (1) the use of microproppants to keep open the natural and induced microfractures during the production, and (2) the dissolution (or etching) effects on increasing pore or aperture sizes using a mixture of the delayed acid generating materials. A series of the proof-of-concept laboratory coreflood experiments were conducted under elevated temperatures on a core plug assembly, which was comprised of a one-half core Eagle Ford sample, another half core of hastelloy core plug, and a mixture of delayed acid generating materials along with small-sized proppants sandwiched by two half cores.

The texture and surface profile of the half core shale plugs were analyzed using a Nanovea PS50 profilometer before and after the mixture of delayed acid generating particles and small-sized proppants treatment. Simulations using the discrete element method (DEM) and the lattice Boltzmann method (LBM) coupling approach for three general different scenarios — 14 cases in total — were also conducted to quantify the permeability changes along the microfractures under different packing and etching conditions.

Experimental Methods

Materials

Rock Sample. The tight organic-rich carbonate source rock samples used in this study were an outcrop from the Eagle Ford shale. Total organic carbon (TOC) of this sample was around 5 wt%. The mineral content determined by X-ray diffraction (XRD) technique shows that it is mainly composed of calcite (66 wt%), quartz (26 wt%), and minor amounts of dolomite (1 wt%), gypsum (2 wt%), pyrite (less than 1 wt%), kaolinite (3 wt%), and illitic clay (1 wt%).

Proppants. Small-sized proppants were used to support the opening of naturally or newly induced microfractures. Since the size of the microproppants is quite small and they tend to be very fluffy, it is very challenging to handle them properly in the laboratory. Instead, 100 mesh (around 150 μm in diameter) white sand was chosen for proving the concept proof study.

Solid Delayed Acid Generating Materials. Solid delayed acid generating material was used to create voids or dimples on the flow path of microfractures by its degradation under elevated temperature and the chemical reaction between the acidic fluid and the calcite formation. One of the degradable ester type chemicals with an average size of 200 μm was used in this study. The generated acid after degradation is considered to be an organic acid, or weak acid.

Preparation Procedure of the Half Core Plug Sample

Half core Eagle Ford outcrop plugs were obtained by splitting one full core of 1" in diameter by 1" in length using a trim saw in the longitudinal direction — similar to the procedure described in Wu et al. (2017)[20]. The rock surfaces were then fine trimmed using a target surface trimmer.

Surface Morphology Characterization

The texture and surface profile of the half core plugs were analyzed using a Nanovea PS50 profilometer. This instrument was designed with leading edge chromatic confocal optical technology (axial chromatism), compliant with both the International Organization for Standardization (ISO) and the American Society for Testing and Materials (ASTM). The technique measures a physical wavelength directly related to a specific height without using complex algorithms. The surface characterization was conducted for rock samples before and after chemical treatment to identify the morphology difference caused by the chemical reactions.

Packing Treatment Chemicals on Rock Surface

Three experiments with different chemical packing patterns were conducted, preferably with single layer packing. Experiment #1 was conducted with intermixed solid delayed acid generating materials and 100 mesh sand particles. In Experiment #1, 23.9 mg of solid delayed acid generating materials, and 31.9 mg of 100 mesh white sand were packed on the surface of the half core Eagle Ford outcrop sample, Fig. 1a.

Experiment #2 was conducted with 51.9 mg of solid delayed acid generating materials alone, Fig. 1b. No white sand was added in this experiment.

Experiment #3 was conducted with solid delayed acid generating materials and 100 mesh sand in four arrays. In this experiment, 23.0 mg of solid delayed acid generating materials and 40.7 mg of 100 mesh sand were packed on the surface of the half core plug sample with four different rows, Fig. 1c. From the top to the bottom of Fig. 1c, the packed materials are white sand, solid delayed acid generating materials, white sand and intermixed sand, and solid delayed acid generating materials.

The distributions of packed treatment materials were

Fig. 1 Photos of the Eagle Ford outcrop sample packed with different treatment chemicals: (a) Experiment #1, packed with intermixed solid delayed acid generating materials and 100 mesh sand; (b) Experiment #2, packed with solid delayed acid generating materials alone; and (c) Experiment #3, packed with solid delayed acid generating materials and 100 mesh sand in different patterns.

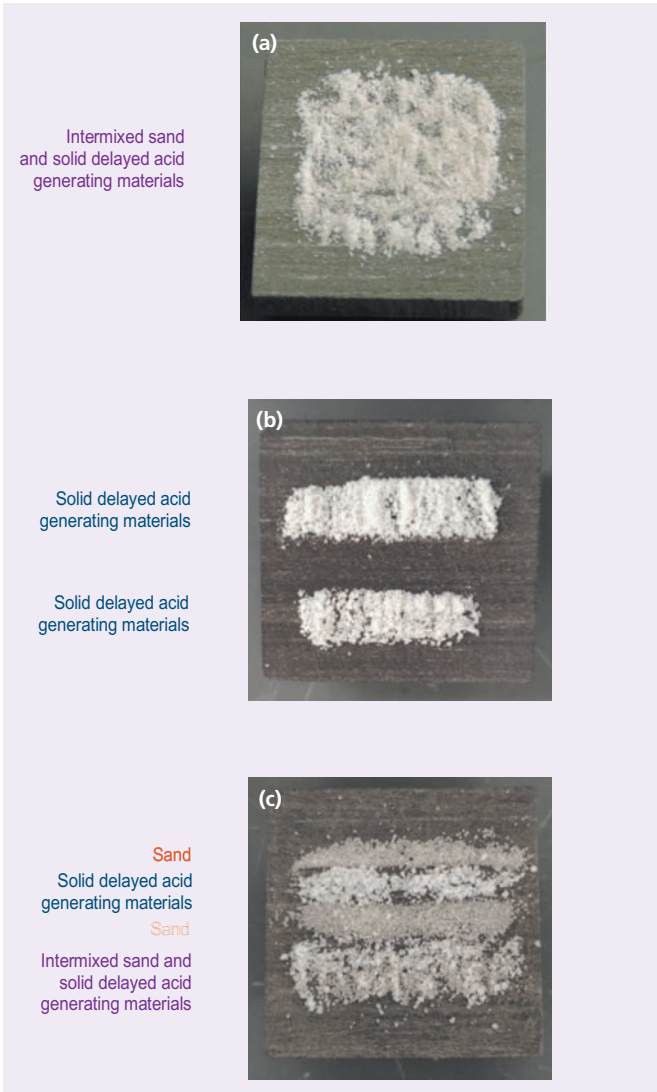

designed in such a way that they reflect the pump consequence of fracturing fluids in practical applications.

Treatment under High-Pressure and Elevated Temperature

The packed half core plug was assembled with a half core spacer made with hastelloy material, Fig. 2. The aperture between the two halves was used to simulate the width of the filled microfracture. The composite core assembly was then placed into a hastelloy core holder for testing under high pressure and elevated temperature. The confining pressure was set at 2,000 psi and back pressure was maintained at 1,000 psi through the test. Potassium chloride (KCl) — 2% — was used as the flowing fluid for all the three coreflood tests. Since the size of the aperture between the half core and the spacer is relatively large (around 150 µm), attempts were made to measure the differential pressure across the composite core assembly, but were not able to detect accurately due to the current pressure gauge's detection limit. After thermal treatment, the half core sample was removed from the coreflood setup and the etched surface was analyzed to identify the morphology difference caused by the chemical reactions.

Testing Condition for Experiment #1. The testing temperature was set at 180 °F, with a 2% KCl fluid flowing through the core assembly at a rate of 1 mL/min for 3 hours. Then the coreflood setup was shut-in overnight. No further fluid flow was conducted and the core assembly was removed from the coreflood setup.

Testing Condition for Experiment #2. The testing temperature was set at 180 °F. A constant flow rate of 2% KCl was maintained at a very slow value of 0.001 mL/min for 90 hours. Then, the core assembly was removed from the coreflood setup.

Testing Condition for Experiment #3. The testing temperature was set at 250 °F. A constant flow rate of 2% KCl was maintained at 0.02 mL/min for 48 hours. Effluents were collected with auto collectors for further analysis. Then, the core assembly was removed from the coreflood setup.

Quantification of Dissolved Calcium Ions and TOC

Effluents collected from Experiment #3 were analyzed using inductively coupled plasma (ICP) equipped with the optical emission spectrometer (OES) technique. Since the rock sample used in this study was Eagle Ford outcrop and contains 66% calcite, it was expected that calcite will react with the acidic components from the degraded solid acid generating materials. Therefore, the concentration of Ca^{2+} was expected to increase in the collected effluents.

Before the ICP measurement for the effluents, Ca^{2+} was first quantified with its own standard solution with a five-point calibration curve, measured in mg/L (or ppm). If a testing sample was found to have concentrations above the upper limit of the standard solution (500 mg/L), further dilution of the testing sample was conducted until the reading was within the calibration range. The values less than the lowest concentration of the standard solution were reported as < 0.1 mg/L.

The concentration of the TOC in the effluents, which could reflect the amount of the degraded/dissolved solid acids, was analyzed by using a Shimadzu TOC analyzer. A calibration curve with a concentration of 0.00 ppm, 0.1 ppm, 1 ppm, 10 ppm, and 100 ppm carbon was conducted before the sample testing.

Numerical Modeling

Due to its resolution limitation, the laboratory pressure gauge cannot accurately quantify the differential pressure across the core assembly setup, so as with the permeability changes of the filled microfracture. Numerical modeling was conducted to estimate the permeability change based on the fracture aperture and the quantified ranges of the etched fracture surfaces.

The DEM-LBM coupling model has been proven to be capable of precisely capturing the fluid flow in the pore space, and the interaction between the pore fluid, solid particles, and confining walls[21, 22], and has been employed to further prove the concept in this work and quantify the difference in the permeabilities and hydraulic conductivities in all the scenarios of interest.

Fig. 2 *An illustration of the core assembly with a half core and spacer for coreflood setup. Solid delayed acid generating materials and proppants were packed in between the two halves.*

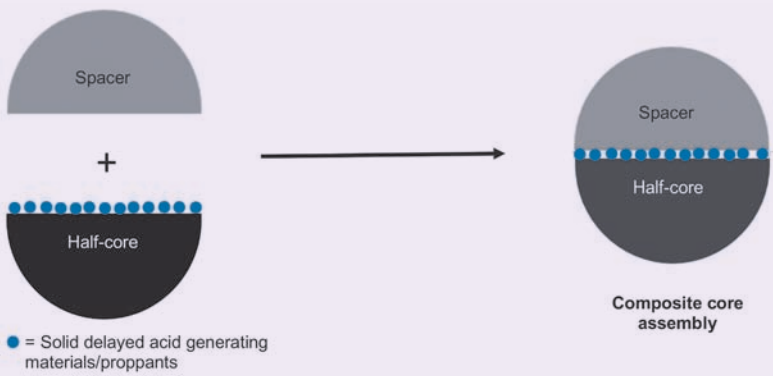

Results and Discussion

Surface Characterization

The texture and surface profile of the half core plug of the Eagle Ford outcrop samples were analyzed using a Nanovea PS50 profilometer before and after chemical treatment. The characterization allows for assessing the impact of the treatment on the surface characteristics and potentially on changes in the fracture flow properties.

Experiment #1. The first experiment was conducted with intermixed solid acids and 100 mesh sand particles. Before packing the chemicals onto the rock surface, the texture and surface profiles of the half core plug of Eagle Ford outcrop Sample I were characterized, Fig. 3. The sample surface was relatively uniform and the small-sized grooves generated during the core preparation process were measured to be around 1 µm to 5 µm, Fig. 3c and Fig. 3e.

Intermixed solid delayed acid generating materials (23.9 mg) and 100 mesh sand particles (31.9 mg) were packed on the surface of the half core Eagle Ford outcrop Sample I, Fig. 4a — same as Fig. 1a. The composite core assembly was treated at 180 °F with 2% KCl fluid flowing through the core assembly at a rate of 1 mL/min for 3 hours, and then the flow was shut-in overnight. After the core assembly was retrieved from the core holder, sand particles and undissolved solid delayed acid generating materials were found on the surface of the half core plug, Fig. 4b.

Figure 5 shows the surface profile of the retrieved half core after removing the sand particles. Figure 5a is the surface scan of one area, 15 mm × 10 mm

Fig. 3 *Surface profile of the Eagle Ford outcrop Sample I — general surface morphology analysis: (a) surface scan of 15 mm × 10 mm area (3D image, scan step in x, y axis was 5 µm); (b) magnified scan image of blue framed area in Fig. 3a (15 mm × 5 mm); (c) height profile along the red dashed line in Fig. 3b; (d) magnified scan image of blue framed area in Fig. 3b (4 mm × 5 mm); and (e) the height profile along the red dashed line in Fig. 3d.*

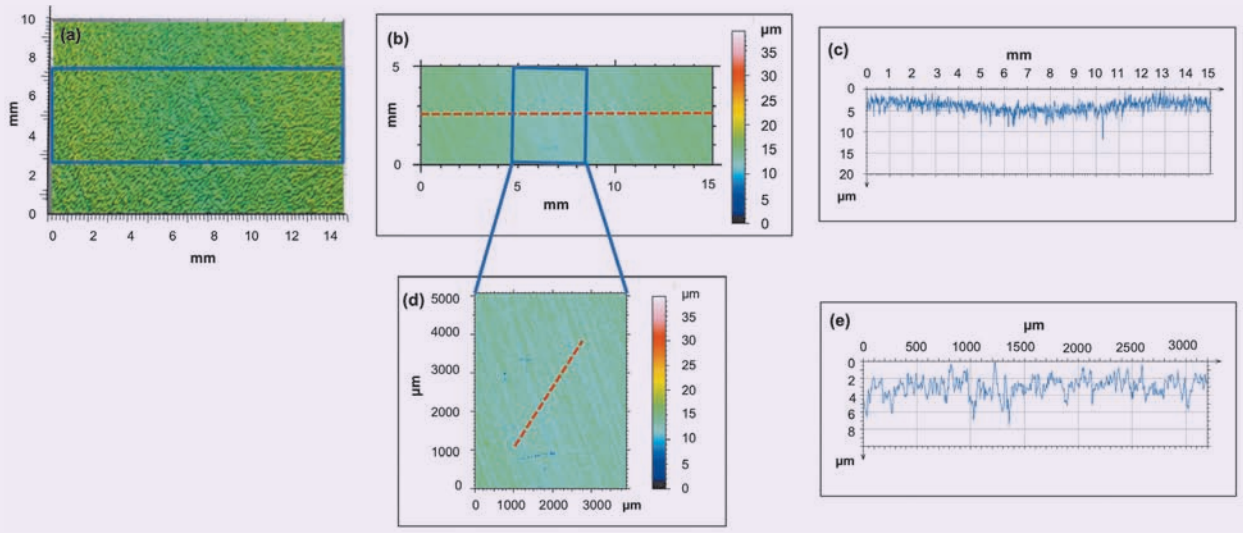

Fig. 4 *Photos of the Eagle Ford outcrop Sample I for Experiment #1: (a) surface of the half core packed with intermixed solid delayed acid generating materials and 100 mesh sand before being put into the coreflood setup; and (b) surface of the core plug after being retrieved from the core holder, and then sand and undissolved solid delayed acid generating materials were removed.*

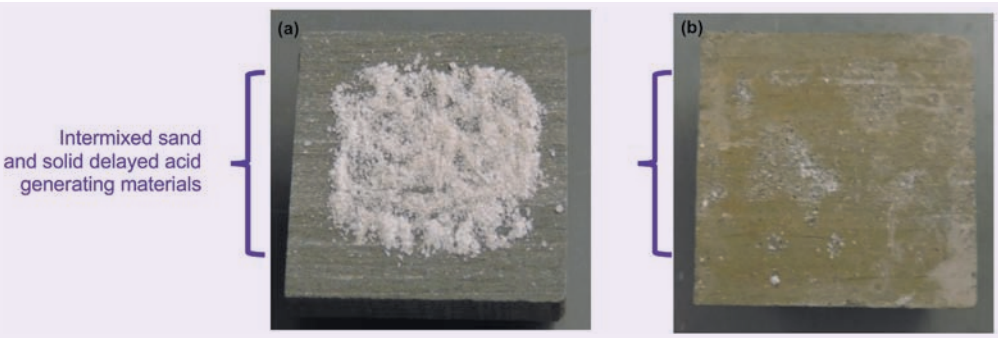

Fig. 5 *The surface profile of the Eagle Ford outcrop Sample I after treatment with mixed solid delayed acid generating materials and 100 mesh sand, and then the sand was removed — general surface morphology analysis: (a) Surface scan of a 15 mm × 10 mm area (3D image, scan step in x, y axis was 5 μm); (b) magnified scan image of the blue framed area in Fig. 5a (15 mm × 5 mm); (c) height profile along the red dashed line in Fig. 5b; (d) magnified scan image of the blue framed area in Fig. 5b (4 mm × 5 mm); and (e) the height profile along the red dashed line in Fig. 5d.*

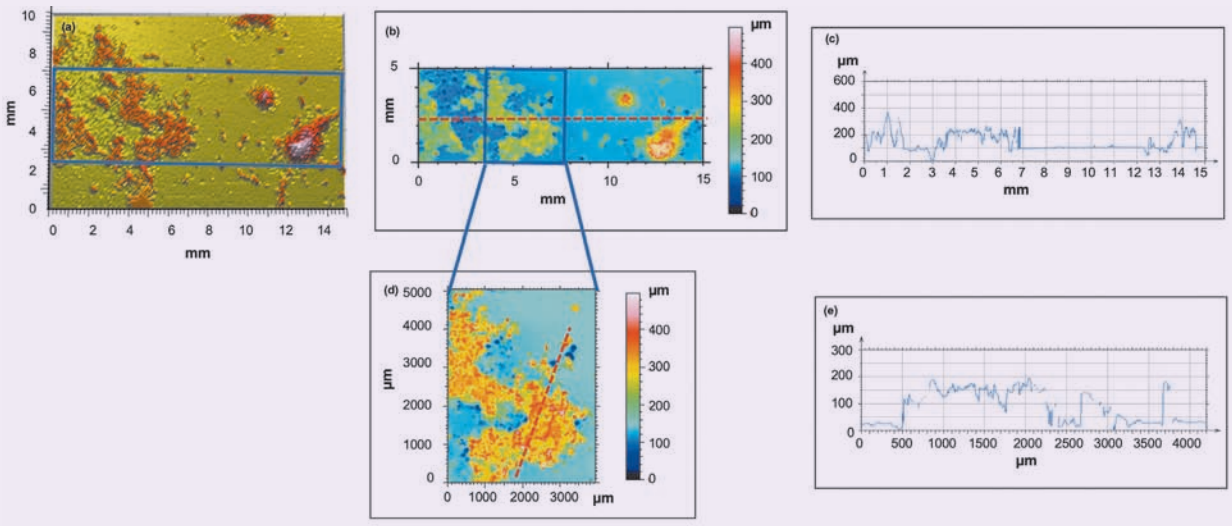

Fig. 6 *The surface profile of the Eagle Ford outcrop Sample I after treatment with mixed solid delayed acid generating materials and 100 mesh sand, then removed the surface undegraded solid delayed acid generating materials — general surface morphology analysis: (a) surface scan of 15 mm × 10 mm area (3D image, scan step in x, y axis was 5 μm); (b) magnified scan image of the blue framed area in Fig. 6a (15 mm × 5 mm); (c) height profile along the red dashed line in Fig. 6b; (d) magnified scan image of the blue framed area in Fig. 6b (5.5 mm × 5 mm); and (e) the height profile along the red dashed line in Fig. 6d.*

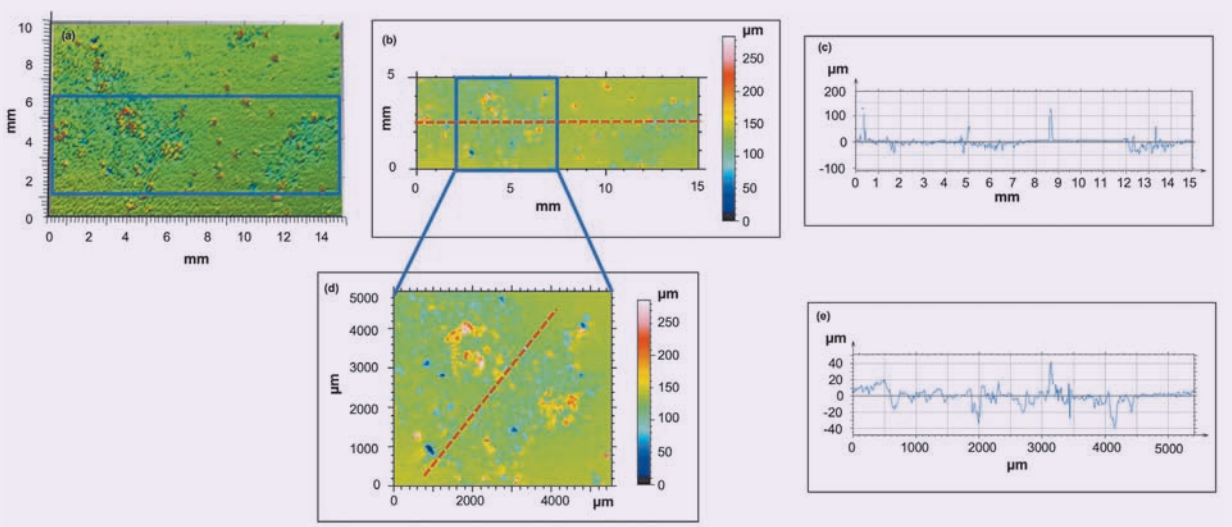

in size. Figure 5b is the magnified scan image of blue framed area in Fig. 5a (15 mm × 5 mm). Figure 5c is the height profile along the red dashed line in Fig. 5b. The height of the white solids coverage measured in Fig. 5c was approximately 100 μm to 150 μm, which was similar to the aperture size of the composite core assembly. Figure 5d is the magnified scan image of the blue framed area in Fig. 5b (4 mm × 5 mm). Figure 5e is the height profile along the red dashed line in Fig. 5d. Similar to Fig. 5c, the height of the white solids coverage measured in Fig. 5e was approximately 100 μm to 150 μm, which is in the same range of the aperture of the composite core assembly — ~150 μm, the diameter of the 100 mesh sand particles.

After the white solids were removed by blowing the sample with an air nozzle, the surface was discovered to be rougher than the original rock surface, with some deeper irregular shaped pockets being formed. The

Fig. 7 *The surface profile of the Eagle Ford outcrop Sample II — general surface morphology analysis: (a) surface scan of a 15 mm × 10 mm area (3D image, scan step in x, y axis was 5 µm); (b) magnified scan image of the blue framed area in Fig. 7a (15 mm × 5 mm); (c) height profile along the red dashed line in Fig. 7b; (d) magnified scan image of the blue framed area in Fig. 7b (3 mm × 5 mm); and (e) the height profile along the red dashed line in Fig. 7d.*

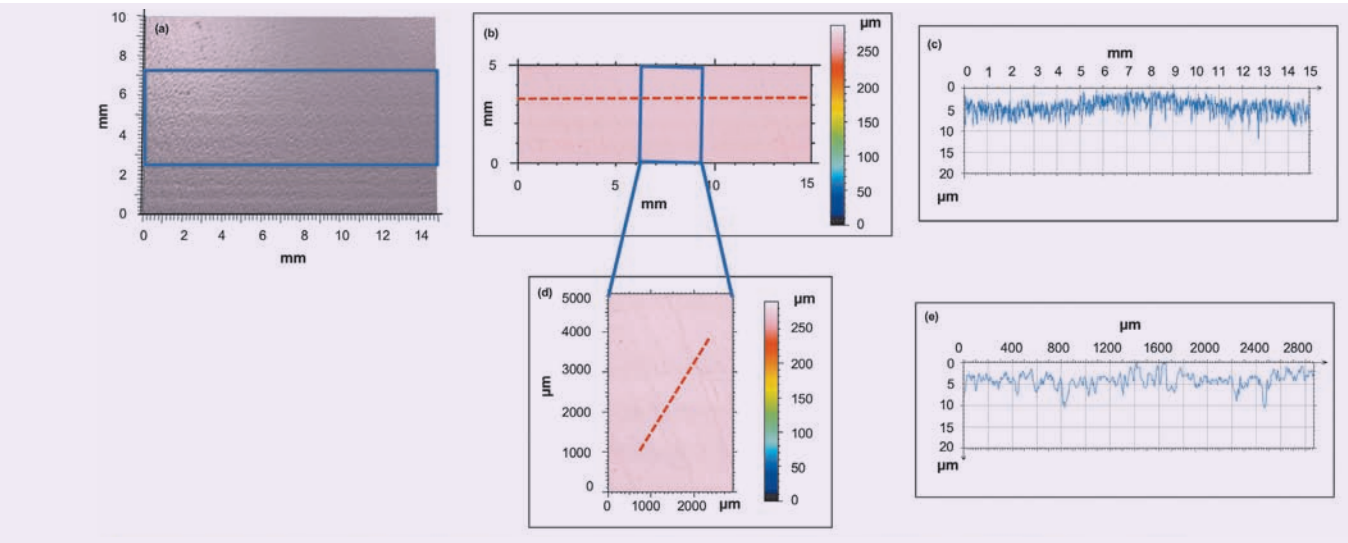

Fig. 8 *Photos of the Eagle Ford outcrop Sample II for Experiment #2: (a) Surface of the half core packed with solid delayed acid generating materials alone before putting into the coreflood setup; and (b) surface of the core plug after being retrieved from the coreflood experiment.*

same area as scanned in Fig. 5 was analyzed with the surface profilometer, Fig. 6. The depth of the irregular etched areas ranged from 5 µm to 40 µm.

Experiment #2. The second experiment was conducted with solid acids along with constant aqueous media exposure to further confirm the reaction between the degraded solid acids and calcite-rich rock sample. Before the chemicals were packed on the rock surface, the texture and surface profiles of the half core plug of the Eagle Ford outcrop Sample II, Fig. 7. Similar to the half core Plug I, the small-sized groves generated during the core preparation process were measured to be around 2 to 5 microns, Fig. 7c and Fig. 7e.

In this experiment, 51.9 mg of solid delayed acid generating materials were packed on the surface of the half core plug Sample II, Fig. 8a — same as Fig. 1b. The composite core assembly was treated at 180 °F with 2% KCl flowing through the core assembly at a constant and very low flow rate of 0.001 mL/min for 90 hours. After the core assembly was retrieved from the core holder, some undissolved solid delayed acid generating materials still remained on the surface of the half core plug. This might be due to the slow flow rate of the aqueous media, which prefers to flow around the two solid acid packed columns, resulting in the solid delayed acid generating materials not being exposed to enough water for full degradation. Figure 8b is the photo of the rock surface after the undissolved solid delayed acid generating materials were removed. Two rough patches with irregular shaped pockets were observed in the areas where the solid delayed acid generating materials were packed.

Figure 9 shows the surface profile of the retrieved half core after removing the undissolved solid delayed acid generating materials. The depth of the patched irregular pockets was determined to be from 10 µm

Fig. 9 *Surface profile of the Eagle Ford outcrop Sample II after treatment with solid delayed acid generating materials alone — general surface morphology analysis: (a) Surface scan of a 15 mm × 20 mm area (3D image, scan step in x, y axis was 5 µm); (b) magnified scan image of the blue framed area in Fig. 9a (3.5 mm × 5 mm); (c) height profile along the red dashed line in Fig. 9b; (d) a magnified scan image of the purple framed area in Fig. 9a (15 mm × 5 mm); and (e) the height profile along the red dashed line in Fig. 9d.*

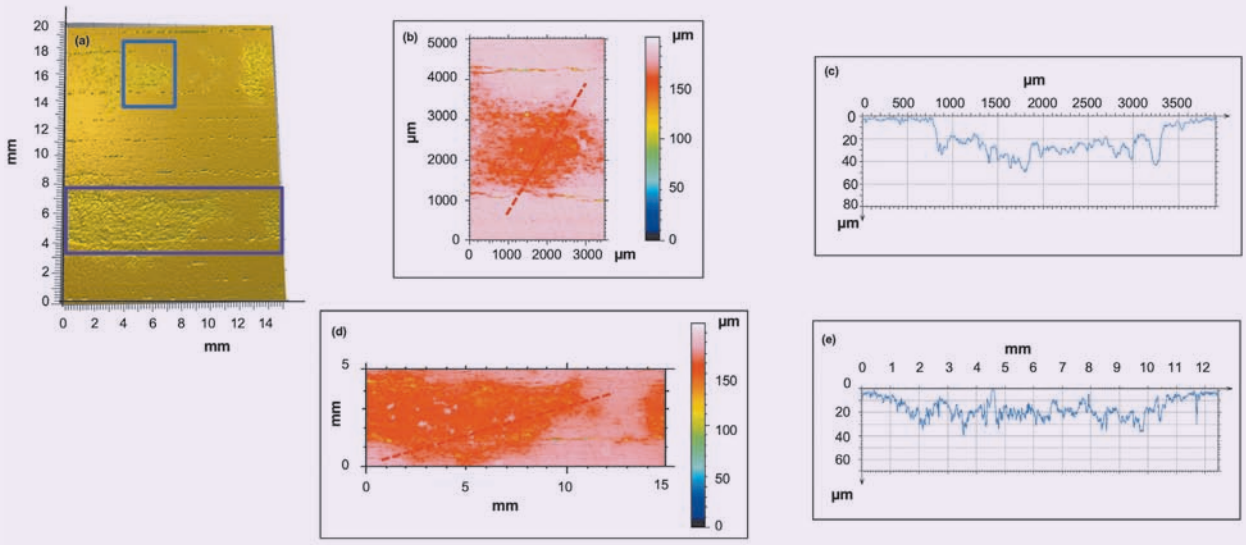

Fig. 10 *Surface profile of the Eagle Ford outcrop Sample III — general surface morphology analysis: (a) surface scan of a 15 mm × 10 mm area (3D image, scan step in x, y axis was 5 µm); (b) a magnified scan image of the blue framed area in Fig. 10a (15 mm × 5 mm); (c) height profile along the red dashed line in Fig. 10b; (d) a magnified scan image of the blue framed area in Fig. 10b (2 mm × 5 mm); and (e) the height profile along the red dashed line in Fig. 10d.*

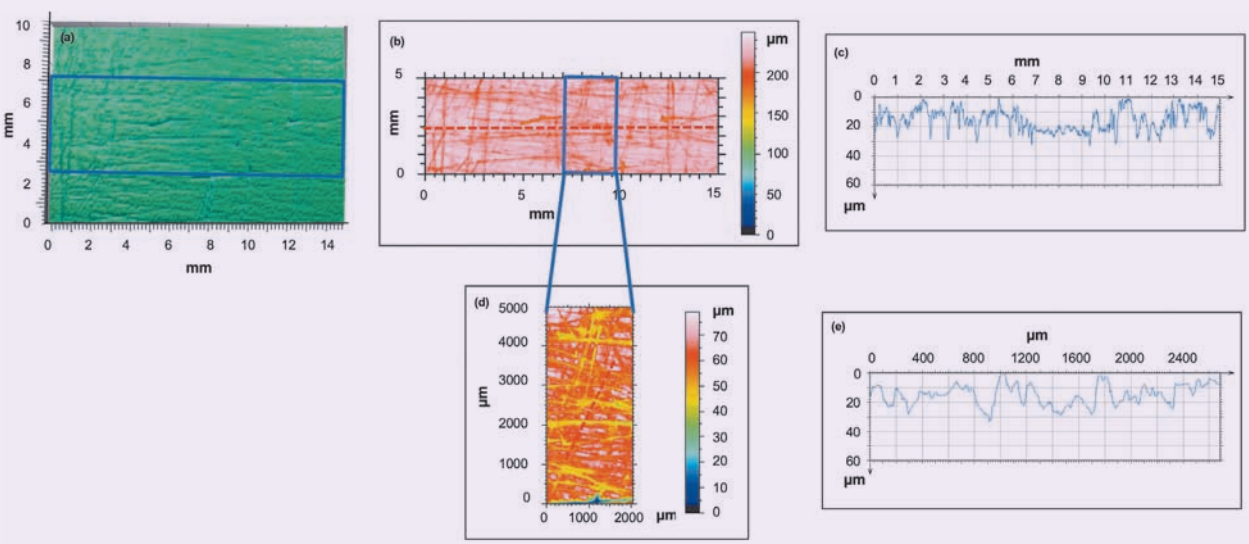

to 50 µm, which was in a similar range as observed in Experiment #1.

Experiment #3. The third experiment was conducted using solid delayed acid generating materials and 100 mesh sand at a temperature of 250 °F. Before packing the chemicals onto the rock surface, the rock surface was roughened a little with 60 grit sandpaper to reduce the particle's movement during the experiment.

Figure 10 shows the texture and surface profiles of the half core plug of the Eagle Ford outcrop Sample III before being packed with treatment chemicals. The groves generated during core preparation and further roughing process were measured to be around 10 to 30 microns, Fig. 10c and Fig. 10e, which were slightly deeper than the rocks used for Experiments #1 and #2.

In this experiment, 23.0 mg of solid delayed acid

Fig. 11 *Photos of the Eagle Ford outcrop Sample III for Experiment #3: (a) surface of the half core packed with solid delayed acid generating materials and 100 mesh sand in four patterns before being put into the coreflood setup; and (b) surface of the core plug after being retrieved from the coreflood experiment.*

Fig. 12 *Surface profile of the Eagle Ford outcrop Sample III after being treated with solid delayed acid generating materials and 100 mesh sand — general surface morphology analysis: (a) surface scan of a 15 mm × 20 mm area (3D image, scan step in x, y axis was 5 µm); (b) a magnified scan image of the blue framed area in Fig. 12a (5.5 mm × 15 mm); (c) the height profile along the red dashed line in Fig. 12b; (d) the magnified scan image of the purple framed area in Fig. 12a (3 mm × 5 mm); and (e) the height profile along the red dashed line in Fig. 12d.*

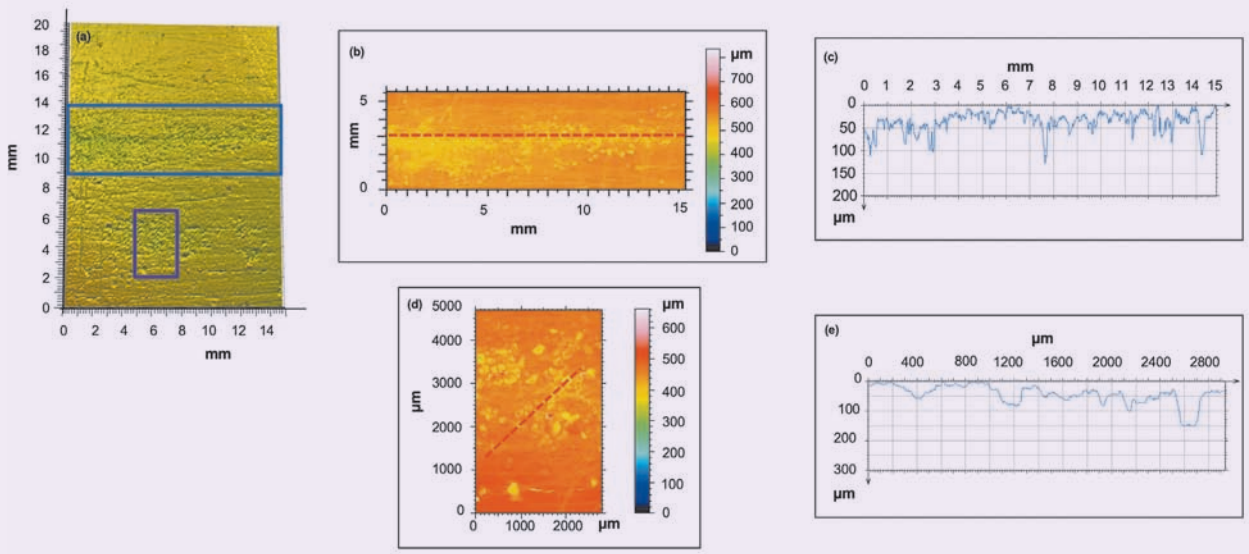

generating materials and 40.7 mg of sand were packed on the surface of the half core plug, Sample III, with four different patterns, Fig. 11a — same photo as Fig. 1c. The composite core assembly was treated at 250 °F with 2% KCl flowing through the core assembly at a constant flow rate of 0.02 mL/min for 48 hours. Effluents were collected with auto-collectors for further analysis. Then, the core assembly was removed from the coreflood setup. Figure 11b is the photo of the rock surface after the sand, and a small amount of undissolved solid delayed acid generating material was removed. Two rough irregular etched areas were observed where the solid acids were packed.

Figure 12 shows the surface profile of the retrieved half core after removing the sand and a small amount of undissolved solid delayed acid generating material. The depth of the etched irregular pockets was determined to be around 50 µm to 150 µm, which was deeper than what was observed in Experiments #1 and #2. This might be due to the faster reaction kinetics at higher temperatures.

Quantification of Dissolved Calcium Ions in the Effluents

Since the major mineral from the Eagle Ford cores was calcite (from the XRD results), the expected major changes of the ions are from Ca^{2+} in the effluents from the coreflood experiment that involves reactions between the acidic components from the degraded solid delayed acid generating materials and the formation rock. The concentrations of Ca^{2+} in each of the effluents from Experiment #3 were analyzed by ICP-OES.

The dissolved Ca^{2+} was calculated for each effluent

Table 1 *Calcium dissolution in the effluents in Experiment #3.*

Effluent #	Sample Volume (mL)	Ca^{2+} (mg/L)	Dissolved Ca^2 (mg)	Dissolved $CaCO_3$ (mg)
1	5	34.32	0.17	0.4
2	3.5	30.71	0.11	0.3
3	3.5	30.62	0.11	0.3
4	3.5	63.36	0.22	0.6
5	4	363.9	1.46	3.6
6	4	943.8	3.78	9.4
7	3.5	844.9	2.96	7.4
8	3.5	641.1	2.24	5.6
9	3.5	560.7	1.96	4.9
10	4	373.2	1.49	3.7
11	4	324.9	1.30	3.2
12	4	291.9	1.17	2.9
13	3.5	284.5	1.00	2.5
14	4	261.4	1.05	2.6
15	3.5	271.3	0.95	2.4
16	3.5	235.5	0.82	2.1

Table 2 *TOC analysis in the effluents in Experiment #3.*

Effluent #	Sample Volume (mL)	TOC (mg/L)	Total Dissolved Carbon in Solids Acids (mg)	Total Dissolved Solids Acids (mg)
1	5	0.0	0.00	0.0
2	3.5	26.3	0.09	0.2
3	3.5	34.9	0.12	0.3
4	3.5	55.3	0.19	0.5
5	4	190.7	0.76	1.9
6	4	641.3	2.57	6.4
7	3.5	549.4	1.92	4.8
8	3.5	351.4	1.23	3.1
9	3.5	282.2	0.99	2.5
10	4	107.2	0.43	1.1
11	4	85.8	0.34	0.9
12	4	77.0	0.31	0.8
13	3.5	84.8	0.30	0.7
14	4	73.8	0.30	0.7
15	3.5	87.6	0.31	0.8
16	3.5	77.1	0.27	0.7

sample and then converted to the amount of dissolved $CaCO_3$, Table 1. The accumulated dissolved calcite was calculated to be around 51.9 mg in this treatment.

Quantification of Dissolved Solid Acids

As mentioned earlier, since the resulting acidic components from the degraded solid delayed acid generating materials will react with the calcite from the rock sample, the analysis of the TOC in the effluents reflected the amount of the degraded/dissolved solid acids. The concentration of TOC in each effluent from Experiment #3 was analyzed using a Shimadzu TOC analyzer, Table 2. A calibration curve with concentrations of 0.00 ppm, 0.1 ppm, 1 ppm, 10 ppm, and 100 ppm carbon was conducted before the sample testing. Assuming that the majority of dissolved organic carbon was from the degraded solid acid, the dissolved solid acid in each effluent sample could be calculated. The total amount of the degraded solid delayed acid generating materials was calculated to be around 25.3 mg, which is very close to the entire amount of solid acids packed in the core assembly.

Results from the above three experiments have demonstrated that the solid delayed acid generating materials were able to create voids or dimples on the flow path of the microfractures by their degradation under elevated temperatures, and the chemical reaction between the generated weak acid and the calcite-rich formation, which likely enhances the permeability of microfractures. Consequently, since the size of the aperture between the half core and the spacer is relatively large — approximately 150 µm, differential pressure across the composite core assembly was not able to be detected accurately because of the pressure gauge's detection limit.

Numerical modeling was further conducted to quantify the conductivity changes due to the placement of small-sized proppants in the microfractures and the etching effect from the interactions of the acid generating material with the fracture faces.

Numerical Modeling

Simulations using the DEM-LBM coupled approach for different scenarios were conducted to further demonstrate the feasibility of the proposed conceptual approach. The basic concept of LBM, and verification of its accuracy in modeling small-scale fluid flow problems, can be found in many publications[23-25]. The DEM is a micromechanics computational method originated by Cundall (1971)[26] and is extended by Cundall and Strack (1979)[27]. Since then, the DEM has been widely applied as an interdisciplinary modeling tool in many scientific and engineering areas. The verification of the coupling of the DEM and LBM to model fluid-particle interaction and fluid flow in porous media can be found in Han and Cundall (2011, 2013)[21, 22].

In this study, three general scenarios are modeled with the DEM-LBM simulations: (1) fluid flow in a rough fracture without proppant, Fig. 13a; (2) fluid flow in a fracture with microproppants, Fig. 13b; and (3) fluid flow in a fracture supported by small-sized proppants and generated voids on the fracture walls, Fig. 13c.

More specifically, the aperture of the fracture is assumed to be 1 µm and 5 µm without proppant (Case 1 and 2 in Table 3, the base case) and 150 µm with the support of proppants — similar to the aperture size tested in the laboratory experiment (Cases 3 to 14 in Table 3). The fracture walls are assumed to be perpendicular to the x-direction, Fig. 14. It is further assumed that a single layer of proppants are placed in the fracture; the proppant particles are distributed uniformly inside the fracture with a particle-to-particle gap of gap_x in the x-direction (which is also the fluid flow direction) and gap_z in the z-direction. The etched depth in the fracture walls can vary from 50 µm to 150 µm. As tabulated in Table 3, the permeability values of the 13 cases are estimated using DEM-LBM simulations.

Simulation results for Cases 3 to 8 indicate that with proppant support, the fracture permeability can be increased by tens to hundreds of times, depending on the gaps between the proppant particles. The permeability of the proppant supported fracture can be further enhanced by the voids created by acid erosion, as shown by results from Cases 9 to 14.

Note that the fluid transport capacity of a fracture is not only related to the permeability of material inside the fracture, but also affected by the fracture aperture. The product of a facture aperture and its permeability is called fracture conductivity. The fracture conductivities of all the simulated cases in Table 3 are computed and provided in the last column. As can be seen, the fracture conductivity in all proppant supported cases

Fig. 13 *Modeled scenarios in the DEM-LBM coupling simulations.*

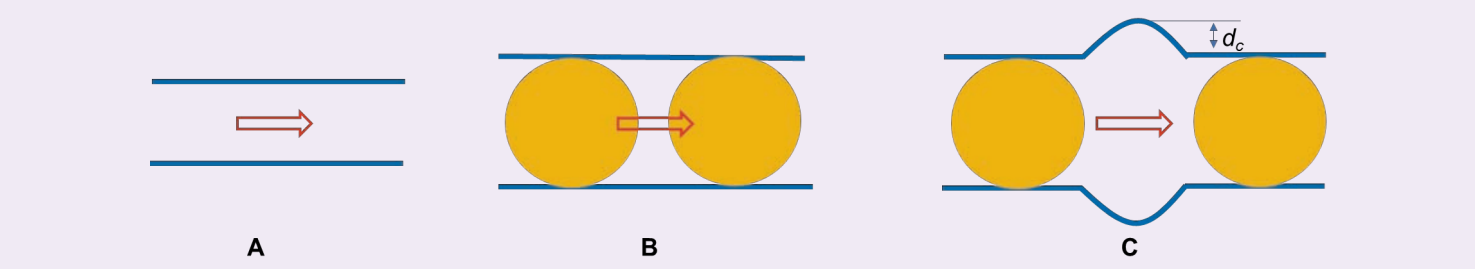

Table 3 *Permeabilities of various scenarios measured by the DEM-LBM simulations (d = 150 μm).*

Case	Fracture Aperture (μm)	Particle Gaps gap_x:gap_z (μm)	Etched Depth, d_c (μm)	Fracture Permeability (md)	Fracture Conductivity (md · ft)
1	1	—	—	8.36×10^1	0.0003
2	5	—	—	2.09×10^3	0.03
3	150	0:0	—	1.90×10^4	9.35
4	150	37.5:37.5	—	9.42×10^4	46.25
5	150	75:75	—	2.87×10^5	141.04
6	150	150:150	—	6.00×10^5	295.20
7	150	75:0	—	2.75×10^4	13.55
8	150	150:0	—	3.41×10^4	16.79
9	150	75:0	50	4.81×10^4	23.65
10	150	75:0	100	4.81×10^4	23.65
11	150	75:0	150	4.86×10^4	23.88
12	150	150:0	50	6.03×10^4	29.65
13	150	150:0	100	6.03×10^4	29.68
14	150	150:0	150	6.10×10^4	30.01

Fig. 14 *Monolayered proppant particles inside a microfracture.*

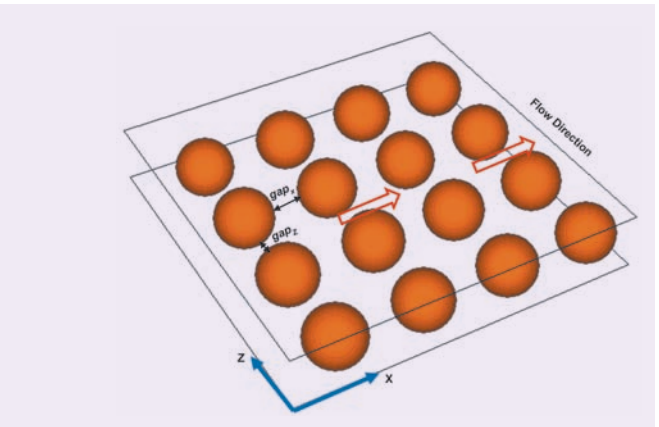

is increased by hundreds to thousands of times in comparison to that of the unsupported fracture.

In summary, our simulation results clearly indicate that the proposed conceptual approach of an improved hydraulic fracturing treatment can significantly increase the flow conductivity of microfractures, and thereby enhance well productivity.

Conclusions

As the bottleneck for hydrocarbon flow from the reservoir to a production well is the low permeability of the formation for unconventional reservoirs, enhancement of the formation permeability is critical for further improving well productivity after the hydraulic fracturing process whose major purpose is to increase the stimulated reservoir volume. The microfractures in a reservoir, as the major contributor to the formation permeability, tend to close during the production. Therefore, to minimize the closure of these fractures during production has many important implications to the hydrocarbon production from unconventional reservoirs.

This work proposes a conceptual approach of an improved hydraulic fracturing treatment to enhance well productivity by combining the advantages of two key elements: (1) the use of microproppants to keep open the natural and induced microfractures during production, and (2) the dissolution effects on increasing pore or aperture sizes using a mixture of the delayed acid generating materials along with microproppants.

The feasibility of the proposed approach is demonstrated by a series of the proof-of-concept laboratory coreflood experiments and numerical modeling results. Experiment results demonstrated that solid delayed acid generating materials were able to create voids or dimples on the flow path of microfractures by their degradation under elevated temperature, and the chemical reaction between the generated weak acid and the calcite-rich formation, which likely enhances the permeability of microfractures. Simulation results also show that the proposed conceptual approach can significantly increase and maintain flow conductivity of microfractures, thereby enhancing well productivity.

Acknowledgments

The authors would like to thank the management of Aramco Services Company for their support and permission to publish this article. The authors would also like to give special thanks to Nam Mai for assisting with the coreflood experiment testing.

References

1. McLeod, H.O.: "Matrix Acidizing," *Journal of Petroleum Technology*, Vol. 36, Issue 12, December 1984, pp. 2055-2069.
2. McLeod, H.O.: "Significant Factors for Successful Matrix Acidizing," SPE paper 20155, presented at the SPE Centennial Symposium at New Mexico Tech, Socorro, New Mexico, October 16-19, 1989.
3. Olsen, T.N. and Karr IV, G.K.: "Treatment Optimization of Acid Fracturing in Carbonate Formations," SPE paper 15165, presented at the SPE Rocky Mountain Regional Meeting, Billings, Montana, May 19-21, 1986.
4. Bybee, K.: "Acid Fracturing a Carbonate Reservoir," *Journal of Petroleum Technology*, Vol. 56, Issue 7, July 2004, pp. 49-52.
5. Nelson, P.H.: "Pore Throat Sizes in Sandstones, Tight Sandstones, and Shales," *AAPG Bulletin*, Vol. 93, Issue 3, March 2009, pp. 329-340.
6. Sondergeld, C.H., Ambrose, R.J., Rai, C.S. and Moncrieff, J.: "Microstructural Studies of Gas Shales," SPE paper 131771, presented at the SPE Unconventional Gas Conference, Pittsburgh, Pennsylvania, February 23-25, 2010.
7. Loucks, R.G., Reed, R.M., Ruppel, S.C. and Hammes, U.: "Spectrum of Pore Types and Networks in Mudrocks and a Descriptive Classification for Matrix-related Mudrock Pores," *AAPG Bulletin*, Vol. 96, Issue 6, June 2012, pp. 1071-1098.
8. Baihly, J.D., Altman, R.M., Malpani, R. and Luo, F.: "Shale Gas Production Decline Trend Comparison over Time and Basins," SPE paper 135555, presented at the SPE Annual Technical Conference and Exhibition, Florence, Italy, September 19-22, 2010.
9. Wang, H.: "What Factors Control Shale Gas Production and Production Decline Trend in Fractured Systems: A Comprehensive Analysis and Investigation," *SPE Journal*, Vol. 22, Issue 2, April 2017, pp. 562-581.
10. Dahl, J., Nguyen, P., Dusterhoft, R., Calvin, J., et al.: "Application of Microproppant to Enhance Well Production in Unconventional Reservoirs: Laboratory and Field Results," SPE paper 174060, presented at the SPE Western Regional Meeting, Garden Grove, California, April 27-30, 2015.
11. Dahl, J., Calvin, J., Siddiqui, S., Nguyen, P., et al.: "Application of Microproppant in Liquid-Rich, Unconventional Reservoirs to Improve Well Production: Laboratory Results, Field Results, and Numerical Simulations," SPE paper 177663, presented at the Abu Dhabi International Petroleum Exhibition and Conference, Abu Dhabi, UAE, November 9-12, 2015.
12. Cheng, Y.: "Impact of Water Dynamics in Fractures on the Performance of Hydraulically Fractured Wells in Gas-Shale Reservoirs," *Journal of Canadian Petroleum Technology*, Vol. 51, Issue 2, March 2012, pp. 143-151.
13. King, G.E.: "Hydraulic Fracturing 101: What Every Representative, Environmentalist, Regulator, Reporter, Investor, University Researcher Neighbor and Engineer Should Know About Estimating Fracturing Risk," *Journal of Petroleum Technology*, Vol. 64, Issue 4, April 2012, pp. 34-42.
14. Soeder, D.J.: *Unconventional: The Development of Natural Gas from the Marcellus Shale*, 1st edition, Boulder, Colorado: Geological Society of America, 2017, 155 p.
15. Bennion, D.B. and Thomas, F.B.: "Formation Damage Issues Impacting the Productivity of Low Permeability, Low Initial Water Saturation Gas Producing Formations," *Journal of Energy Resources Technology*, Vol. 127, Issue 3, April 2005, pp. 240-247.
16. Roychaudhuri, B., Tsotsis, T.T. and Jessen, K.: "An Experimental and Numerical Investigation of Spontaneous Imbibition in Gas Shales," SPE paper 147652, presented at the SPE Annual Technical Conference and Exhibition, Denver, Colorado, October 30-November 2, 2011.
17. Liang, F., Lai, B., Zhang, J., Liu, H-H., et al.: "An Experimental Study on Interactions between Imbibed Fracturing Fluid and Organic-Rich Tight Carbonate Source Rocks," *SPE Journal*, Vol. 23, Issue 6, December 2018, pp. 2133-2146.
18. Liang, F., Zhang, J., Liu, H-H. and Bartko, K.M.: "Multiscale Experimental Studies on Interactions between Aqueous-based Fracturing Fluids and Tight Organic-rich Carbonate Source Rocks," *SPE Reservoir Evaluation & Engineering*, Vol. 22, Issue 2, May 2019, pp. 402-417.
19. Wu, W. and Sharma, M.M.: "Acid Fracturing in Shales: Effect of Dilute Acid on Properties and Pore Structure of Shale," *SPE Production & Operations*, Vol. 32, Issue 1, February 2017, pp. 51-63.
20. Wu, W., Russell, R. and Sharma, M.M.: "An Experimental Method to Study the Impact of Fracturing Fluids on Fracture Conductivity in Heterogeneous Shales," URTEC paper 2669936, presented at the Unconventional Resources Technology Conference, Austin, Texas, July 24-26, 2017.
21. Han, Y. and Cundall, P.A.: "Resolution Sensitivity of Momentum Exchange and Immersed Boundary Methods for Solid Fluid Interaction in the Lattice Boltzmann Method," *International Journal for Numerical Methods in Fluids*, Vol. 67, Issue 3, September 2011, pp. 314-327.
22. Han, Y. and Cundall, P.A.: "LBM-DEM Modeling of Fluid-Solid Interaction in Porous Media," *International Journal for Numerical and Analytical Methods in Geomechanics*, Vol. 37, Issue 10, June 2013, pp. 1391-1407.
23. Succi, S., Foti, E. and Higuera, F.: "Three-Dimensional Flows in Complex Geometries with the Lattice Boltzmann Method," *Europhysics Letters*, Vol. 10, Issue 5, 1989, p. 433.
24. Kutay, M.E., Aydilek, A.H. and Masad, E.: "Laboratory Validation of Lattice Boltzmann Method for Modeling Pore-scale Flow in Granular Materials," *Computers and Geotechnics*, Vol. 33, Issue 8, December 2006, pp. 381-395.
25. Han, Y. and Cundall, P.A.: "Coupling the Lattice Boltzmann Method with PFC. Part 1: Verification of LBM as a Hydrodynamic Code," *Proceedings of the 2nd International FLAC/DEM Symposium*, February 2011, pp. 649-660.
26. Cundall, P.A.: "A Computer Model for Simulating Progressive, Large-Scale Movement in Blocky Rock System," *Proceedings of the International Symposium on Rock Mechanics*, Vol. 2, 1971, pp. 2-8.
27. Cundall, P.A. and Strack, O.D.L.: "A Discrete Numerical Model for Granular Assemblies," *Geotechnique*, Vol. 29, Issue 1, March 1979, pp. 47-65.

About the Authors

Dr. Feng Liang

Ph.D. in Organic Chemistry, Rice University

Dr. Feng Liang is currently a Research Science Specialist at the Aramco Services Company, Aramco Research Center-Houston. She has now been with the company for over five years.

Prior to joining the Aramco Research Center, Feng was a Principal Scientist at Halliburton for nearly eight years. Her research interests are the new materials and product development in fracturing fluid, advanced fluid additives, waterless fracturing technologies, bio-degradable diversion materials, sand control products, cement additives and nanomaterials reinforced elastomers.

Feng is a contributor to many patents and technical papers. She holds over 40 issued U.S. patents and 30 additional published patent applications. Feng is the author and coauthor of more than 60 technical papers, with a few in very high impact factor journals such as the *Journal of the American Chemical Society* and also *Nano Letters*. She has also coauthored two book chapters as well. Feng's publications have received over 3,000 citations.

She is a member of the Society of Petroleum Engineers (SPE) and the American Chemical Society (ACS). Feng received the 2017 SPE Production and Operations Award for the Gulf Coast North American Region. She also received the 2017 Effective Publication Award from Saudi Aramco's Exploration and Petroleum Engineering Center – Advanced Research Center (EXPEC ARC).

Feng received her Ph.D. degree in Organic Chemistry from Rice University, Houston, TX.

Dr. Yanhui Han

Ph.D. in Computational Geomechanics, University of Minnesota

Dr. Yanhui Han is a Petroleum Engineering Specialist at the Aramco Research Center-Houston. His research interests are computational geomechanics related research, development, and applications. Yanhui's previous positions include the primary FLAC Developer and Geomechanics Consultant at Itasca Consulting Group for 10 years, Principal Technical Professional at Halliburton for 1 year and Production Technologist at Shell for 2 years.

Yanhui is the recipient of the 2013 N.G.W. Cook Award from the American Rock Mechanics Association. He is also a Registered Professional Engineer in the United States. Yanhui is currently serving as an Associate Editor for the *Journal of Petroleum Science and Engineering*.

He received his Ph.D. degree in Computational Geomechanics from the University of Minnesota, Minneapolis, MN

Dr. Hui-Hai Liu

Ph.D. in Soil Physics, Auburn University

Dr. Hui-Hai Liu is a Senior Petroleum Engineering Consultant at the Aramco Research Center in Houston. Before joining Aramco in 2014, he was a Staff Scientist and the Head of the Hydrogeology and Reservoir Dynamics Department at Lawrence Berkeley National Laboratory (LBNL) and an Adjunct Distinguished Professor at the China University of Mining and Technology in Beijing.

Hui-Hai has more than 25 years of experience in developing models for subsurface fluid flow and coupled hydromechanical processes, and in applying them to shale gas recovery, carbon dioxide geological sequestration, enhanced coalbed methane recovery, geological disposal of high-level nuclear waste, and groundwater flow and transport. Since joining Aramco, he has focused on research activities related to reservoir property measurement and production prediction for unconventional reservoirs.

Hui-Hai's work has been documented in one book, more than 130 peer-reviewed journal articles, and numerous patents. He has received several awards for his research and achievements, including the Society of Petroleum Engineers (SPE) Distinguished Membership, the LBNL Director's Award for Exceptional Achievement, Fellowship of the Geological Society of America, and the Emil Truog Research Award from the Soil Science Society of America.

Hui-Hai received his B.S. in Mechanical Engineering from Beijing Agricultural Engineering University, Beijing, China, his M.S. degree in Applied Fluid Mechanics from Huazhong University of Science and Technology, Wuhan, China, and a Ph.D. degree in Soil Physics (Multiphase Flow in Porous Media) from Auburn University, Auburn, AL.

Dr. Rajesh K. Saini

Ph.D. in Organic Chemistry, Kurukshetra University

Dr. Rajesh K. Saini is a Research Science Specialist in the Production Technology Team at the Aramco Research Center-Houston. He has more than 22 years of experience in the oil and gas industry, and chemical research. Rajesh is a subject matter expert in oil field stimulation, production and operations technology. He specializes in product development, scaling up, intellectual property, sales and commercialization of new products/processes for hydraulic fracturing, sand control, acidizing, production technology, oil field chemicals, and water conformance. Prior to joining Aramco in 2017, Rajesh played critical roles at Halliburton, Weatherford, and Lubrizol in the capacity from Research Scientist to R&D Manager.

He has served as a technical reviewer for major journals, including the *Journal of American Chemical Society*, and the *Journal of Organic Chemistry and Organic Letters*. Rajesh is a Technical Editor for the Society of Petroleum Engineers (SPE) *Production and Operations Journal*. He is serving on the SPE Annual Technical Conference and Exhibition (ATCE) well stimulation committee. Rajesh holds 54 U.S. patents, 21 U.S. patent applications, and has published one book chapter and 48 peer-reviewed journal articles.

He served as the Distinguish Lecture's Program Chair and Director of the SPE-Southwest Oklahoma Section during 2009-2012. Rajesh received the Maximizing Value-Added Performance (MVP) award at Halliburton for developing environmental fracturing fluid (CleanStim®) and breaker for AquaLinear® fluid. In 2018, he was also awarded the SPE Gulf Coast Regional award for Production and Operations.

Rajesh received his MBA from Oklahoma State University, Stillwater, OK, and his Ph.D. degree in Organic Chemistry from Kurukshetra University, Haryana, India. He was a postdoctoral fellow at Rice University working with Prof. W.E. Billups and Richard E. Smalley (Nobel Laureate in Chemistry).

Dr. Jose I. Rueda

Ph.D. in Petroleum Engineering, Texas A&M University

Dr. Jose I. Rueda joined Saudi Aramco in November 2016, and is the Head of the Technical Support Unit of the Well Completion & Production Engineering Department for Unconventional Resources in Dhahran, Saudi Arabia. During his extensive 25+ year career, Jose previously worked for Ecopetrol, Schlumberger, and BP, and was primarily involved in applied research projects related to hydraulic fracturing for both conventional and unconventional reservoirs. His experience includes managing hydraulic fracturing projects in several countries, including Colombia, Venezuela, USA, Russia, Algeria, U.K., Mexico, and Saudi Arabia.

Jose's current research interests in unconventional resources include maximizing effective stimulated reservoir volumes, cluster efficiency, geomechanics of hydraulic fracturing, optimum fracture design, and rate transient analysis.

He has authored and coauthored more than 30 technical papers.

Jose received his B.S. degree in Petroleum Engineering from Universidad Industrial de Santander, Colombia. He also received an M.S. degree and a Ph.D. degree in Petroleum Engineering, both from Texas A&M University, College Station, TX.

Jose is an active member of the Society of Petroleum Engineers (SPE).

A New Mathematical Formulation for Estimating Flow Capacity and Phase Mobility in Oil-Water Segregated Flow Systems

Dr. Hasan A. Nooruddin and Dr. N.M. Anisur Rahman

Abstract / A new analytical procedure is introduced for the interpretation of pressure transient data in oil producers with pronounced water production. The new mathematical model is applicable to flow conditions where segregated flow dominates the displacement process in the reservoir. Here, formation flow capacity and individual magnitudes of oil- and water-phase mobility are also determined, allowing accurate reservoir characterization under such complex flow conditions.

Segregated flow is very common in natural porous rocks and is characterized by a sharp interface between oil and water. Therefore, our new mathematical model mimics the dynamics of this flow mechanism by taking into consideration the individual contributions of oil and water from each reservoir zone. This novel mathematical model is utilized to extract formation flow capacity and mobility for both phases. An average fluid saturation can also be determined with a reasonable accuracy.

The reservoir system in hand is represented by a two-layer model with no crossflow between the different zones in the reservoir. Because of gravity effects, oil is produced from the top layer while water is produced from the bottom one. Each reservoir layer has its own distinct static and dynamic properties, such as porosity, permeability, thickness, and petrophysical properties. A case study based on synthetic reservoir data is presented to demonstrate the application of the mathematical model in characterizing formation rocks. It is observed that conventional well testing methods could produce inaccurate results when applied to reservoir systems influenced by segregated flow. Using the new model, a correction factor is derived to estimate absolute permeability values from the conventional well testing analysis, producing a one-to-one transformation between dispersed and segregated flow.

The conventional way of interpreting pressure transient data for two-phase flow displacements under segregated conditions is based on an equivalent single-phase flow model that might produce inaccurate results and invalid estimates of flow capacity and phase mobility. Our new approach, therefore, is more representative for the system under consideration and captures the flow mechanism more robustly.

Introduction

Pressure transient analysis (PTA) can be viewed as an experiment, which is conducted in the field to acquire certain information about the productivity or injectivity of a tested well and to characterize the in situ properties of the near wellbore reservoir region. Properties derived from well testing are very important in characterizing reservoir formations and understanding their dynamic behavior under in situ conditions. In typical well testing operations, pressure responses and flow rates are measured as a function of time, commonly using high resolution gauges, either from the surface or downhole. These responses are then analyzed and interpreted by identifying flow regimes using appropriate well and reservoir models. Well testing today has become sophisticated with many numerical and analytical approaches.

Under certain multiphase flow conditions, gravity forces dominate the displacement process motivating fluids to segregate from each other, so that heavier fluids slump down to the base of the reservoir and lighter fluids rise up. The segregated flow is considered as one of the most frequently encountered flow mechanisms in nature, and is characterized by a sharp interface between oil and water phases[1]. This flow mechanism is governed by some key geometric parameters of the formation, i.e., reservoir thickness and length; petrophysical parameters, i.e., reservoir vertical and horizontal permeability; in addition to other parameters related to in situ fluids, i.e., density difference and components of average fluid velocity in the vertical and horizontal directions.

The most common methodology in the industry to analyze PTA for multiphase use is the method introduced by Perrine (1956)[2]. His approach is based on an equivalent single-phase flow model that replaces the individual, single-phase properties with some effective total properties representing the multiphase systems[2].

A key assumption is that both capillary and gravity forces are ignored. In addition, saturation gradients are considered negligible[3, 4].

Chu et al. (1986)[5] investigated the Perrine method using a 2D numerical model applicable to oil and water systems. They showed that the Perrine method could be used to interpret pressure transient data for simultaneous production of oil and water when saturation gradients are significant in the vertical direction only. In addition, the estimated individual magnitudes of phase mobility represent thickness averaged magnitudes of mobility in the investigated zone. In case of nonuniform saturation gradients in the horizontal direction, the Perrine method may give unreliable estimates for the individual magnitudes of phase mobility. The magnitude of total mobility can be determined with reasonable accuracy.

Sharp interfaces between oil and water in partially flooded regions are repeatedly observed from conventional log analysis, saturation monitoring and production logging tools. Analyzing pressure transient data under segregated flow conditions using conventional multiphase flow methods that are currently in use in the industry may not be adequate, and could result in misleading magnitudes of formation flow capacity and individual phase mobility, and skin factors. To overcome this problem, a new mathematical model is introduced, where segregated flow is derived analytically. The new methodology provides better estimation of the formation flow capacity in addition to the oil and water phase mobility.

A Closer Look into Segregated Flow

Segregated flow is considered as "the most common flooding conditions encountered in nature"[1]. Under this flooding condition, gravity dominates the displacement process and activates the crossflow of fluids, giving that a high degree of pressure equilibrium exists across the entire thickness of a reservoir. The interface between oil and water is sharp, and can be represented with a step function, assuming that the dynamic capillary transition zone is negligible as compared to the total reservoir thickness. As pointed out by Dake (2001)[1], this assumption is valid for most waterflood conditions and has been confirmed theoretically and experimentally. The sharp interface between oil and water at their boundary is observed usually from in situ production and formation analysis logs.

Many researchers have extensively investigated the segregated flow mechanism[6-9]. For example, Dietz (1953)[10] presented a theoretical analysis of the displacement stability in dip reservoirs. He introduced two dimensionless numbers to indicate whether a displacement process is stable or not: the dimensionless gravity number, G, and the end-point mobility ratio, M_R. Dietz (1953)[10] showed that stable displacements take place when the angle measured between the main direction of the flow and the interface of the fluids stay constant. This condition is satisfied when $G > (M_R - 1)$ for $M_R > 1$. Nevertheless, the displacement process is found to be unconditionally stable when $M_R \leq 1$.

Another dimensionless number, Eqn. 1, is frequently used to identify segregated flow by virtue of vertical equilibrium[6, 11-13]:

$$R_L = \frac{L}{H}\sqrt{\frac{k_v}{k_h}} \quad (1)$$

The likelihood of having segregated flow in a given system increases for large values of R_L. Some numerical simulation studies have indicated that segregated flow would most likely occur for $R_L \geq 5$, Waggoner et al. (1991)[14].

Elements of the Analytical Model

In this section, we present key elements and assumptions of the analytical solution. The model assumes two-phase flow in radial coordinates for a vertical well that fully penetrates a reservoir rock with uniform properties in the horizontal direction. In the vertical direction, however, the model assumes a two-layer system with nonuniform properties. Fluids are immiscible and slightly compressible with constant compressibility.

Figure 1 shows a schematic of the segregated two-phase flow of oil and water in a well. Under this flow condition, oil is produced separately from a clearly distinguished zone with distinct static and dynamic properties — thickness, permeability, porosity, total compressibility, residual water saturation and relative permeability of oil at residual water saturation. Similarly, for water, only water is produced from a well-defined zone, located at the bottom of the reservoir with distinct static and dynamic properties — thickness, permeability, porosity, total compressibility, residual oil saturation and relative permeability of water at residual oil saturation. Each zone has its own porosity, permeability, total compressibility and residual saturations. After leaving the sandface, oil and water mix in the wellbore. The mixture is produced and measured at the surface, where the percentage of water in the mixture is determined, which is most commonly referred to as the water cut ratio.

Once oil and water exit the sandface and enter the wellbore, the flowing bottom-hole pressure (FBHP) of both phases is considered to be the same at a given depth inside the wellbore. In normal practices, the FBHP is measured at a gauge depth inside the wellbore, at which the pressure of both the oil and water phases are considered identical. Nooruddin and Rahman (2018)[15] have provided the main equations for infinite acting reservoirs. The governing equations are presented in Appendix A.

The thicknesses of the oil zone, h_o, and water zone, h_w, are required to be known *a priori* for the calculations of the pressure responses, using the segregated flow model. In the presence of valid production logs, such information can be estimated with reasonable accuracy. In most cases, production logs are absent, and only the total reservoir thickness, h, is available. Fortunately, under segregated flow conditions, the thicknesses of the oil and water zones can be estimated from the definition of the fractional flow of water, f_w, by utilizing the individual phase production rates,

Fig. 1 *A schematic of the segregated two-phase flow conditions around a fully penetrating vertical well.*

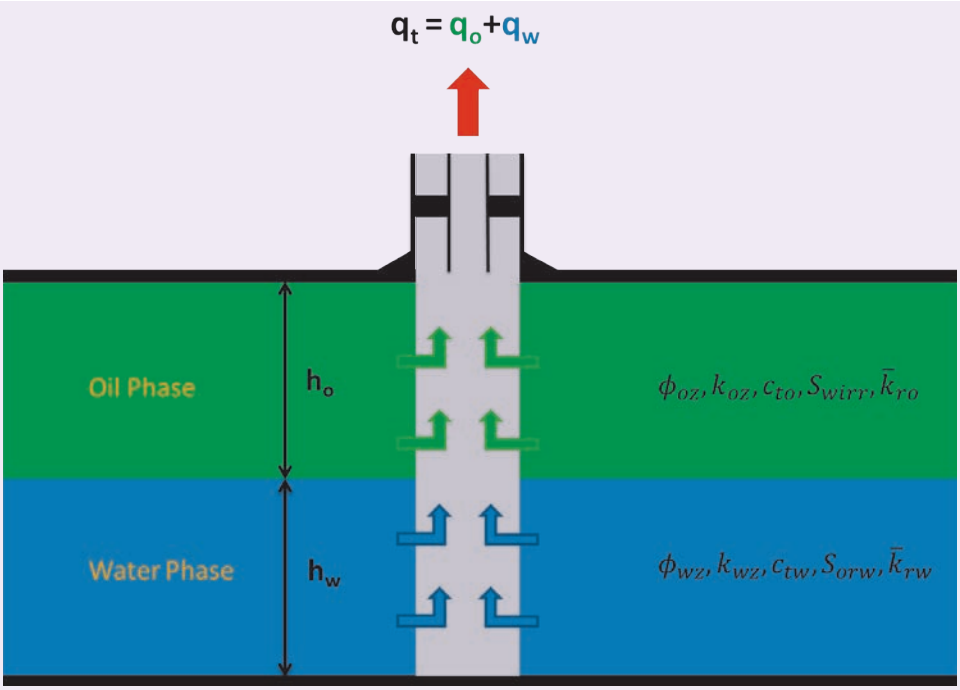

Table 1 *The properties used in the case study.*

Initial pressure (p_i)	5,000 psia
Absolute permeability (k)	100 md
Reservoir thickness (h)	100 ft
Wellbore storage coefficient (C)	0.01 bbl/psia
Wellbore radius (r_w)	0.3 ft
Skin (s)	0
Oil viscosity (μ_o)	3.0 cP
Water viscosity (μ_w)	0.3 cP
Oil formation volume factor (B_o)	1.3 bbl/stb
Water formation volume factor (B_w)	1.0 bbl/stb
Residual water saturation (S_{wirr})	0.15
Residual oil saturation to water (S_{orw})	0.25
End-point relative permeability to oil (k_{ro})	1
End-point relative permeability to water (k_{rw})	0.5
Oil compressibility (c_o)	9.53325E-6 $psia^{-1}$
Water compressibility (c_w)	2.97670E-6 $psia^{-1}$
Rock compressibility (c_r)	3.00000E-6 $psia^{-1}$
Production period before shut-in	1,000 hr
Shut-in duration	1,000 hr

fluid properties, and some petrophysical parameters of each zone. The detailed derivations are provided in Appendix B.

Once a satisfactory match is obtained between the model and the measured pressure transient data, the flow capacity for oil phase, the water phase, and the equivalent oil phase (assuming dry-oil production), respectively, are calculated as:

$$\text{Flow capacity for oil} = k_{oz}\,\bar{k}_{ro}\,h_o \quad (2)$$

$$\text{Flow capacity for water} = k_{wz}\,\bar{k}_{rw}\,h_w \quad (3)$$

$$\text{Equivalent oil phase flow capacity} = \bar{k}_{ro}\left(k_{oz}\,h_o + k_{wz}\,h_w\right) \quad (4)$$

Case Study

In this section, a case study is presented based on synthetic data to demonstrate the applicability of the new model to diagnose two-phase flow, and derive

Fig. 2 *Pressure, pressure drop and derivative, and production profiles generated using the segregated flow model (black), and Perrine's method (red) at a low water cut ratio of 20%.*

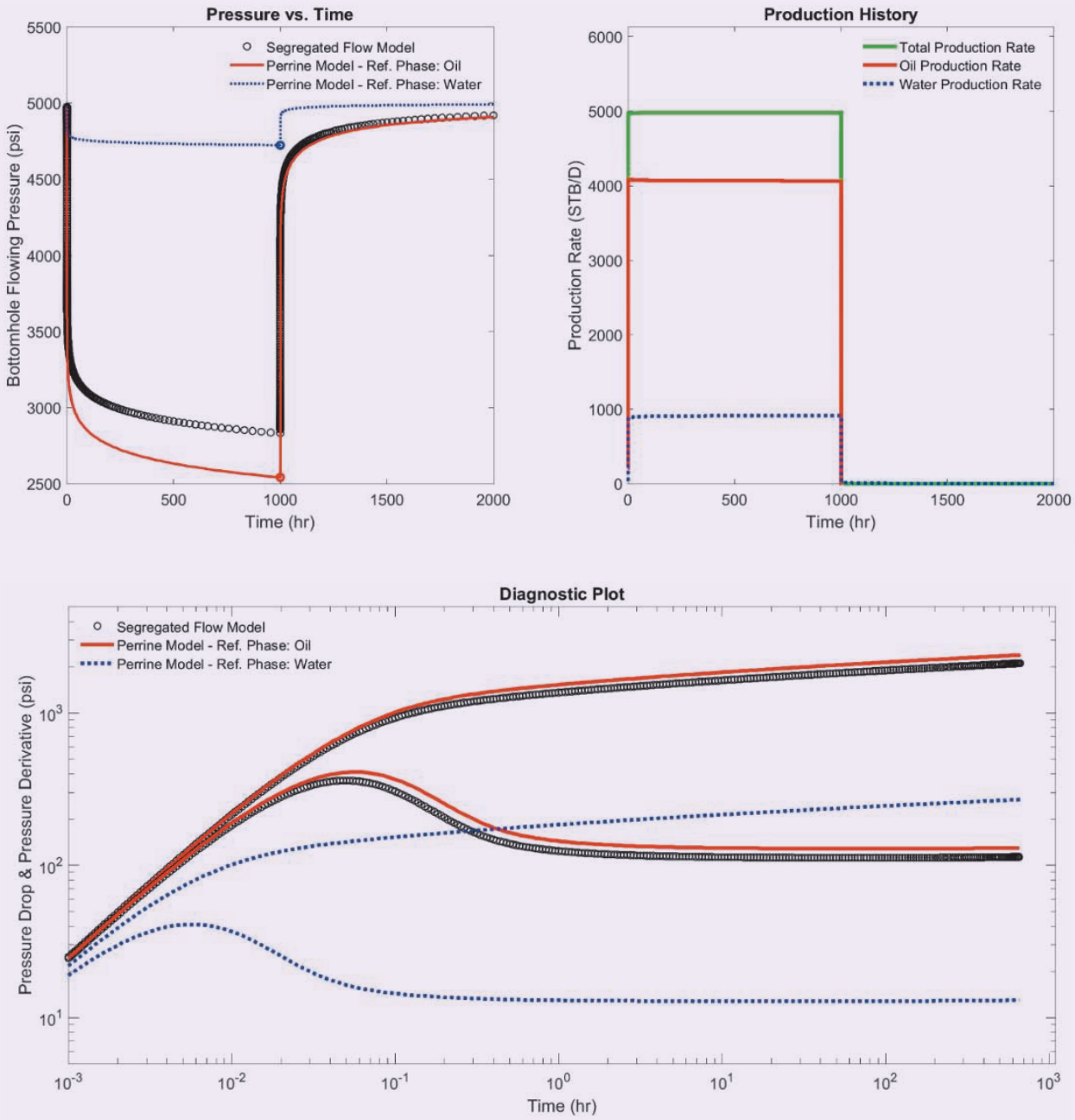

Fig. 3 *Pressure, pressure drop and derivative, and production plots generated using the segregated flow model (black), and Perrine's model (red) at a high water cut ratio of 80%.*

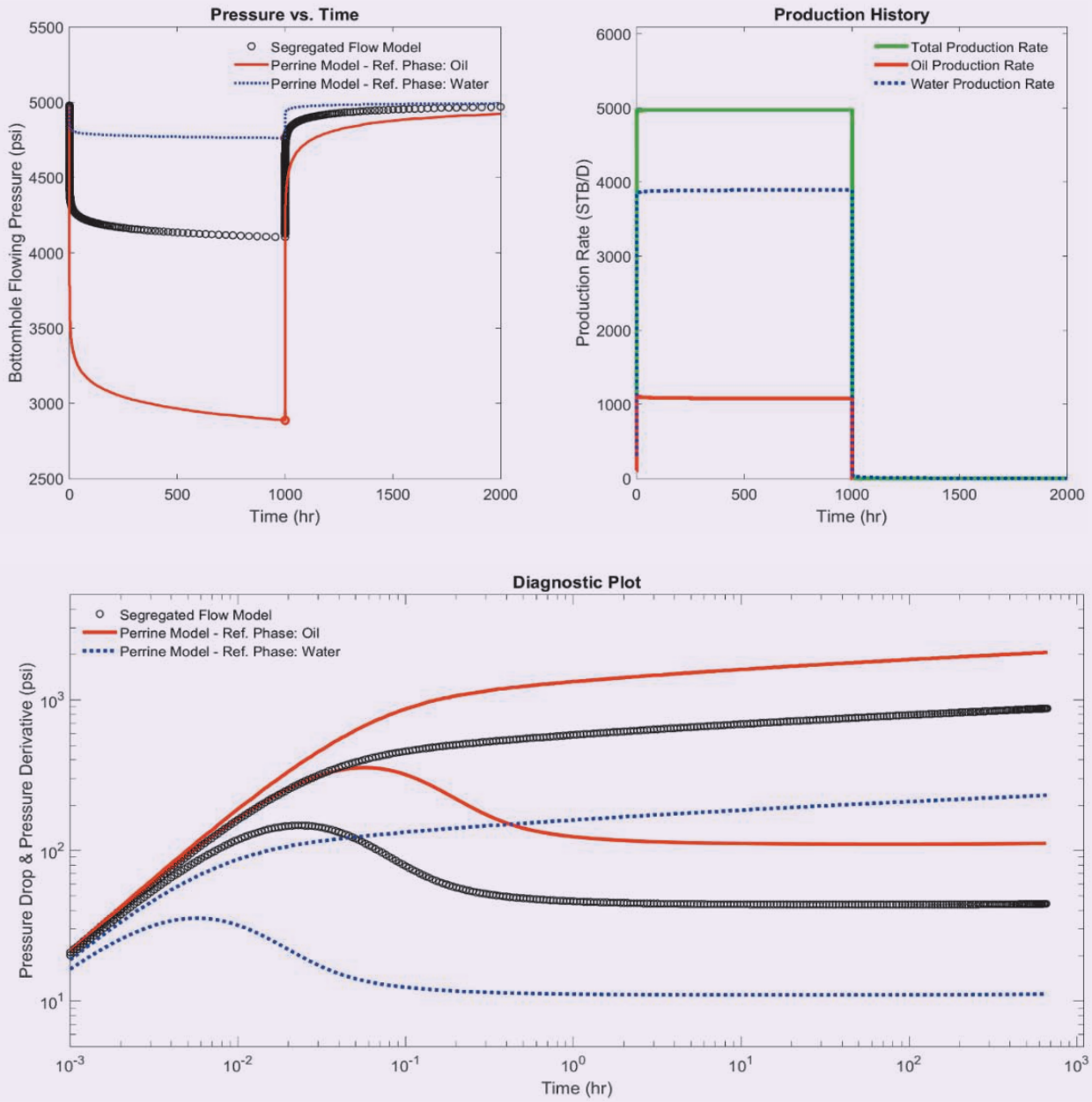

estimates of formation flow capacity and phase mobility. A fully penetrating vertical well produces for a period of 1,000 hours before shut-in for the same duration. It is assumed that the reservoir is unbounded and homogeneous. Table 1 contains all parameters used in the case study, including reservoir, fluids, and petrophysical properties.

For the implementation of Perrine's method, a numerical code has been developed and validated against a commercial well testing package as illustrated in Appendix C. As previously mentioned, Perrine assumes equivalent single-phase properties to represents two-phase flow, one of which is the viscosity, which takes the value of a reference phase specified by the user. Usually, oil is chosen as the reference phase, irrespective of the water cut ratio. In this study, we investigate the impact of selecting either oil or water as the main reference phase for computing values of properties, including viscosity.

Results of both the segregated and Perrine models are shown in Figs. 2 and 3, in which pressure responses from the segregated model are shown in black for high and low water cut ratios (20% and 80%). Responses with Perrine estimates are shown in red and blue,

Table 2 *Comparison between two models, and deviations from the segregated flow model.*

Case Input				Perrine Estimates		Segregated Flow Model		Deviation From Segregated Flow Model	
q_w (stb/d)	q_o (stb/d)	Water Cut (%)	Reference Phase	$k_o h$ (md-ft)	$k_w h$ (md-ft)	$k_o h_o$ (md-ft)	$k_w h_w$ (md-ft)	$\Delta k_o h$ (%)	$\Delta k_w h$ (%)
4,000	1,000	80	Oil	2,453	755	6,190	1,905	60.4	60.4
4,000	1,000	80	Water	24,528	7,547	6,190	1,905	296	296
1,000	4,000	20	Oil	8,387	161	9,630	185	13	13
1,000	4,000	20	Water	83,871	1,613	9,630	185	771	771

Fig. 4 *Pressure, pressure drop and derivative, and production plots generated using the segregated flow model (black), and Perrine's model using the corrected permeability (red) for a low water cut case.*

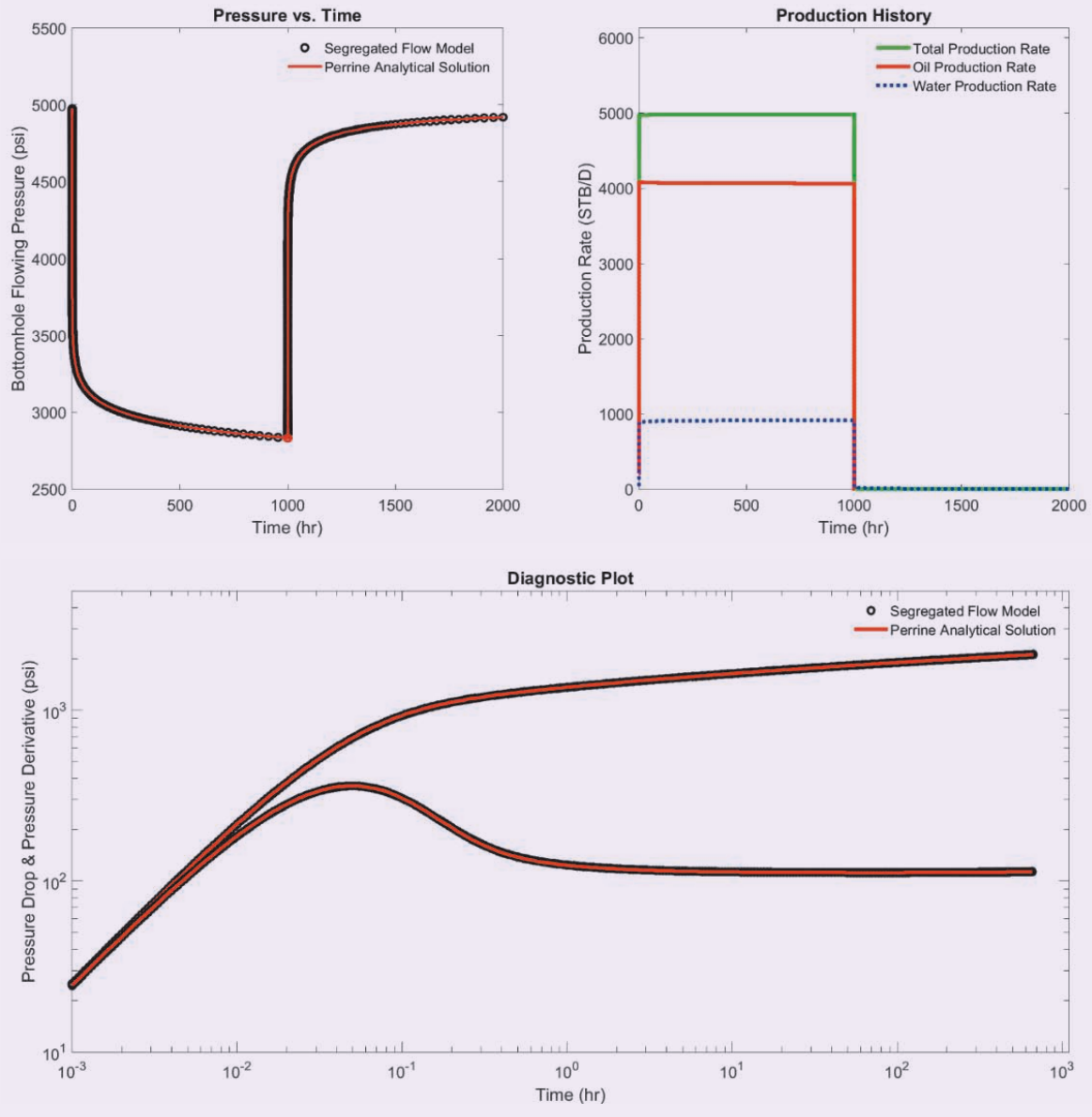

Fig. 5 *Pressure, pressure drop and derivative, and production plots generated using the segregated flow model (black), and Perrine's model using the corrected permeability (red) for a high water cut case.*

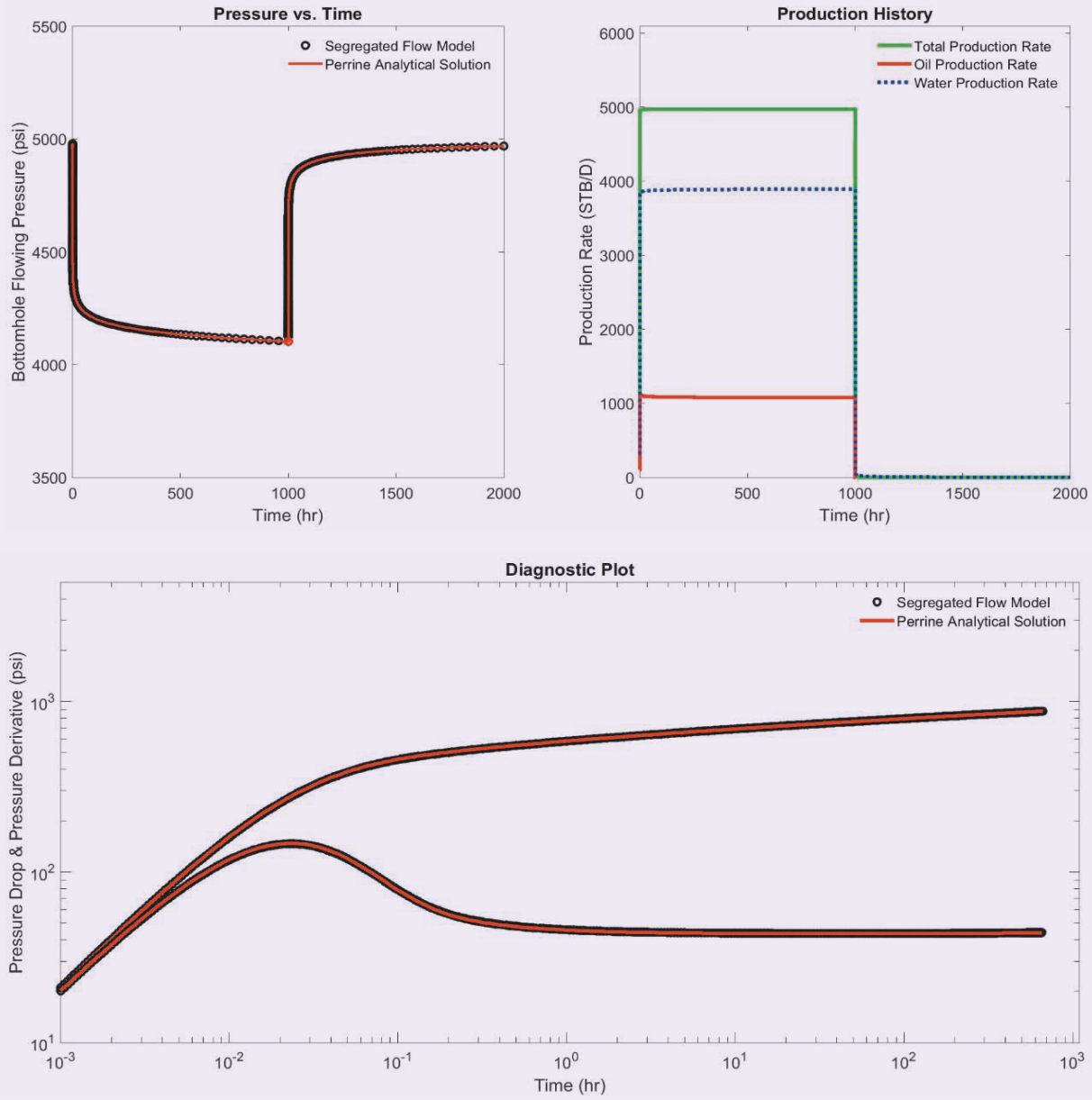

depending on the selected reference phase for viscosity, such that red indicates oil as the reference phase, while blue indicates water.

Figures 2 and 3 display the pressure and rate responses for the case when the properties in Table 1 are used for both models. Significant differences are observed, especially when the reference phase is water with a low water cut. The Perrine model exhibits substantial differences when compared to the segregated flow model, regardless of the chosen reference phase for a high water cut.

Table 2 summarizes the results of the comparison study between the two models and the deviations from the segregated flow model in the two-phase flow capacities, calculated using Eqns. 2 and 3 for the segregated model, and using Eqns. C-4 and C-5 for the Perrine model.

Correction to Perrine's Model

Earlier, we demonstrated that Perrine's approach could produce inaccurate results under segregated flow. We now provide a correction factor that can be used to adjust the calculated two-phase flow properties under such flow conditions. Note that the developed segregated flow is an explicit representation of the mechanism

Table 3 *A comparison between the segregated flow model and Perrine's method.*

Case Input		Perrine's Method		Segregated Flow Model		Corrected Perrine's Method	
Water Cut (%)	Reference Phase	k_{eq} (md)	Skin	k (md)	Skin	k_{cor} (md)	k_{eq}/k_{cor}
80	Oil or Water	252.38	+0.20	100.00	0	100.00	2.524
20	Oil or Water	114.81	+0.05	100.00	0	100.00	1.148

under consideration. The proposed correction is to force Perrine's estimates to match phase mobility values with those from the segregated flow model, Eqn. 5:

$$k_{cor} = k_{eq}\left[\frac{\mu_w}{\bar{k}_{rw}\,\mu_{ref}}\{M_R(1-f_w)+f_w\}\right] \quad 5$$

The correction factor of Eqn. 5 can only be used to correct the absolute permeability from Perrine's model — usually called the equivalent permeability — when segregated flow is anticipated.

Corrected permeability values, using Eqn. 5, are used to replicate Perrine's model to reproduce the pressure responses of the reservoir parameters as used in the previous section, and compared against those of the segregated flow model. Figures 4 and 5 show the results indicating a perfect match to the segregated model response for both high and low water cut ratios, irrespective of the chosen reference phase for viscosity.

Table 3 summarizes the results. In this particular example, it is shown that at a high water cut, Perrine's equivalent permeability overestimates the true reservoir permeability by more than a factor of two. The corrected values, nevertheless, match the true permeability precisely. The computed skin, however, indicates a slight deviation, which is of no major impact.

Conclusions

In this article, a new mathematical model to describe two-phase flow systems under a segregated flow mechanism is introduced and compared to the Perrine model. The new model describes the system more robustly, since it captures segregated flow as a two-layer system, allowing oil to flow through the top layer and water through the bottom layer. The Perrine model, on the other hand, treats the system as a single-phase and computes respective, effective properties to capture two-phase flow.

Synthetic reservoir data has been utilized to present a case study with multiple production scenarios, where both the segregated flow and the Perrine models have been compared. It has also been shown that the Perrine model could provide misleading estimates of phase flow capacity and phase mobility. Based on the segregated model, a new correction factor has been proposed to correct Perrine's absolute permeability under segregated flow conditions. An application of the new correction factor demonstrates a perfect match with the responses under multiple production cases, indicating a one-to-one transformation between the two models.

Acknowledgments

The authors would like to thank the management of Saudi Aramco for their support and permission to publish this article. The authors would also like to thank Saud A. Bin Akresh for his review comments, which have certainly helped improve clarity in certain sections in this article.

This article was submitted for presentation at the International Petroleum Technology Conference, Dhahran, Saudi Arabia, January 13-15, 2020.

Greek Symbols

η	Diffusivity constant for single-phase flow, defined in Eqn. A-2, md-psia/cP
η_o, η_w	Diffusivity constants for oil and water zones, respectively, md-psia/cP
ϕ_{oz}, ϕ_{wz}	Porosity in oil and water zones, respectively, fraction
λ_t	Total mobility ratio, defined in Eqn. C-2, md/cP
μ_o, μ_w	Viscosity of oil and water phases, respectively, cP
μ_{ref}	Viscosity of reference phase, cP

References

1. Dake, L.P.: *The Practice of Reservoir Engineering (Revised Edition), Developments in Petroleum Science, Vol. 36*, Elsevier Science, 2001, 572 p.
2. Perrine, R.L.: "Analysis of Pressure Buildup Curves," API paper 56-482, presented at the Drilling and Production Practice Conference, New York, NY, January 1956.
3. Martin, J.C.: "Simplified Equations of Flow in Gas Drive Reservoirs and the Theoretical Foundation of Multiphase Pressure Buildup Analysis," *Petroleum Transactions, AIME*, Vol. 216, 1959, pp. 321-323.
4. Weller, W.T.: "Reservoir Performance during Two-Phase Flow," *Journal of Petroleum Technology*, Vol. 18, Issue 2, February 1966, pp. 240-246.
5. Chu, W-C., Reynolds, A.C. and Raghavan, R.: "Pressure Transient Analysis of Two-Phase Flow Problems," *SPE Formation Evaluation*, Vol. 1, Issue 2, April 1986, pp. 151-164.
6. Coats, K.H., Dempsey, J.R. and Henderson, J.H.: "The Use of Vertical Equilibrium in Two-Dimensional Simulation of Three-Dimensional Reservoir Performance," *Society of*

Petroleum Engineers Journal, Vol. 11, Issue 1, March 1971, pp. 63-71.

7. Bear, J.: *Dynamics of Fluids in Porous Media*, American Elsevier Publishing Company Inc., NY, 1972, 764 p.
8. Fayers, F.J. and Muggeridge, A.H.: "Extensions to Dietz Theory and Behavior of Gravity Tongues in Slightly Tilted Reservoirs," *SPE Reservoir Engineering*, Vol. 5, Issue 4, November 1990, pp. 487-494.
9. Yortsos, Y.C.: "A Theoretical Analysis of Vertical Flow Equilibrium," SPE paper 22612, presented at the SPE Annual Technical Conference and Exhibition, Dallas, Texas, October 6-9, 1991.
10. Dietz, D.N.: "A Theoretical Approach to the Problem of Encroaching and Bypassing Edge Water," in *Koninklijke Nederlandse Akademie van Wetenschappen*, B56, 1953, pp. 83-92.
11. Lake, L.W.: *Enhanced Oil Recovery*, Prentice Hall, NY, 1989, 550 p.
12. Lake, L.W., Kasap, E. and Shook, M.: "Pseudofunctions — The Key to Practical Use of Reservoir Description," *North Sea Oil and Gas Reservoirs — II*, 1990, pp. 297-308.
13. Yortsos, Y.C.: "Analytical Studies for Processes at Vertical Equilibrium," paper presented at the 3rd European Conference on the Mathematics of Oil Recovery, Delft, the Netherlands, June 17-19, 1992.
14. Waggoner, J.R., Zapata, V.J. and Lake, L.W.: "Viscous Mixing in Unstable Miscible Displacements," SPE paper 22235, submitted for publication, but not published, 1991.
15. Nooruddin, H.A. and Rahman, N.A.M.: "Estimating Measures of Formation Flow Capacity and Phase Mobility from Pressure Transient Data under Segregated Oil and Water Flow Conditions," U.S. Patent 10,094,202, 2018.

Appendix A — Governing Differential Equations of the Segregated Flow Model

The diffusivity equation in radial coordinates for a single-phase flow is given as:

$$\frac{1}{r}\frac{\partial}{\partial r}\left(r\frac{\partial p}{\partial r}\right)=\frac{1}{\eta}\frac{\partial p}{\partial t} \quad \text{A-1}$$

where the diffusivity constant given by:

$$\eta=\frac{2.6376\ \mathrm{e}{-4}\ k}{\phi\ \mu\ c_t} \quad \text{A-2}$$

Eqn. A-1 is subject to the following initial condition:

$$p(r,0)=p_i \quad \text{A-3}$$

The sandface pressures are to be evaluated at the equivalent wellbore radius due to the presence of the skin factor. Therefore, the skin factor, s, of the subject well is considered through the equivalent wellbore radius of a physical wellbore radius, r_w, as:

$$r_{wa}=r_w\exp(-s) \quad \text{A-4}$$

The effective wellbore radius, defined in Eqn. A-4, can deal with both positive and negative values of the skin factors. Also the sandface pressure will be equal to the flowing wellbore pressure, which means that:

$$p_{wf}=p|_{r_{wa}} \quad \text{A-5}$$

Accounting for the wellbore storage phenomenon, the wellbore flowing pressure is related to the nominal production rate and the sandface production rate by the following material balance equation:

$$\frac{khr_w}{141.2B\mu}\frac{\partial p}{\partial r}\Big|_{r_w}+24C\frac{\mathrm{d}p_{wf}}{\mathrm{d}t}=q_t \quad \text{A-6}$$

Eqns. A-1 through A-6 can be readily solved by the Laplace transform technique. Individual phase equations are organized for dealing with the segregated flow model, as previously seen in Fig. 1. As such, the individual phase rates are related to the total production rate by the following equation:

$$q_t=q_o(t)B_o+q_w(t)B_w \quad \text{A-7}$$

As shown in Eqn. A-7, the total production rate at downhole conditions is constant, although the individual phase rates can vary with time. We also define c_{to} and c_{tw}, total compressibility in the oil and the water zones, respectively, as:

$$c_{to}=c_r+(1-S_{wirr})\,c_o+S_{wirr}\,c_w \quad \text{A-8}$$

$$c_{tw}=c_r+(1-S_{orw})\,c_w+S_{orw}\,c_o \quad \text{A-9}$$

In the presence of skin factors in the oil and water layers, the apparent wellbore radii in the oil and water zones, respectively, are computed as:

$$r_{wo}=r_w\exp(-s_o) \quad \text{A-10}$$

$$r_{ww}=r_w\exp(-s_w) \quad \text{A-11}$$

Therefore, the inner-boundary conditions can be expressed mathematically as functions of time:

$$p_{wf}(r_{wa},t)=p_o(r_{wo},t)=p_w(r_{ww},t) \quad \text{A-12}$$

Final expressions for the wellbore pressures, and the oil and water flow rates with wellbore storage and skin effects have been presented[15].

Appendix B — Derivation of h_w and h_o

The fractional flow of water under reservoir conditions can be defined as:

$$f_w=\frac{q_wB_w}{q_wB_w+q_oB_o} \quad \text{B-1}$$

At steady-state flow conditions, for radial flow, q_wB_w and q_oB_o can be determined using Darcy's equation as:

$$q_wB_w=\frac{2\pi h_wk_{wz}\bar{k}_{rw}\ \Delta p}{\mu_w\ln\left(\frac{r_e}{r_w}\right)} \quad \text{B-2}$$

$$q_oB_o=\frac{2\pi h_ok_{oz}\bar{k}_{ro}\ \Delta p}{\mu_o\ln\left(\frac{r_e}{r_w}\right)} \quad \text{B-3}$$

The fractional flow in Eqn. B-1 is then updated by Eqns. B-2 and B-3 as:

$$f_w=\frac{1}{1+\frac{h_ok_{oz}\bar{k}_{ro}\,\mu_w}{h_wk_{wz}\bar{k}_{rw}\,\mu_o}} \quad \text{B-4}$$

Solving Eqn. B-4 for $\frac{h_o}{h_w}$ gives:

$$\frac{h_o}{h_w} = \frac{k_{wz}\bar{k}_{rw}\,\mu_o}{k_{oz}\bar{k}_{ro}\,\mu_w}\left(\frac{1}{f_w} - 1\right) \quad \text{B-5}$$

Since, we get:

$$h_w = \frac{h}{\frac{k_{wz}\bar{k}_{rw}\,\mu_o}{k_{oz}\bar{k}_{ro}\,\mu_w}\left(\frac{1}{f_w}-1\right)+1} \quad \text{B-6}$$

and

$$h_o = h - h_w \quad \text{B-7}$$

The average fluid saturation in the reservoir can be estimated as:

$$S_w = \frac{\phi_{wz}\,h_w(1-S_{orw})+\phi_{oz}\,h_o\,S_{wirr}}{\phi_{wz}\,h_w+\phi_{oz}\,h_o} \quad \text{B-8}$$

An interesting relationship between fractional flow and average saturation can be drawn from Eqn. B-8 for segregated flow systems. From the fraction flow equation, the only variable parameter is $\frac{h_o}{h_w}$, which can be related to the average saturation as:

$$\frac{h_o}{h_w} = \frac{\phi_{wz}}{\phi_{oz}}\left(\frac{1-S_{orw}-S_w}{S_w-S_{wirr}}\right) \quad \text{B-9}$$

Fractional flow Eqn. B-4 then becomes:

$$f_w = \frac{1}{1+\frac{\phi_{wz}}{\phi_{oz}}\left(\frac{1-S_n}{S_n}\right)\frac{k_{oz}\bar{k}_{ro}\,\mu_w}{k_{wz}\bar{k}_{rw}\,\mu_o}} \quad \text{B-10}$$

where

$$S_n = \frac{S_w - S_{wirr}}{1-S_{orw}-S_{wirr}} \quad \text{B-11}$$

In the case of homogeneous reservoir formation, each ratio, $\frac{\phi_{wz}}{\phi_{oz}}$ and $\frac{k_{oz}}{k_{wz}}$, is unity in Eqn. B-10, and the equation simplifies to:

$$f_w = \frac{1}{1+\left(\frac{1-S_n}{S_n}\right)\frac{\bar{k}_{ro}\,\mu_w}{\bar{k}_{rw}\,\mu_o}} \quad \text{B-12}$$

This demonstrates that under segregated flow conditions, relative permeability can be represented by the Cory function with the exponents n_o and n_w, being equal to unity as:

$$k_{ro} = \bar{k}_{ro}\,(1 - S_n) \quad \text{B-13}$$

$$k_{rw} = \bar{k}_{rw}\,S_n \quad \text{B-14}$$

The water cut trends can also be evaluated under segregated flow conditions using the fractional flow equation at surface conditions for homogeneous reservoirs.

Fig. B-1 *Water cut as a function of dimensionless water thickness and* M_R *values:* $B_o = 1.3$ *and* $B_w = 1.0$.

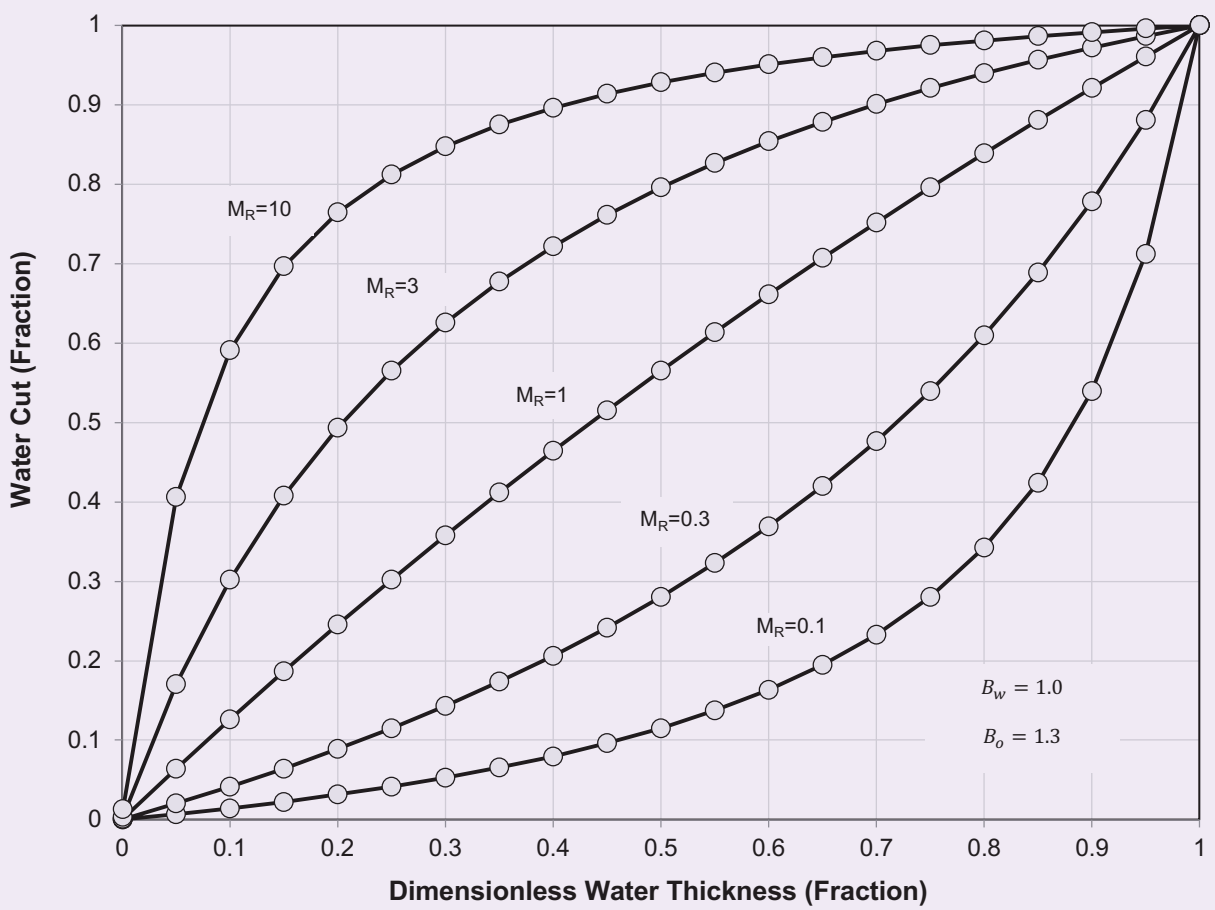

Starting from the definition of water cut and the rates in Eqns. B-2 and B-3, one finds:

$$WC = \frac{1}{1+\frac{h_o \bar{k}_{ro}\, \mu_w B_w}{h_w \bar{k}_{rw}\, \mu_o B_o}} \quad \text{B-15}$$

We define the M_R as:

$$M_R = \frac{\bar{k}_{rw}\, \mu_o}{\bar{k}_{ro}\, \mu_w} \quad \text{B-16}$$

Similarly, by defining the dimensionless water column height in the reservoir as:

$$h_{wD} = \frac{h_w}{h} \quad \text{B-17}$$

The parameter $\frac{h_o}{h_w}$ can be written in terms h_{wD} as:

$$\frac{h_o}{h_w} = \frac{1-h_{wD}}{h_{wD}} \quad \text{B-18}$$

Water cut from Eqn. B-15 can be rewritten as:

$$WC = \frac{1}{1+\frac{(1-h_{wD})B_w}{h_{wD}\, M_R B_o}} \quad \text{B-19}$$

Figure B-1 presents variations of water cut with h_{wD} for different M_R values.

Appendix C — Mathematical Model Built with Perrine's Estimates

As suggested by Perrine (1956)[2], multiphase flow properties are converted into single-phase flow properties with substitution of some effective total properties. These properties are total mobility, total compressibility, and equivalent production rate. Following Martin (1959)[3], the single-phase equivalent total compressibility, c_t, and total mobility, λ_t, to the respective multiphase quantities can be defined as:

$$c_t = c_o(1 - S_w) + c_w S_w + c_r \quad \text{C-1}$$

$$\lambda_t = \frac{k_o}{\mu_o} + \frac{k_w}{\mu_w} \quad \text{C-2}$$

Note that the c_t in Eqn. C-1 is evaluated with the known average water saturation, S_w, which requires the knowledge of the fractional flow vs. the saturation relationship. In addition, relative permeability functions must be known beforehand.

The effective total rate is defined as:

$$q_{et} = \frac{q_t}{B_{ref}} = \frac{q_o B_o + q_w B_w}{B_{ref}} \quad \text{C-3}$$

The individual phase permeability can be determined as:

$$k_o = \frac{q_o B_o}{q_{et} B_{ref}} \lambda_t\, \mu_o \quad \text{C-4}$$

Table C-1 *Properties used in the validation experiment.*

Initial pressure (p_i)	5,000 psia
Absolute permeability (k)	33.333 md
Reservoir thickness (h)	30 ft
Wellbore storage coefficient (C)	0.01
Wellbore radius (r_w)	0.3 ft
Skin (s)	0
Oil viscosity (μ_o)	0.487564 cP
Water viscosity (μ_w)	0.294823 cP
Oil formation volume factor (B_o)	1.28647 bbl/stb
Water formation volume factor (B_w)	1.02649 bbl/stb
Water production rate (q_w)	1,000 stb/d
Oil production rate (q_o)	2,000 stb/d
Residual water saturation (S_{wirr})	0.1
Residual oil saturation to water (S_{orw})	0.1
End-point relative permeability to oil (k_{ro})	1
End-point relative permeability to water (k_{rw})	[1]
Total compressibility (c_t)	1.25332E-5 $psia^{-1}$
Production period before shut-in	1,000 hr
Shut-in duration	1,000 hr

$$k_w = \frac{q_w B_w}{q_{et} B_{ref}} \lambda_t \, \mu_w \qquad \text{C-5}$$

The equivalent permeability is defined as:

$$k_{eq} = \lambda_t \, \mu_{ref} \qquad \text{C-6}$$

Note that the equivalent permeability depends on μ_{ref}, the viscosity of the reference phase specified by the user, which is usually selected as the oil phase. The values of equivalent permeability should be used with caution.

We now present a validation process of the implemented Perrine method in our numerical code against a commercial well testing package. The objective of this exercise is to make sure that our implementation is arithmetically correct. We have used the following solution in the Laplace space to generate the pressure responses at the wellbore with the parameters estimated from the Perrine method:

$$\bar{p}_{wf} = \frac{\frac{p_i}{l} + \frac{141.2\,(24\,Cp_i - q_t/l) K_0(r_{wa}\sqrt{l/\eta_t})}{\lambda_t h r_w \sqrt{l/\eta_t}\; K_1(r_w\sqrt{l/\eta_t})}}{1 + \frac{(24)(141.2) Cl\, K_0(r_{wa}\sqrt{l/\eta_t})}{\lambda_t h\, r_w \sqrt{l/\eta_t}\; K_1(r_w\sqrt{l/\eta_t})}} \qquad \text{C-7}$$

As shown in Eqn. C-7, the estimated parameters from the Perrine method contribute to the transient pressure through λ_t and n_t.

Table C-1 summarizes the parameters used in the validation process, and Fig. C-1 displays the comparative pressure responses.

Fig. C-1 *The comparison between the comparative pressure responses of Perrine's model generated from two different sources: A commercial well testing package and numerical code in this study.*

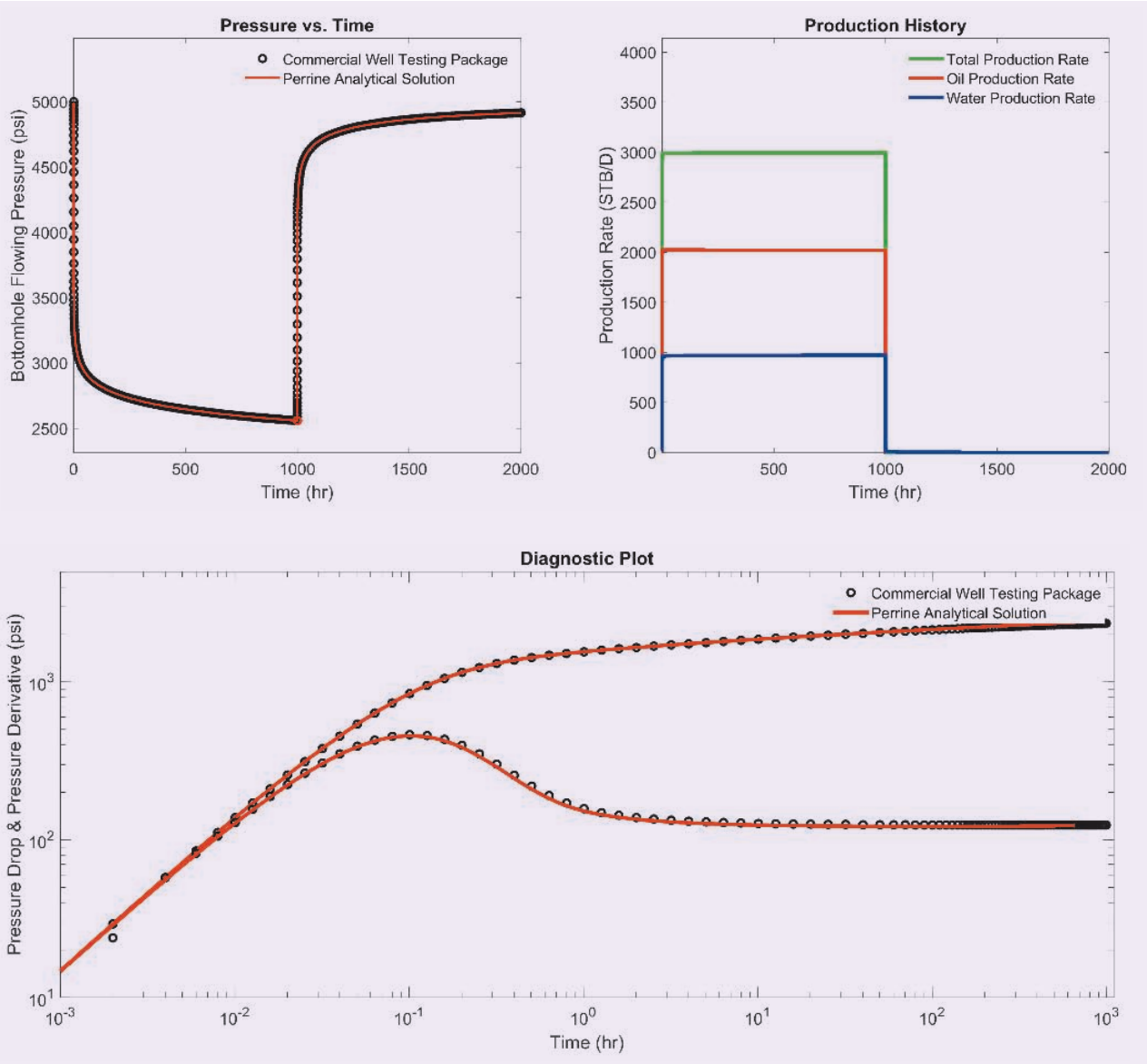

About the Authors

Dr. Hasan A. Nooruddin

Ph.D. in Petroleum Engineering, Imperial College London

Dr. Hasan A. Nooruddin is a Senior Petroleum Engineer currently working in the Reservoir Simulation Division of Saudi Aramco's Reservoir Description and Simulation Department. He has more than 13 years of experience in reservoir simulation, reservoir management, petrophysics, and well testing.

Since 2011, Hasan has published more than 15 papers in various peer-reviewed journals and conference proceedings, covering a wide range of research areas, including mathematical modeling, petrophysics, well testing, artificial intelligence, and machine learning.

He has three granted patents in well testing.

Hasan is a participant in the company's Petroleum Engineering Technologist Development Program, specializing in waterflooding optimization and modeling. He is a member of the Society of Petroleum Engineers (SPE), and a SPE Certified Petroleum Engineer.

Hasan received his B.S. and M.S. degrees from King Fahd University of Petroleum and Minerals (KFUPM), Dhahran, Saudi Arabia, and a Ph.D. degree from Imperial College London, London, U.K., all in Petroleum Engineering.

Dr. N.M. Anisur Rahman

Ph.D. in Petroleum Engineering, University of Alberta

Dr. N.M. Anisur Rahman is a Senior Petroleum Engineering Consultant with the Well Testing Division of the Reservoir Description and Simulation Department at Saudi Aramco, where he designs and interprets transient tests on hydrocarbon production and water injection wells. Anisur Rahman has also developed analytical solutions to a number of pressure transient models, including methods for short well tests. His interests include production technology, reservoir characterization and pressure transient analysis.

Prior to joining Saudi Aramco in 2009, Anisur Rahman worked for the Bangladesh University of Engineering and Technology, the University of Alberta, Fekete Associate Inc., and Schlumberger.

He has authored or coauthored 37 technical papers for publication in refereed journals and conference proceedings, and 12 patent documents, of which eight patents have already been granted by the U.S. Patent and Trademark Office. Anisur Rahman was a recipient of the 2016 Society of Petroleum Engineers (SPE) Middle East Regional Reservoir Description and Dynamics Award for his contributions to exceptional service and leadership, and for making significant contributions to the technical discipline. He also serves as a PTA/Well Testing Champion under the Petroleum Engineering Technical Excellence (PETE) and Support Network in Saudi Aramco.

Anisur Rahman received both his B.S. and M.S. degrees in Mechanical Engineering from the Bangladesh University of Engineering and Technology, Dhaka, Bangladesh, and his Ph.D. degree in Petroleum Engineering from the University of Alberta, Edmonton, Alberta, Canada.

He is registered as a Professional Engineer in the Province of Alberta, Canada.

Wettability Alteration of Oil-Wet Calcite: A Mechanistic Study

Dr. Ahmed Gmira, Dr. Mohamed A. Hammami, Dr. Sultan M. Al Enezi, and Dr. Ali A. AlYousef

Abstract /

Enhancing oil recovery in naturally fractured reservoirs by injecting chemistry optimized water has been widely investigated recently, and has demonstrated its efficiency in both laboratory and field trials. There are extensive ongoing efforts in the industry to characterize and understand the responsible mechanisms at scales ranging from nano-scale to field scale. The ionic formulation of the injected brine dramatically affects the crude oil/brine/rock interfaces, altering rock wettability and improving oil recovery efficiency.

In this experimental work, a mechanistic study is performed utilizing analytical methods to study the effect of the ionic composition and ionic strength on the rock sample's wettability. The combination of thermogravimetric analysis (TGA) and Fourier transform infrared (FTIR) spectroscopy is a timesaving experimental approach, suitable for wettability alteration quantification of rock samples.

The results indicate that stearic acid stretching vibrational bands decrease with the decrease of the brine's ionic strength, indicating a partial release of adsorbed organic material from the calcite surface. Single ion brines impacted the calcite wettability, and the sulfate ions were found to be the most effective in stearic acid release followed by sodium (Na), calcium (Ca) and magnesium (Mg). TGA confirmed the observed trend and the calcite weight loss due to the decrease of stearic acid decomposition with decreasing brine ionic strength, and confirmed the fact that sulfate ions are the most effective in partial release of adsorbed stearic acid from the calcite surface.

Introduction

There is increasing evidence that SmartWater flooding, through the tuning of injection water chemistry and ionic composition, has a significant impact on reservoir wettability, and on the recovered oil. This approach can potentially provide higher ultimate oil recovery with minimal investment assuming that waterflooding facilities are already in place. When compared to other enhanced oil recovery (EOR) techniques, it could avoid massive capital investment associated with conventional EOR methods. Injection of chemistry optimized water can be applied in the late life cycle of reservoirs, and also in early stages of production. The efficiency of oil recovery by waterflooding is strongly dependent on the complex interaction between oil, rock, and brine, and the balance of in situ competing forces. Since the mid-1990s, evidence has grown to show that injecting low salinity water into petroleum reservoirs give rise to significant increases in oil recovery[1-3].

The efforts in the past two decades have been devoted to understand recovery mechanisms of low salinity waterflooding, and various ideas have been proposed, including fine migration[4, 5], mineral dissolution[6], pH increase leading to interfacial tension (IFT) reduction[7], multiple ion exchange[8], double layer expansion[9, 10], and wettability alteration[11]. The mechanisms causing wettability alteration are not fully understood and are under debate due to the complexity of the carbonate reservoirs, i.e., fluid-fluid and fluid-rock interactions in place. Different mechanisms for wettability alteration have been proposed[12-15], including surface charges alteration by adsorption of SO_4^{2-} with co-adsorption of Ca^{2+} on the chalk rock surface, and substitution of Ca^{2+} on the chalk rock surface by Mg^{2+} because of increasing ionic reactivity at higher temperatures.

Yousef et al. (2010, 2011, 2012, 2012)[16-19] have demonstrated the positive impact of brine ionic strength on oil recoveries using numerous experimental methods, including IFT, contact angle, zeta potential, and coreflooding; corroborated later on by field tests in carbonate reservoirs[20]. Those fundamental studies pointed out that the carbonate rock wettability alteration was the main cause for the substantial increase in oil recovery observed in reported coreflood experiments. They attributed the wettability shift with SmartWater from oil-wet toward more water-wet to the interplay of key determining ions (Ca^{2+}, Mg^{2+}, and SO_4^{2-}) along with connectivity enhancement between micropores and macropores caused by anhydrite dissolution.

At nanoscale, atomic force microscopy measurements of the calcite surface[21] allowed a visualization of surface alteration such as dissolution, adsorption, and precipitation, initiated by the injected brine ionic content. Alotaibi and Yousef (2015)[22] described, by zeta potential measurements on carbonates, the contribution of individual ions and SmartWater recipes in changing the rock surface charges, which is considered a key mechanism in

rock wettability alteration. The impact of determining key ions in a crude oil-brine interface have recently been under focus, and studies have shown the impact of ions in enhancing interfacial viscoelastic properties; Alvarado et al. (2014)[23], reported an enhancement in interface elasticity at a lower sulfate content; Alves et al. (2014)[24] found that interfacial rheological properties are enhanced with an increase in salt content.

Sulfate ions were found to play a critical role in interface rheology as they increase elastic and viscous moduli at the oil-brine interface[25]. The interfacial compressibility of monolayers formed at the oil-brine interface were measured and have shown a sensitivity to various parameters such as aging time, ionic strength level, and ionic composition[26]. The effect of the salinity of single ion brines on the wettability have recently been reported by different authors. Lashkarbolooki et al. (2014)[27], have studied the effect of salinity on the wettability of crude oil in carbonate rocks.

They have measured the IFT and contact angles at various concentrations of sodium chloride (NaCl), magnesium chloride ($MgCl_2$), and calcium chloride ($CaCl_2$), and reported the impact of brine salinity on the contact angles and rock wettability. IFT measurements have also shown that the lowest IFT values are obtained at high salinity levels, especially if divalent ions are utilized. High values of IFT are obtained if monovalent salts are used. Aslan et al. (2016)[28], have also investigated the change in calcite wettability caused by injecting NaCl and $MgCl_2$ over a wide concentration. This shows a dual regime for the contact angle; an increase of the contact angle reaching a maximum, and then a decrease with an increasing salt concentration.

The action of tuning injected water is a complex process involving not only a comprehensive understanding of fluid-fluid and fluid-rock interactions, but also an understanding of the synergy between competing forces acting at the interfaces.

The goal of this work is to investigate the sensitivity of an experimental workflow combining thermogravimetric analysis (TGA) and Fourier transform infrared (FTIR) spectroscopy to different injected brines. In this study, we discuss the influence of brine ionic strength and the effect of single ion brines on the adsorbed amount of polar components in a modal oil, onto a calcite surface and adsorption bands, in an attempt to provide information on the potential mechanisms responsible for altering carbonate wettability using tuned water injection.

Experimental Section

A pure calcium carbonate disk was obtained from Italy, as a white, fine-grained rock. A ceramic mortar and pestle were utilized to crush the disk into fine powder. The purity of the calcite sample was determined by using X-ray powder diffraction (XRD) and scanning electron microscope techniques. The XRD results indicate that the calcite disk contained more than 99 wt% of calcium carbonate. Advanced grinding and sieve analysis techniques were avoided to minimize the contamination issues. Modal oil was used in this study to control the properties affecting the wettability alteration process. Stearic acid or octadecanoic acid ($CH_3(CH_2)_{16}COOH$), in n-decane is considered as a modal oil in this study. The n-decane of 99% purity and stearic acid were purchased from Thermo Fischer Scientific and Fluka, respectively, and the concentration of stearic acid in n-decane was set to 0.1M. Distillated deionized water from Scientific Nanopure™ was used for preparation of the brines. The brine samples were prepared using the following salt compounds from Fischer Scientific (ACS grade): magnesium chloride hexahydrate, NaCl, calcium chloride dihydrate, sodium sulfate anhydrous, and sodium hydrogen carbonate, including brines with various ionic strengths and single ion brines, Table 1.

A batch of calcium carbonate powder was poured into deionized water and agitated with modal oil (0.1M stearic acid in n-decane). The aged calcium carbonate was then separated by centrifugation at 6,000 rpm for 30 minutes and oven dried overnight at 50 °C. The oil-wet powder was then treated with single ions and complex brines by agitation for 48 hours at 75 °C. The powder was then separated from the liquid suspension by centrifugation at 6,000 rpm for 30 minutes and oven dried overnight at 50 °C.

Table 1 *Composition of the brines.*

	Brine 1	Brine 2	Brine 3	Brine 4	Brine 5	Brine 6	Brine 7
Na^+	18,240	9,120	1,824	2,266	—	—	*1,865*
Mg^{2+}	2,110	1,055	211	—	—	1,471	—
Ca^{2+}	650	325	65	—	2,080	—	—
SO_4^{2-}	4,290	2,145	429	—	—	—	3,896
Cl^-	32,200	16,100	3,220	3,495	3,681	4,290	—
HCO_3^-	120	60	12	—	—	—	—
TDS (ppm)	57,610	28,805	5,761	5,761	5,761	5,761	5,761

FTIR spectroscopy was performed to evaluate the structural changes of the functional groups during the surface treatment. The FTIR spectrum of the calcium carbonate samples were recorded in the wavenumber range of 400 cm^{-1} to 4,000 cm^{-1}. FTIR spectroscopy is a powerful qualitative technique for observing oscillations arising from the vibration of molecules[29-31]. A change in vibration of a molecule can be used to investigate the interaction of the molecules with the surrounding environment. Untreated and treated samples were analyzed to quantify the wettability alteration of oil-wet calcium carbonates by the application of single and complex brines.

TGA was performed to evaluate the extent of the wettability alteration caused by various brine compositions. The method measures the mass change as a function of temperature, and the amount of adsorbed components onto the surface was calculated for treated and untreated calcium carbonate samples. A thermogravimetric analyzer with a balance resolution of ± 0.1 µg was used to record the weight loss as a function of temperature. The samples were placed in an aluminum pan and heated at 10 °C/min under a constant flow of dried air, up to 900 °C.

Results and Discussions

Several studies has shown that the acidic compounds, especially carboxylic acid, in the crude oil can adsorb onto the carbonate surface and alter the initial rock surface wetting properties[32, 33]. Stearic acid is known as one of the most active wettability altering agents in crude oil[34] as stearate groups are chemically adsorbed on the calcite surface and form a chemisorbed stearate layer[35]. TGA was used to measure the amount of adsorbed stearate on the calcite surface before and after treatment with modified brines.

Figure 1 presents the TGA results of calcite and aged calcite in modal oil (Decane/0.1M stearic acid). The TGA curve of the calcite sample consists of one step, starting from 620 °C onward. The observed single sharp weight loss is a confirmation of the calcite purity as it demonstrates the decomposition of calcium carbonate into calcium oxide and carbon dioxide. The weight loss of calcite after aging in modal oil follows three different steps.

Fig. 1 *The TGA analysis of calcite and aged calcite treated with 0.1M stearic acid.*

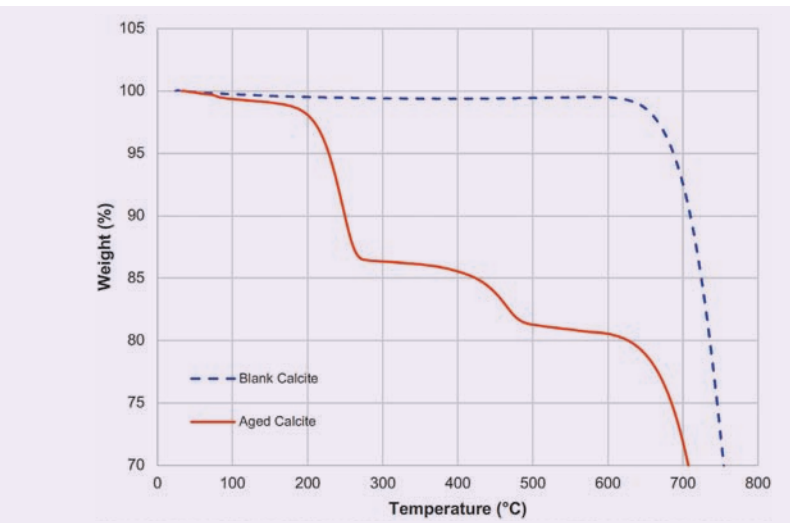

The first stage, 30 °C to 210 °C, is associated with the removal of physically adsorbed materials from the surface, starting from the weaker bonds. When the temperature increased up to 360 °C, the stronger bonds — chemical bonds between acids and active sites of the calcite surface — become weaker. The weight loss at this stage is essentially due to the decomposition of chemisorbed material. A double deflection point is also observed in the region 420 °C to 500 °C, and is probably caused by the release of multiple layers of the chemisorbed material. The thermal region, 210 °C to 500 °C, is used to compare the amounts of adsorbed stearic acids on the calcite surface exposed to injected brines with various compositions. The last stage is characterized by the calcite thermal degradation, starting from 600 °C onward. The TGA results for the oil-wet calcite is given in Fig. 2 for samples treated with high, medium, and low ionic strength brines, and in Fig. 3 for the calcite samples treated with single ion brines: $CaCl_2$, NaCl, $MgCl_2$, and Na_2SO_4.

Three stages of weight loss are also noticed in the thermal decomposition process in Figs. 2 and 3. As already mentioned, the first stage was caused by water loss and the decomposition of the physisorbed materials. The second stage is related to decomposition of chemisorbed materials, and the last stage is caused by calcite thermal degradation. The results of the oil-wet calcite treated with high, medium, and low ionic strength brines are compared with calcite aged only in the modal oil.

The weight loss due to the chemical bonds degradation and elimination of the stearate layers in the second stage is 1.5 wt% for calcite exposed to highly ionic strength brine, which is less than the aged calcite, 12 wt%. Calcite treated with lower ionic strength brine is also impacting the weight loss of the chemisorbed organic materials, Fig. 2. The weight loss in stage two was 0.9 wt% and 0.7 wt% for brines with medium and low ionic strength, respectively. This indicates that the adsorbed component on the calcite surface was decreased with decreasing ionic strength. The TGA results vs. ionic strength variations is in total accordance with previous results obtained by the contact angle, IFT, and coreflooding[16-18].

Figure 3 is the TGA results of the oil-wet calcite sample treated with brines composed only of potential determining ions (Ca^{2+}, Na^{+}, Mg^{2+}, and SO_4^{2-}), believed to be key determining ions in rock wettability alteration. After the aged calcite was treated with single ion brines, the lowest weight loss due to the decomposition of adsorbed stearate on the surface was caused by Na_2SO_4 (0.8 wt%), followed by $CaCl_2$ (2.5 wt%), NaCl (3 wt%), and $MgCl_2$ (7 wt%). The

presence of sulfate ions enhances the partial release of stearate ions from the surface, contributing to alter calcite wettability toward more water wet. TGA has shown that adsorbed modal oil on the calcite surface depends strongly on the brine's ionic strength and ionic composition. Weight losses of calcite due to the decomposition of chemisorbed material vs. brine ionic strength and single ion brines are summarized in Figs. 4a and 4b, respectively.

Fig. 2 *The TGA results of the oil-wet calcite treated with high, medium, and low ionic strength brines.*

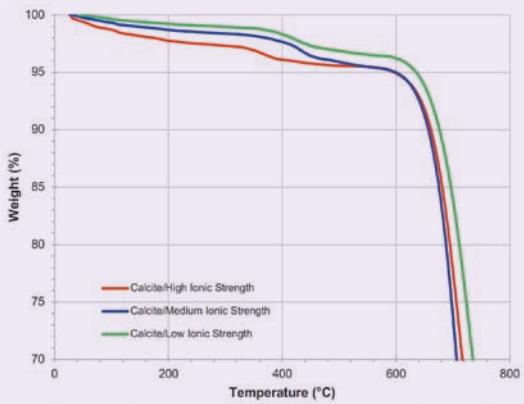

Fig. 3 *The TGA results of the oil-wet calcite treated with single ion brines: $CaCl_2$, NaCl, $MgCl_2$, and Na_2SO_4.*

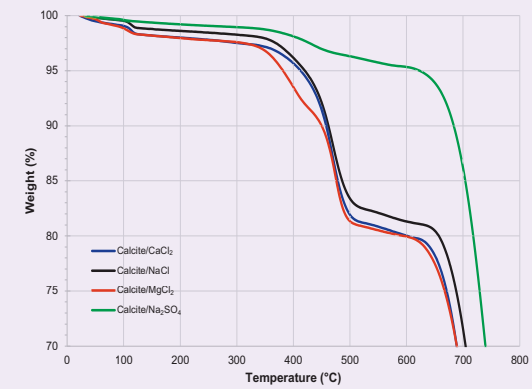

FTIR spectroscopy was used to provide complementary evidence about the calcite surface wettability alteration mechanisms, and also to investigate the impact of injected brine ionic strengths and ionic composition. A change in molecular bond length (stretching) or bond angle (bending) results in changes in the vibration of a molecule. Those changes reflect some of the characteristics of the chemical bonds within the molecule, and can be used to identify the functional groups in the molecules and the adsorbed compounds on the calcite surface. Figure 5 illustrates the transmittance spectrum of a dry calcite and after aging in a Decane/0.1M stearic acid solution within the wavenumber range of 500 cm^{-1} to 5,000 cm^{-1}.

In the calcite spectrum, four transmittance bands are characteristics of a pure calcium carbonate: (1) in-plane bending vibration located at 725 cm^{-1}, (2) out-of-plane bending centered at 875 cm^{-1}, (3) carbon-oxygen (C-O) asymmetric stretching centered at 1,403 cm^{-1}, and (4) C-O symmetric stretching centered at 1,805 cm^{-1}. The broad and symmetrical band at 1,403 cm^{-1} is one of the main characteristics of a carbonate group produced by C-O stretching vibration, and the two infrared bands at 725 cm^{-1} and 875 cm^{-1} are the bending vibrations of the carbonate group. Those infrared bands are in good agreement with previous studies[36, 37]. The spectrum of the calcite aged in modal oil reveals new infrared bands added due to the adsorption of stearate on a calcite surface. A new peak at 1,542 cm^{-1} is referred to as related to the C-O asymmetric stretching vibration[30], a peak located at 2,850 cm^{-1} referred to the carbon-hydrogen (C-H) symmetric stretching vibration[31], and the 2,915 cm^{-1} peak referred to the C-H asymmetric stretching vibration. The water adsorbed on the surface produced a sharp band in the 3,200 cm^{-1} to 3,800 cm^{-1}, due to oxygen-hydrogen stretching.

Figure 6 presents the FTIR spectrum of aged calcite

Fig. 4 *Weight loss of aged calcite treated with: (a) brines with high, medium, and low ionic strength, and (b) single ion brines ($CaCl_2$, NaCl, $MgCl_2$, and Na_2SO_4).*

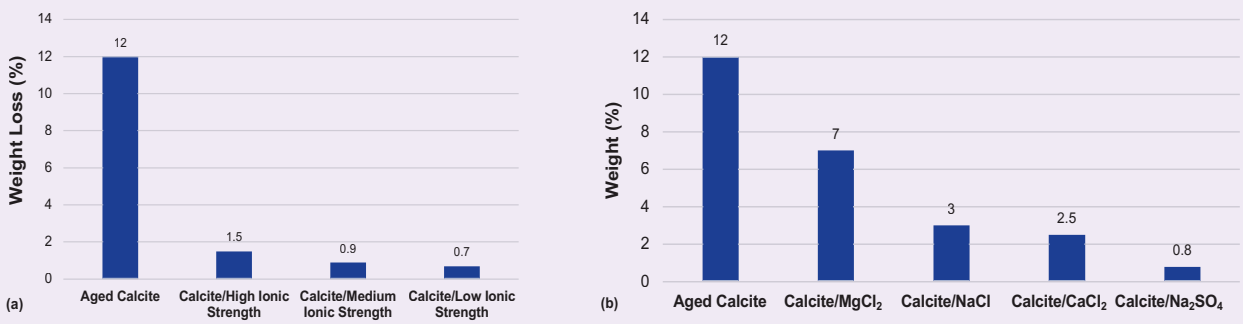

Fig. 5 *The FTIR spectrum (transmittance vs. wavenumbers) of calcite (blue) and aged calcite in modal oil (red).*

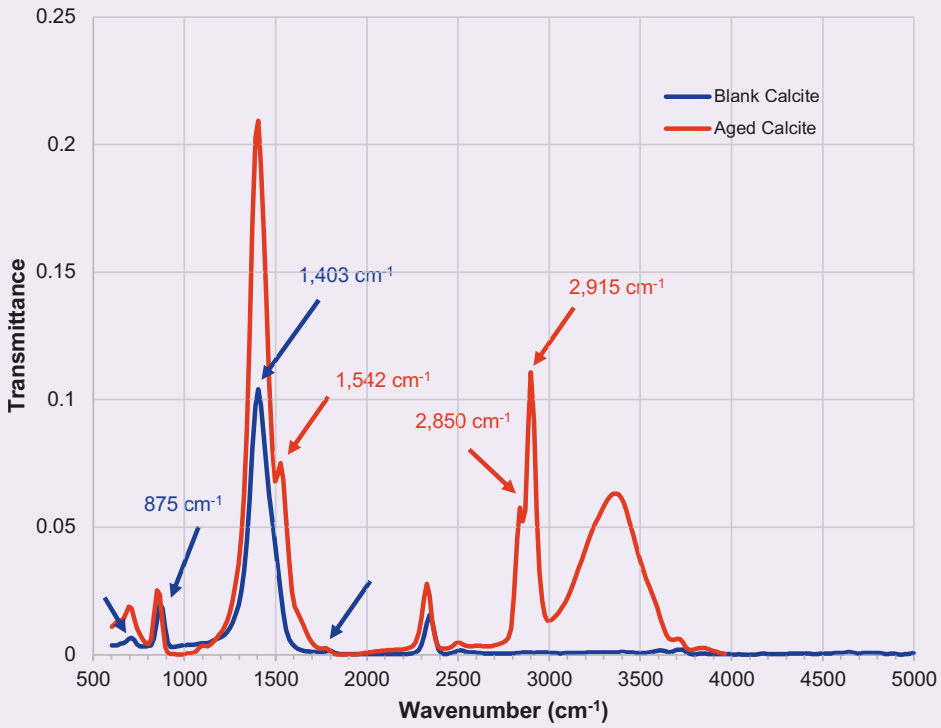

Fig. 6 *The FTIR spectrum of aged calcite treated with high, medium, and low ionic strength brines.*

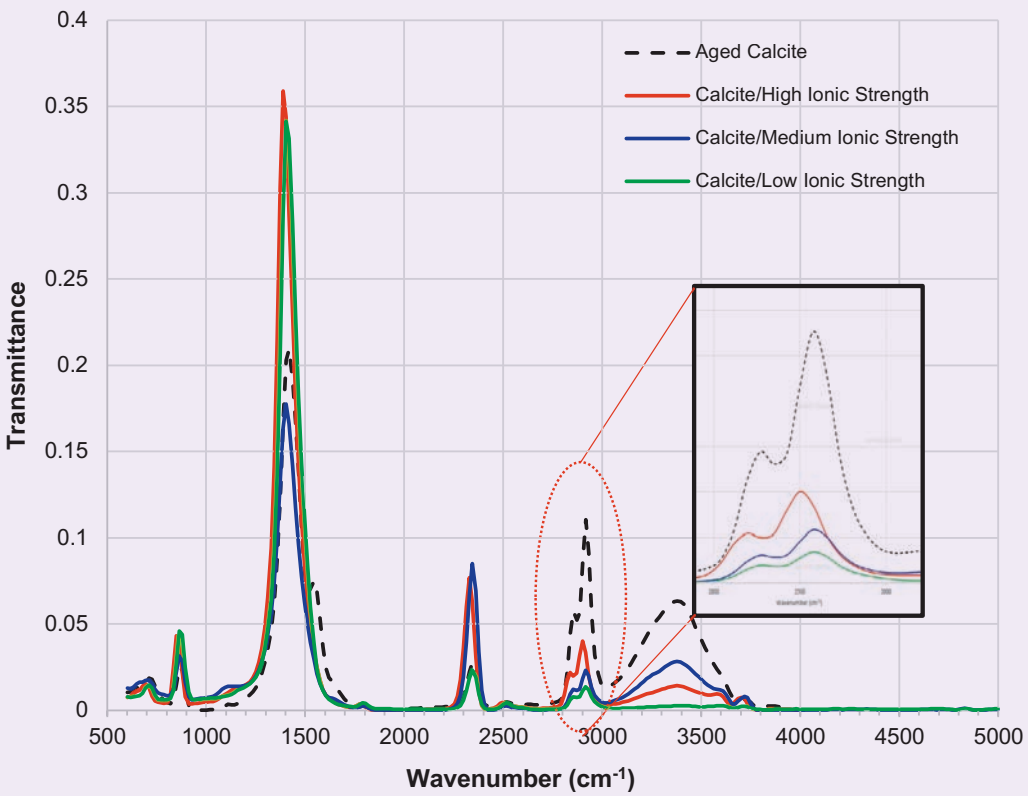

treated with high, medium, and low ionic strength brine. The general pattern of the FTIR spectrum did not change after the calcite was treated with brines. The characteristics of the vibrational bands of the calcite structure remain similar to the ones observed for pure calcite, except for the disappearance of the C-O asymmetric stretching vibration band at 1,542 cm^{-1}.

This is mainly caused by the partial desorption of stearate ions from the calcite surface. The vibrational peaks are getting broader in the wavenumber ranges of 2,600 cm^{-1} to 3,200 cm^{-1} with a decrease in the brine's ionic strength. There were also a decrease in the intensity of C-H stretching symmetric and asymmetric vibrations at 2,850 cm^{-1} and 2,915 cm^{-1}, respectively, with a decrease in the brine's ionic strength (inset in Fig. 6). This indicates that decreasing ionic strength of the injected brine is responsible for partial removal of adsorbed stearate from the calcite surface.

Figure 7 presents the FTIR spectrum of aged calcite treated with single ion brines: $CaCl_2$, NaCl, $MgCl_2$, and Na_2SO_4. The general pattern is similar to the one from the aged calcite with modal oil with main calcium carbonate peaks in place. The peak located at 1,542 cm^{-1} — the C-O asymmetric stretching vibration band — disappeared when the calcite was treated with Na_2SO_4, indicating a partial desorption of the stearate from the calcite surface. We also observed broad peaks in the case of $CaCl_2$, $MgCl_2$, and NaCl. There was also a significant decrease in the C-H stretching symmetric and asymmetric vibrations at 2,850 cm^{-1} and 2,915 cm^{-1}, respectively. The highest decrease of C-H stretching vibrations was observed after the aged calcite was treated with Na_2SO_4, followed by NaCl, $CaCl_2$, and $MgCl_2$ (inset in Fig. 7).

This indicates that sulfate ions are the most effective in removing the adsorbed stearate from the calcite surface, compared to other key ions. There was no noticeable change in the FTIR spectrum pattern, such as the additional presence of vibrational peaks that could be related to adsorption of specific ions on the calcite surface. This observation rules out the adsorption of determining ions on the calcite surface as one of the mechanisms responsible for stearate release in agreement with recent studies by Wei et al. (2017)[38] and Al-Hashim et al. (2018)[39].

This data, obtained from TGA and FTIR, allowed us to come to several observations about the characterization process and the effect of the brine's ionic composition on calcite wettability. Aged calcite treated with sulfate brine has shown the lowest weight loss and the lowest intensity for the symmetric and antisymmetric C-H vibrational bands, related to stearic acid. The FTIR spectroscopy did not show signs of adsorbed ions in general and sulfate ions in particular

Fig. 7 *The FTIR spectrum of calcite aged in modal oil and treated with single ion brines ($CaCl_2$, NaCl, $MgCl_2$, and Na_2SO_4).*

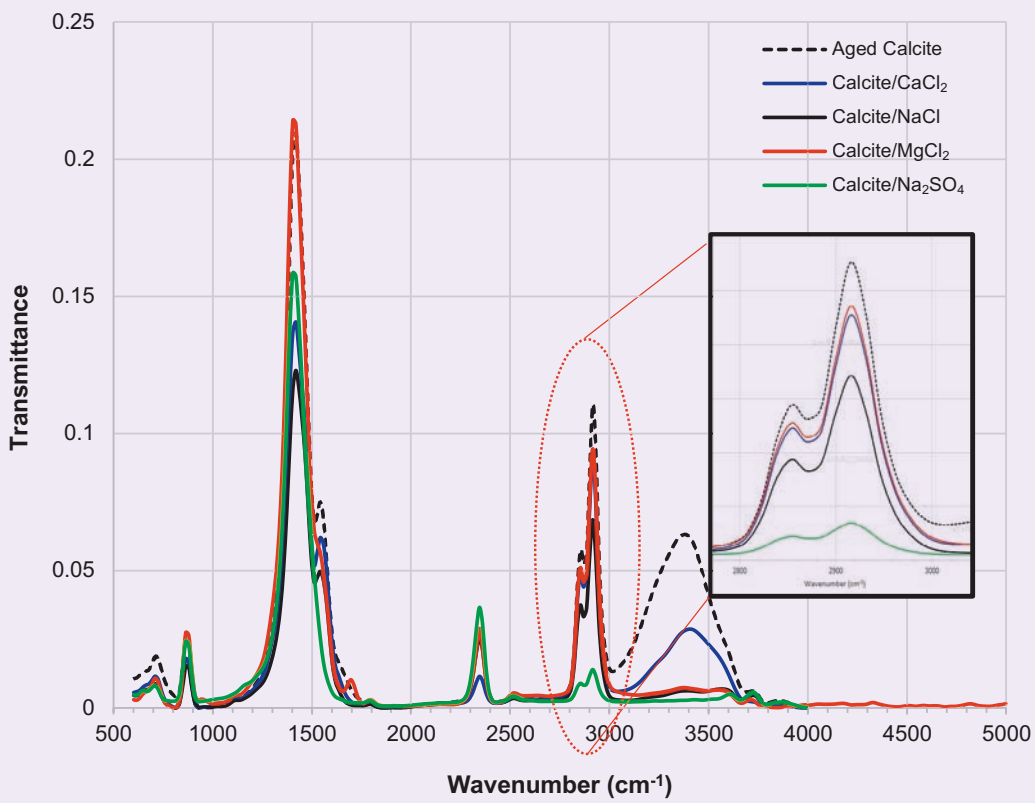

on the calcite surface, an absence that could be explained by the fact that ionic exchange between sulfate and adsorbed stearate on the calcite is not responsible for the desorption of the organic material from the calcite surface.

The responsible mechanism for stearate desorption from the calcite surface is dependent of the ionic make-up of the injected brine. Sodium sulfate and NaCl solutions are known for significantly reducing the charges at oil-water interface[22]. For sulfate anions, a combination of two mechanisms could explain the stearate desorption from the calcite surface: an ionic exchange between hydroxide anions and adsorbed stearate, caused by the increase in the hydroxide concentration during sodium sulfate dissolution and the interaction between sulfate anions and calcium, which is attached to the stearate ion, resulting in the removal of calcium ions along with attached stearate from the calcite surface.

The ionic exchange mechanism between hydroxide anion and stearate ions can also explain the impact of NaCl in the organic material desorption as the hydroxide concentration increases during the NaCl dissolution. A decrease in the concentration of the adsorbed stearate is also observed when adding $MgCl_2$ and $CaCl_2$. An increase in the solution hardness through dissolving more calcium and Mg ions results in a surface charge increase, as reported in previous studies[22,40]. The impact of those divalent cations can be explained by their strong bonding to adsorbed stearate and their ability to play a role in the interactions at the rock-fluid interface.

Conclusions

The impact of a brine ionic composition on the calcite wettability alteration was investigated using brine recipes with different ionic strengths, and brines composed solely of individual ions, believed to be active in wettability alteration mechanisms. The mechanistic study investigated the weight loss by TGA and vibrational bands by FTIR. The following conclusions can be drawn:

- The combination of TGA and FTIR is an effective experimental approach to investigate the impact of the brine's ionic composition on rock wettability alteration.
- Low ionic strength brine is the most effective in releasing adsorbed stearate from the calcite surface.
- Among the single ions brines, sulfate ions are the most effective in calcite wettability alteration by desorbing stearate ions from the calcite surface by a combination of ionic exchange and ionic interactions.
- Brines with divalent cations are the least effective in calcite wettability alteration, but still contribute to stearate desorption.

Acknowledgments

The authors would like to thank the management of Saudi Aramco for their support and permission to publish this article.

This article was presented at the SPE Kingdom of Saudi Arabia Annual Technical Symposium and Exhibition, Dammam, Saudi Arabia, April 23-26, 2018.

References

1. Jackson, M.D., Vinogradov, J., Hamon, G. and Chamerois, M.: "Evidence, Mechanisms and Improved Understanding of Controlled Salinity Waterflooding Part 1: Sandstones," *Fuel*, Vol. 185, December 2016, pp. 772-793.
2. Myint, P.C. and Firoozabadi, A.: "Thin Liquid Films in Improved Oil Recovery from Low-Salinity Brine," *Current Opinion in Colloid and Interface Science*, Vol. 20, Issue 2, April 2015, pp. 105-114.
3. Sheng, J.J.: "Critical Review of Low-Salinity Waterflooding," *Journal of Petroleum Science and Engineering*, Vol. 120, August 2014, pp. 216-224.
4. Tang, G-Q. and Morrow, N.R.: "Influence of Brine Composition and Fines Migration on Crude Oil/Brine/Rock Interactions and Oil Recovery," *Journal of Petroleum Science and Engineering*, Vol. 24, Issues 2-4, December 1999, pp. 99-111.
5. Song, W. and Kovscek, A.R.: "Functionalization of Micromodels with Kaolinite for Investigation of Low Salinity Oil Recovery Processes," *Lab on a Chip*, Vol. 15, Issue 16, August 2015, pp. 3314-3325.
6. Lager, A., Webb, K.J., Black, C.J.J., Singleton, M., et al.: "Low Salinity Oil Recovery — An Experimental Investigation 1," *Petrophysics*, Vol. 49, Issue 1, February 2008, pp. 28-35.
7. McGuire, P.L., Chatham, J.R., Paskvan, F.K., Sommer, D.M., et al.: "Low Salinity Oil Recovery: An Exciting New EOR Opportunity for Alaska's North Slope," SPE paper 93903, presented at the SPE Western Regional Meeting, Irvine, California, March 30-April 1, 2005.
8. Lager, A., Webb, K.J., Black, C.J.J., Singleton, M., et al.: "Low Salinity Oil Recovery — An Experimental Investigation," paper presented at the International Symposium of the Society of Core Analysts, Trondheim, Norway, September 12-16, 2006.
9. Ligthelm, D.J., Gronsveld, J., Hofman, J., Brussee, N., et al.: "Novel Waterflooding Strategy by Manipulation of Injection Brine Composition," SPE paper 119835, presented at the EUROPEC/EAGE Conference and Exhibition, Amsterdam, the Netherlands, June 8-11, 2009.
10. RezaeiDoust, A., Puntervold, T., Strand, S. and Austad, T.: "'Smart Water' as Wettability Modifier in Carbonate and Sandstone," paper presented at the 15th European Symposium on Improved Oil Recovery, Paris, France, April 17-29, 2009.
11. Morrow, N.R., Tang, G-Q. Valat, M. and Xie, X.: "Prospects of Improved Oil Recovery Related to Wettability and Brine Composition," *Journal of Petroleum Science and Engineering*, Vol. 20, Issues 3-4, June 1996, pp. 267-276.
12. Austad, T., Strand, S., Hognesen, E.J. and Zhang, P.: "Seawater as IOR Fluid in Fractured Chalk," SPE paper 93000, presented at the SPE International Symposium on Oil Field Chemistry, The Woodlands, Texas, February 2-4, 2005.
13. Austad, T., Strand, S., Madland, M.V., Puntervold, T., et al.: "Seawater in Chalk: An EOR and Compaction Fluid," *SPE Reservoir Evaluation & Engineering*, Vol. 11, Issue 4, August 2008, pp. 648-654.

14. Strand, S., Hognesen, E.J. and Austad, T.: "Wettability Alteration of Carbonates — Effects of Potential Determining Ions (Ca^{2+} and SO_4^{2-}) and Temperature," *Colloids and Surfaces A: Physicochemical Engineering Aspects*, Vol. 275, Issues 1-3, March 2006, pp. 1-10.

15. Zhang, P. and Austad, T.: "Wettability and Oil Recovery from Carbonates: Effects of Temperature and Potential Determining Ions," *Colloids and Surfaces A: Physicochemical and Engineering Aspects*, Vol. 279, Issues 1-3, May 2006, pp. 179-187.

16. Yousef, A.A., Al-Saleh, S., Al-Kaabi, A.U. and Al-Jawfi, M.S.: "Laboratory Investigation of Novel Oil Recovery Method for Carbonate Reservoirs," SPE paper 137634, presented at the Canadian Unconventional Resources and International Petroleum Conference, Calgary, Alberta, Canada, October 19-21, 2010.

17. Yousef, A.A., Al-Saleh, S. and Al-Jawfi, M.S.: "SmartWater Flooding for Carbonate Reservoirs: Salinity and Role of Ions," SPE paper 141082, presented at the SPE Middle East Oil and Gas Show and Conference, Manama, Bahrain, September 25-28, 2011.

18. Yousef, A.A., Al-Saleh, S. and Al-Jawfi, M.S.: "The Impact of the Injection Water Chemistry on Oil Recovery from Carbonate Reservoirs," SPE paper 154077, presented at the SPE EOR Conference at Oil and Gas West Asia, Muscat, Oman, April 16-18, 2012.

19. Yousef, A.A., Al-Saleh, S. and Al-Jawfi, M.S.: "Improved/Enhanced Oil Recovery from Carbonate Reservoirs by Tuning Injection Water Salinity and Ionic Content," SPE paper 154076, presented at the SPE Improved Oil Recovery Symposium, Tulsa, Oklahoma, April 14-18, 2012.

20. Yousef, A.A., Liu, J., Blanchard, G., Al-Saleh, S., et al.: "SmartWater Flooding: Industry's First Field Test in Carbonate Reservoirs," SPE paper 159526, presented at the SPE Annual Technical Conference and Exhibition, San Antonio, Texas, October 8-10, 2012.

21. Abdallah, W. and Gmira, A.: "Wettability Assessment and Surface Compositional Analysis of Aged Calcite treated with Dynamic Water," *Energy & Fuels*, Vol. 28, Issue 3, 2014, pp. 1652-1663.

22. Alotaibi, M.B. and Yousef, A.A.: "The Impact of Dissolved Species on the Reservoir Fluids and Rock Interactions in Carbonates," SPE paper 177983, presented at the SPE Saudi Arabia Section Annual Technical Symposium and Exhibition, al-Khobar, Saudi Arabia, April 21-23, 2015.

23. Alvarado, V., Bidhendi, M.M., Garcia-Olvera, G., Morin, B., et al.: "Interfacial Viscoelasticity of Crude Oil Brine: An Alternative EOR Mechanism in Smart Waterflooding," SPE paper 169127, presented at the SPE Improved Oil Recovery Symposium, Tulsa, Oklahoma, April 12-16, 2014.

24. Alves, D.R., Carneiro, J.S.A., Oliveira, L.F., Facanha Jr., F., et al.: "Influence of the Salinity on the Interfacial Properties of a Brazilian Crude Oil Brine Systems," *Fuel*, Vol. 118, February 2014, pp. 21-26.

25. Ayirala, S.C., Saleh, S.H. and Yousef, A.A.: "Microscopic Scale Study of Individual Water Ion Interactions at Complex Crude Oil-Water Interface: A New SmartWater Flood Recovery Mechanism," SPE paper 179590, presented at the SPE Improved Oil Recovery Conference, Tulsa, Oklahoma, April 11-13, 2016.

26. Gmira, A., Al-Enezi, S.M. and Yousef, A.A.: "Interfacial Rheology at the Crude Oil/Brine Interface — A Microscopic Insight of SmartWater Flood," poster presented at the 19th European Symposium on Improved Oil Recovery, Stavanger, Norway, April 24-27, 2017.

27. Lashkarbolooki, M., Ayatollahi, S. and Riazi, M.: "Effect of Salinity, Resin, and Asphaltene on the Surface Properties of Acidic Crude Oil/SmartWater/Rock System," *Energy & Fuels*, Vol. 28, Issue 11, November 2014, pp. 6820-6829.

28. Aslan, S., Najafabadi, N.F. and Firoozabadi, A.: "Non-monotonicity of the Contact Angle from NaCl and $MgCl_2$ Concentrations in Two Petroleum Fluids on Atomistically Smooth Surfaces," *Energy & Fuels*, Vol. 30, Issue 4, March 2016, pp. 2858-2864.

29. Christy, A.A., Ozaki, Y. and Gregoriou, V.G.: *Modern Fourier Transform Infrared Spectroscopy, Vol. 35*, 1st edition, Elsevier Science: Amsterdam, 2001, 376 p.

30. Derrick, M.R., Stulik, D.C. and Landry, J.M.: *Infrared Spectroscopy in Conservation Science. Scientific Tools for Conservation*, Los Angeles, California: Getty Conservation Institute, 1999, 248 p.

31. Stuart, B.H.: *Infrared Spectroscopy: Fundamentals and Applications*, John Wiley and Sons Ltd., NY, 2004, 244 p.

32. Lagerge, S., Rousset, P., Zoungrana, T., Douillard, J.M., et al.: "Adsorption of Benzoic Acid from Organic Solvents on Calcite and Dolomite: Influence of Water," *Colloids and Surfaces A: Physicochemical and Engineering Aspects*, Vol. 80, Issues 2-3, December 1993, pp. 261-272.

33. Madsen, L., Grahl-Madsen, L., Gron, C., Lind, I., et al.: "Adsorption of Polar Aromatic Hydrocarbons on Synthetic Calcite," *Organic Geochemistry*, Vol. 24, Issue 12, December 1996, pp. 1151-1155.

34. Rezaei Gomari, K.A., Hamouda, A.A. and Denoyel, R.: "Influence of Sulfate Ions on the Interaction between Fatty Acids and Calcite," *Colloids and Surfaces A: Physicochemical and Engineering Aspects*, Vol. 287, Issues 1-3, September 2006, pp. 29-35.

35. Mihajlović, S.R., Vučinić, D.R., Sekulić, Z.T., Milićević, S.Z., et al.: "Mechanism of Stearic Acid Adsorption to Calcite," *Powder Technology*, Vol. 245, September 2013, pp. 208-216.

36. Tanur, A.E., Gunari, N., Sullan, R.M.A., Kavanagh, C.J., et al.: "Insights into the Composition, Morphology, and Formation of the Calcareous Shell of the Serpulid *Hydroides dianthus*," *Journal of Structural Biology*, Vol. 169, Issue 2, February 2010, pp. 145-160.

37. Long, X., Nasse, M.J., Ma, Y. and Qi, L.: "From Synthetic to Biogenic Mg Containing Calcites: A Comparative Study Using FTIR Microspectroscopy," *Physical Chemistry Chemical Physics*, Vol. 14, 2012, pp. 2255-2263.

38. Wei, B., Lu, L., Li, Q., Li, H., et al.: "Mechanistic Study of Oil/Brine/Solid Interfacial Behaviors during Low-Salinity Waterflooding Using Visual and Quantitative Methods," *Energy & Fuels*, Vol. 31, Issue 6, May 2017, pp. 6615-6624.

39. Al-Hashim, H., Kasha, A., Abdallah, W. and Sauerer, B.: "Impact of Modified Seawater on Zeta Potential and Morphology of Calcite and Dolomite Aged with Stearic Acid," *Energy & Fuels*, Vol. 32, Issue 2, January 2018, pp. 1644-1656.

40. Chen, L., Zhang, G., Wang, L., Wu, W., et al.: "Zeta Potential of Limestone in a Large Range of Salinity," *Colloids and Surfaces A: Physicochemical and Engineering Aspects*, Vol. 450, May 2014, pp. 1-8.

About the Authors

Dr. Ahmed Gmira

Ph.D. in Physico-Chemistry, University of Orléans

Dr. Ahmed Gmira is a Petroleum Scientist with the SmartWater Team of Saudi Aramco's Exploration and Petroleum Engineering Center – Advanced Research Center (EXPEC ARC). His main interests are enhanced oil recovery, SmartWater Flooding, fluids-fluids interfaces and fluids-rocks interfaces.

Ahmed joined Saudi Aramco in April 2015. Prior to this, he worked as a Research Scientist in the Schlumberger Research Centers in Dhahran, Saudi Arabia, and in Rio de Janeiro, Brazil. He also worked as a Research Fellow in a postdoctoral position with the Department of Physics at the Norwegian University of Science and Technology, Trondheim, Norway.

Ahmed received his Ph.D. degree in Physico-Chemistry from the University of Orléans, Orléans, France.

Dr. Mohamed A. Hammami

Ph.D. in Chemical Science, King Abdullah University of Science and Technology

Dr. Mohamed A. Hammami is a Postdoctoral Associate in the Department of Materials Science and Engineering, at Cornell University. His main interests are enhanced oil recovery, carbon dioxide foam, oil emulsions, and nanotechnology for smart release.

As part of his Ph.D. studies, Mohamed joined Saudi Aramco for a research internship working in the Reservoir Engineering Technology Division of the Exploration and Petroleum Engineering Center – Advanced Research Center (EXPEC ARC).

In 2012, he received his B.S. and M.S. degrees in Material Engineering from École Nationale Supérieure d'Ingénieurs Sud Alsace, Mulhouse, France. In 2017, Mohamed received his Ph.D. degree in Chemical Science from King Abdullah University of Science and Technology (KAUST), Thuwal, Saudi Arabia.

Dr. Sultan M. Al-Enezi

Ph.D. in Petroleum and Natural Gas Engineering, Pennsylvania State University

Dr. Sultan M. Al-Enezi is a Petroleum Engineering Specialist. Currently, he is the Group Leader of the Special Core Analysis (SCAL) Group with the Petrophysics Unit of Saudi Aramco's Exploration and Petroleum Engineering Center – Advance Research Center (EXPEC ARC). Previously, Sultan was the Focus Area Champion of the SmartWater Focus Area. His research interests include petrophysics, fluid flow in porous media, enhanced oil recovery, and digital rock physics.

Sultan is an active member of the Society of Petroleum Engineers (SPE), and has participated as co-chair, session chair, technical committee member, and discussion leader in various international SPE events.

He received his B.S. degree in Industrial Chemistry from King Fahd University of Petroleum and Minerals (KFUPM), Dhahran, Saudi Arabia. Sultan also received his M.S. and Ph.D. degrees in Petroleum and Natural Gas Engineering from Pennsylvania State University, University Park, PA.

Dr. Ali A. AlYousef

Ph.D. in Petroleum Engineering, University of Texas at Austin

Dr. Ali A. AlYousef is a Senior Petroleum Engineering Consultant and Chief Technologist of the Reservoir Engineering Technology Division in Saudi Aramco's Exploration and Petroleum Engineering Center – Advanced Research Center (EXPEC ARC). He has more than 25 years of experience in upstream research and technology. Since joining Saudi Aramco, Ali has been involved in applied research projects on improved oil recovery (IOR), waterflooding, and enhanced oil recovery (EOR). He played a pivotal role in planning, developing and implementing the EOR roadmap for the company.

Ali is currently leading more than 50 IOR/EOR scientists, engineers, and technicians. This group of IOR/EOR researchers are dedicated to the development of various EOR processes, including SmartWater, carbon dioxide, and chemical EOR technologies, as well as other novel processes with the clear target of meeting company objectives.

He is the recipient of Saudi Aramco's 2015 President and CEO Excellence Award. In 2016, Ali was the recipient of the prestigious Society of Petroleum Engineers (SPE) IOR Pioneer Award for his pioneering contributions made to the advancement of recovery technologies in the field of IOR/EOR. He also received the Kingdom's top prize, the prestigious award of the Custodian of The Two Holy Mosques Prize for Inventors and Talents in 2018.

Ali has written over 62 technical papers and reports and has more than 25 granted patents. He is currently an active member of SPE and has chaired several SPE workshops and forums, helped organize several petroleum engineering related conferences, and taught courses on IOR/EOR and waterflooding.

Ali received his B.S. degree in Chemical Engineering from King Fahd University of Petroleum and Minerals (KFUPM), Dhahran, Saudi Arabia, and his M.S. and Ph.D. degrees, both in Petroleum Engineering, from the University of Texas at Austin, Austin, TX.

Innovative Production Logging Solution Enabled Comprehensive Horizontal Well Evaluation in Challenging Downhole Conditions

Khaled J. Alsunnary, Mohammed S. Almuslem, Yousif A. Al-Abdulmohsin, Mustafa A. Bawazir, and Zouhir Zaouali

Abstract / Challenging downhole environments require an unconventional integrated production logging solution that is reliable and efficient. Production logging provides information during production operations and beyond. Subsequently, conventional production logging in extended reach horizontal wells, equipped with electric submersible pumps (ESPs), is complicated, as the locations of water- and oil-producing zones are uncertain due to the impurity of the borehole, caused by the presence of debris and thick material. Such downhole conditions affect the production logging tool sensors and lowers the measurement's resolution.

Downhole conditions can present challenges for cased hole and open hole evaluation programs, and each horizontal well presents a different complexity. The technique relies on the combination of the advanced multiphase production logging tool (PLT) and the pulsed neutron logging tool (PNLT). Measuring the flow rate downhole, the PNLT's data were acquired to complement the advanced multiphase PLT spinner data when flowing at both high and low choke settings, and shut-in surveys. The acquisition procedure is to allow unfavorable conditions to be logged at varying flow rates, to identify the fluid flow profile.

We have studied wells equipped with ESPs to gain insight into the job planning, deployment and integration of results for horizontal well production profiling. The examples illustrate the optimization performed during the job that led to successful execution. The first example is an open hole horizontal well logging case using a conventional logging solution. This is followed by the second well, showing the effect of a harsh environment in the open hole section on the logging tool and sensors. The last two field examples were recently logged, and the measurements and interpretation techniques are analyzed in detail in the article.

This innovative production logging solution has resulted in the successful assessment of downhole fluid entries with high confidence and safe operation despite the challenging downhole environment. Such logging is necessary to understand reservoir fluid dynamics, which is fundamental for effective reservoir management, and planning more efficient workovers.

Introduction

Horizontal wells are drilled to enhance reservoir performance by placing a long wellbore section within the reservoir. Horizontal drilling has reduced water and gas coning, because of reduced drawdown in the reservoir for a given production rate, thereby reducing the remedial work required in the future. Producing horizontal wells is certain to present new challenges for the artificial lift industry. Electric submersible pumps (ESPs), in particular, will play a key role in producing these wells due to their inherent ability to lift large volumes of fluid at low bottom-hole pressures. A rapid production decline and increase in water requires a deep understanding of the flow profile across the open hole horizontal section. This mandated the operators to run production logs to help unlock the full potential of horizontal wells. Elements contributing to a challenging logging environment include:

- The wellbore environment with a strong presence of scale, asphaltenes, wax, rocks, and bushy material.
- The hydrocarbon production by fracture network and faults.
- The highly deviated and horizontal well profiles.
- The downhole continuous multiphase flow.
- The downhole logging tool accessibility.
- The open hole completion.
- The ESP performance.

Fig. 1 *A diagram of the production tubing and use of the Y-tool.*

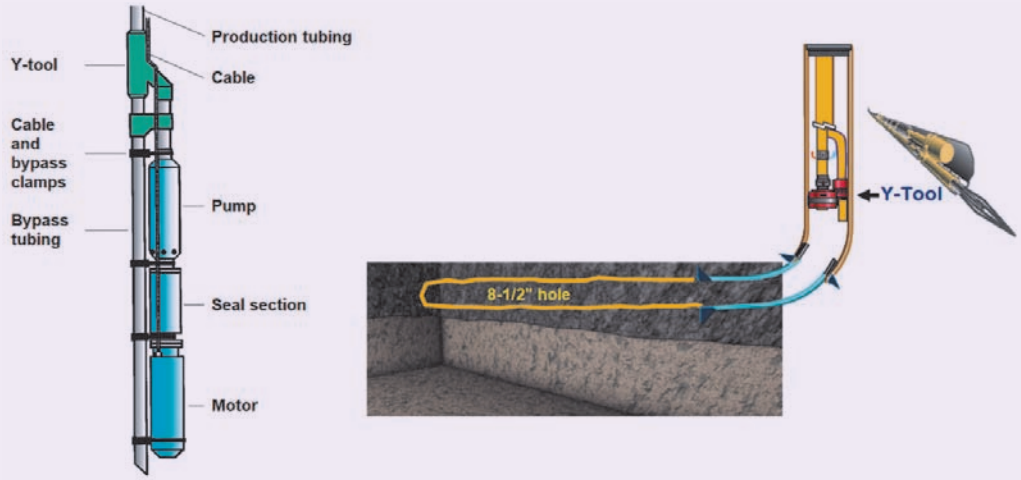

Fig. 2 *Three main types of flow regimes can occur in a two-phase (water-oil) system.*

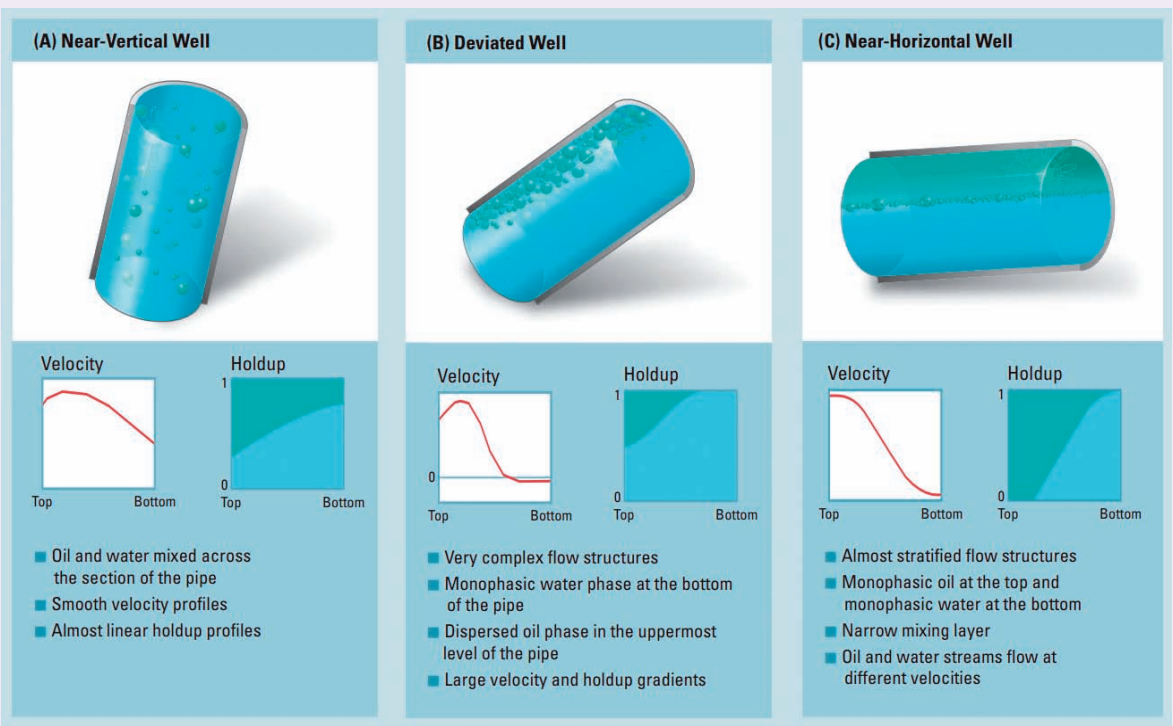

This article reviews field examples of the production logging campaign in horizontal wells equipped with ESPs, with a special emphasis on the operational and interpretation challenges experienced during the campaign. Background information on the tools used to establish the downhole profiles will be demonstrated. Furthermore, the article discusses the methodology used to diagnose this challenging environment and how accurate quantification of the downhole zonal oil and water flow contributions was obtained using a combination of the advanced multiphase production logging tool (PLT) and the pulsed neutron logging tool (PNLT).

Horizontal Well Access for Logging Operations

The Y-tool, Fig. 1, is installed on the production tubing, providing two separate conduits[1]. One conduit

is concentric with the production tubing and enables access to the reservoir below the ESP. The second conduit is offset, and used to support the ESP system.

The objective of the intervention is to perform production logging over the horizontal section with a coiled tubing (CT) logging plug through a single or dual Y-tool ESP completion. Considering the hole restrictions, the operation will include moving downward from the upper ESP bypass section to the lower ESP bypass section. The bottom-hole assembly consists of a CT plug, which includes a connector, a sleeve and a bottom crossover. These parts are covered by the CT plug's external body, which has a seal assembly in addition to the PLT. The CT plug is required to prevent production circulation across the bypass section while operating the ESP[2].

In addition, the challenge of reaching maximum achievable depth and obtaining useful measurements is further complicated by the increasingly complex well configurations. Friction is created within the fluid as it flows through small-diameter tubulars or similar restrictions. Utilizing the friction reduction for logging tools in cased holes allows wireline services to reach further in deviated wells, and increases data quality through a smoother movement.

Advanced Multiphase PLT — Visualize the Flow Regimes

Knowledge of expected flow regimes allows operators to choose measurements suitable for the downhole

Fig. 3 *The advanced multiphase PLT provides scanning features and real-time continuous flow rates.*

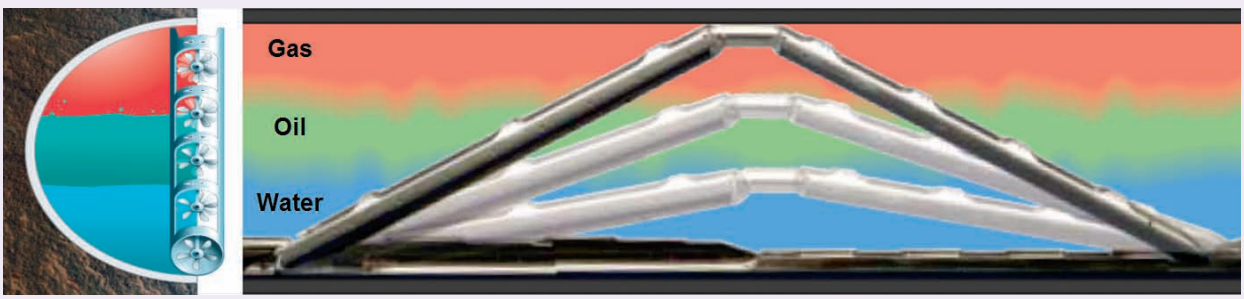

Fig. 4 *A diagram of the three-phase holdup log determination from the PNLT.*

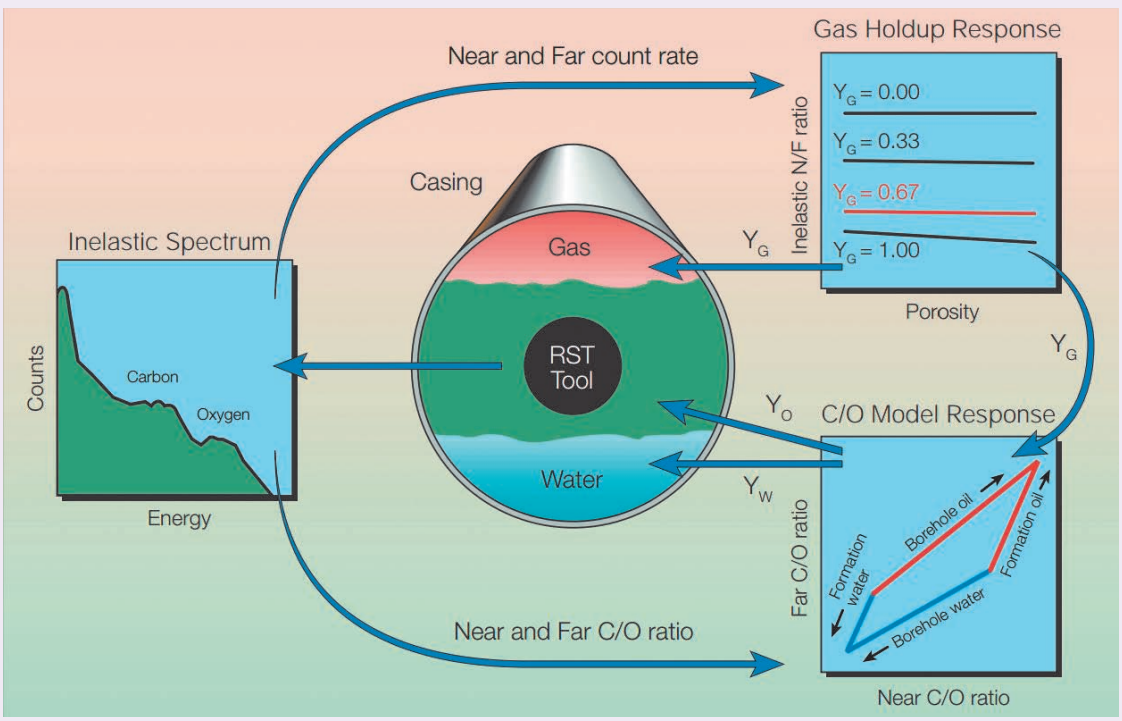

Fig. 5 *The water flow log acquisition from the PNLT.*

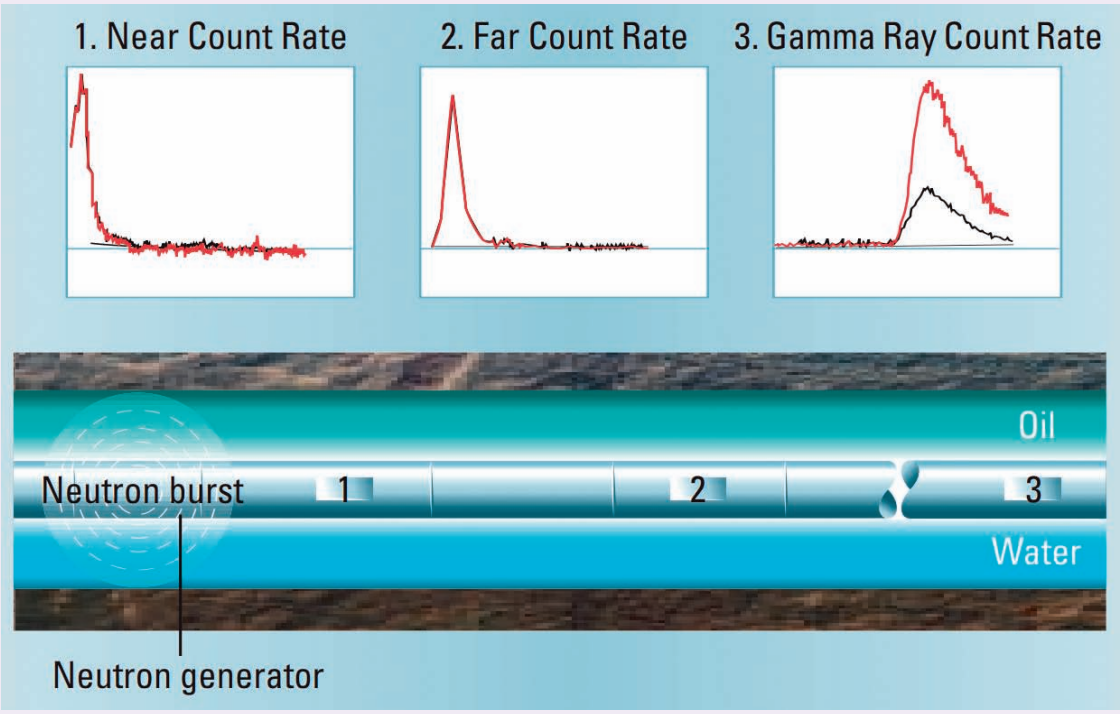

Fig. 6 *Images showing the strong presence of scale, wax, rocks, and metal from the wellbore.*

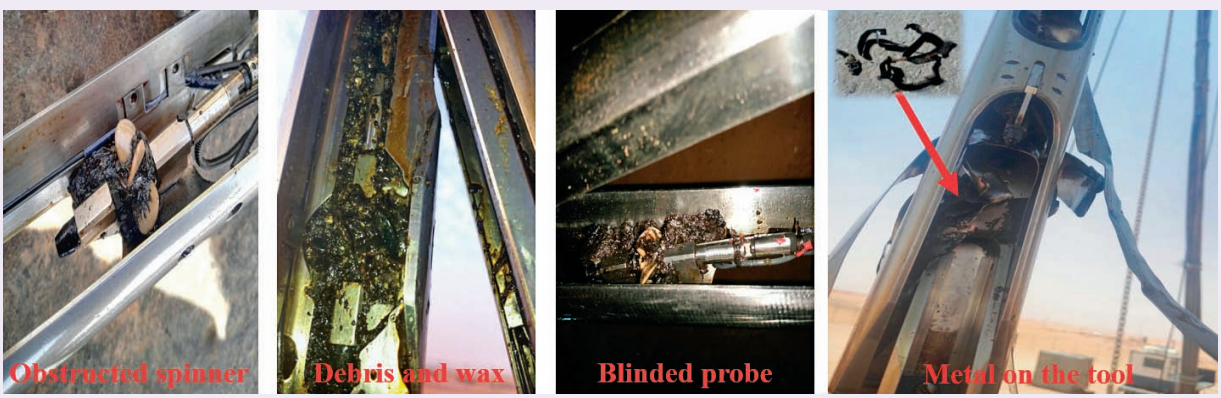

Fig. 7 *A diagram of the advanced multiphase PLT and pulsed neutron log integrated into one string.*

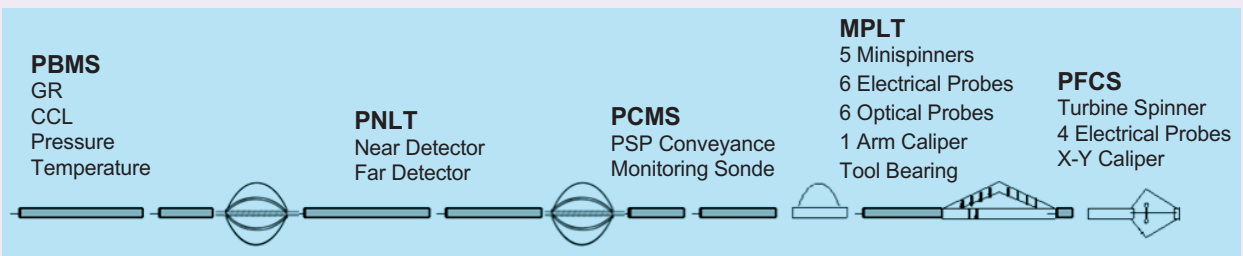

Fig. 8 *Well-X: The advanced multiphase production logging answer in an open hole completion.*

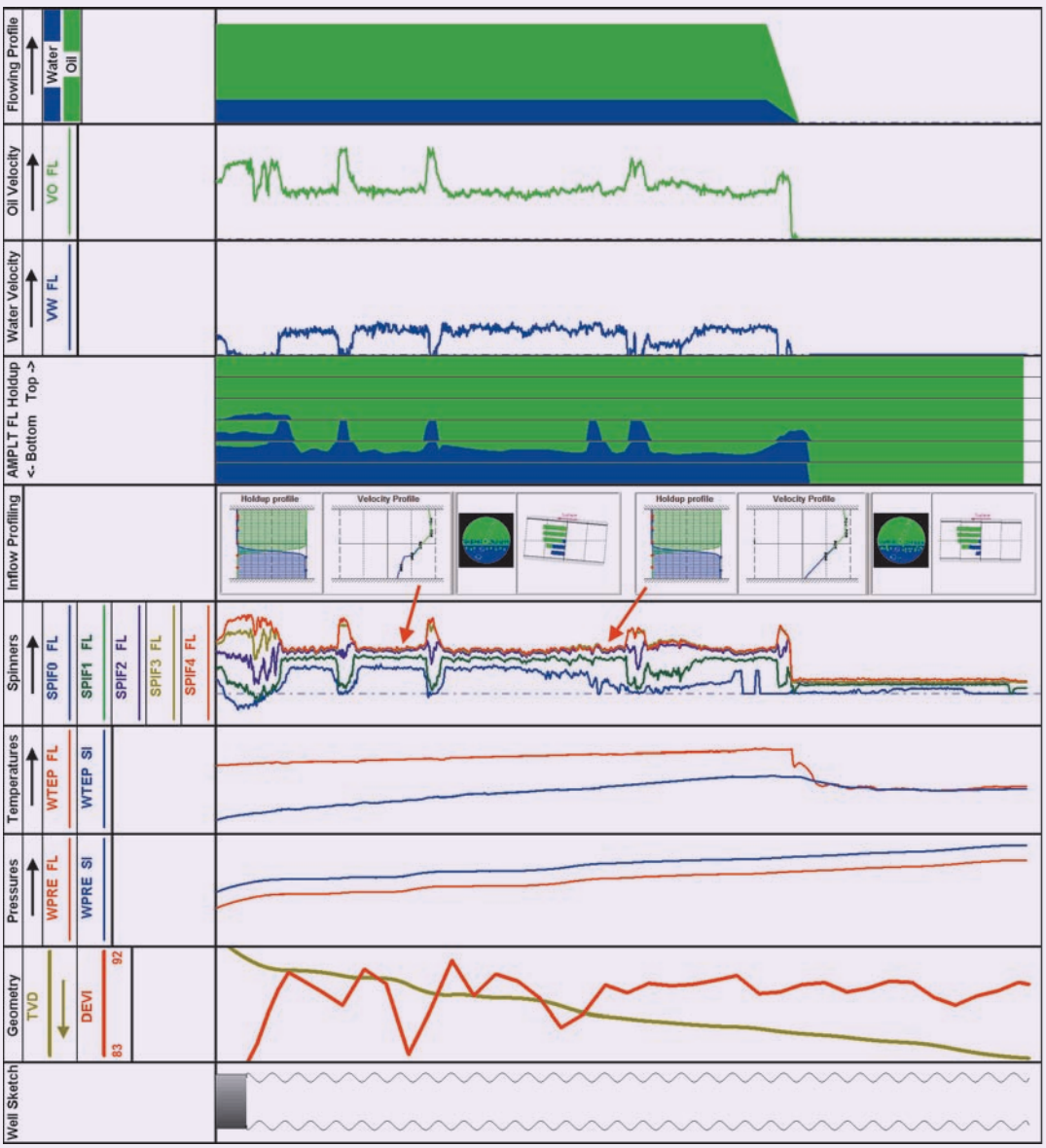

conditions[3], Fig. 2.

In horizontal and deviated wells, advanced multiphase PLTs, optimized for three-phase production logging, provides a complete analysis of complex downhole flow regimes[4]. This advanced multiphase PLT consists of two retractable arms that are equipped with sensors for deployment along the vertical diameter of the wellbore. Five directional mini-spinners are mounted across the vertical axis of the pipe (spinners 0, 1, 2, 3, and 4) to measure the phase velocity profile, Fig. 3. On the other arm, two arrays of six electrical probes (e-probes) and six optical probes are placed to scan water and gas holdup, respectively. In addition, the tool string includes an eccentralizer, relative bearing, pressure, temperature sonde, casing collar locater, knuckle joints, gamma ray, and platform flow meter caliper sonde sensors[5].

The PNLT is a combined pulsed neutron capture and pulsed neutron spectroscopy logging tool capable of evaluating oil saturation in a wide range environment. The PNLT has also been developed for use in production logging applications. This includes the three-phase holdup log from pulsed neutron measurements and the water flow log measurements[6].

The three-phase holdup log is a technique for measuring the holdup of water, oil, and gas phases in the borehole using the slim $1^{11}/_{16}$" PNLT. This technique was developed especially for horizontal wells where the wellbore fluids tend to segregate, but it can also be applied in vertical wells. Figure 4 is a diagram of the

Fig. 9 *Well-A: The advanced multiphase PLT spinners' data from the shut-in survey confirmed the accumulation of debris downhole.*

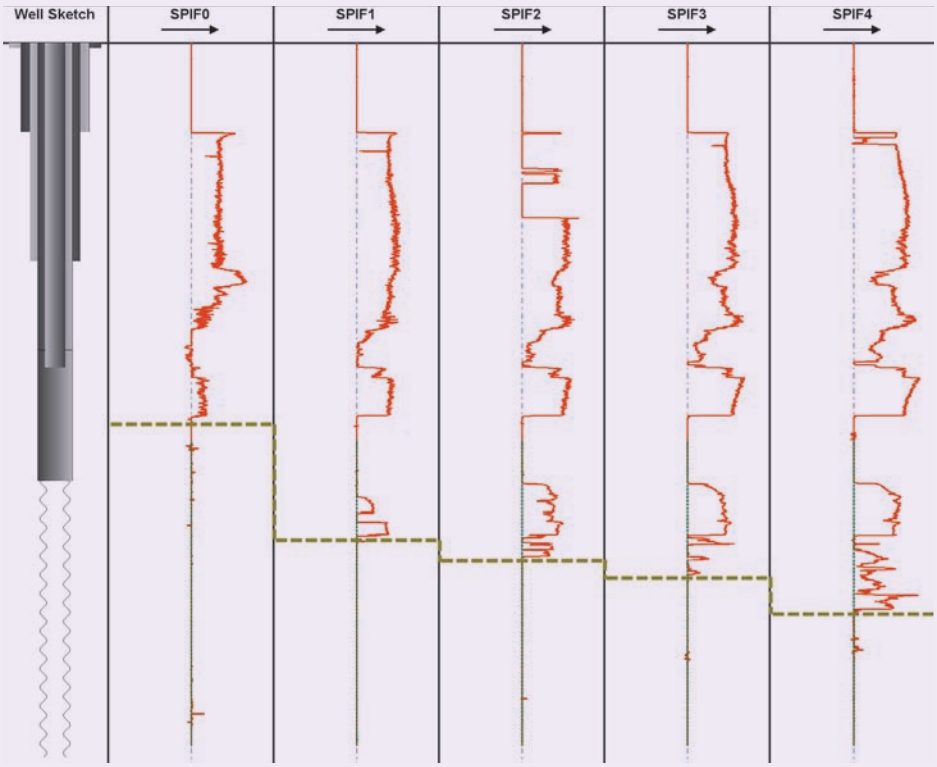

three-phase holdup log, which uses the yields-based carbon-oxygen ratios from the near and far detectors that are primarily sensitive to oil and water[7], and a net inelastic (capture background removed) count rate ratio between the detectors for providing information about borehole gas.

The water flow log is based on neutron activation of oxygen. The basic principle involves the activation of oxygen atoms of the moveable water near the PNLT, and the measurement of the subsequent released gamma rays on the PNLT detectors, mounted downstream of the neutron source[8]. Measuring the time from the neutron source to the peak of the detector signal and using the distance from the pulsed neutron generator to the detector allows a velocity to be computed, Fig. 5.

Furthering the Capabilities of Production Logging in Horizontal Wells

Although information gathering is an important objective, it should remain subordinate to well condition and integrity considerations. Therefore, it is important to ensure that the cost of acquisition can be justified by the value of information generated. Thereafter, the information is effectively managed.

Figure 6 shows several mechanical devices — advanced multiphase PLTs — that have been strongly influenced by the scale, wax, rocks, and metal material sticking to the logging tool. Exposing the advanced multiphase PLT to such severe conditions caused severe damage to the sensors and wires.

Achieving the logging objectives in such a harsh downhole environment is one of the challenges. The other challenge is to provide quality wireline measurements. Because of the expectation of dirty boreholes in these complex conditions, the wellbore environment will limit the advanced multiphase PLT measurements. Therefore, the pulsed neutron log, including the water flow log and the three-phase holdup log, will be integrated into one string with the advanced multiphase PLT to provide confident results, Fig. 7. Leak detection is another application of this integration between the logging tools[9].

Proactive Approach for Profiling Horizontal Wells in a Sensible Wellbore Enviornment

This approach is an opportunity to improve the existing conventional production logging process. Many benefits can be accrued if it is implemented as the main part of the horizontal well evaluation. It can help production, technical, and field engineers to operate effectively in unfavorable wellbore environments. The approach is summarized into four main sections as follows.

Data Gathering

The following procedures should be considered when collecting the data:

1. Discuss the job objectives, logging procedure, and

Fig. 10 *Well-A: The advanced multiphase PLT and pulsed neutron logging integrated answer.*

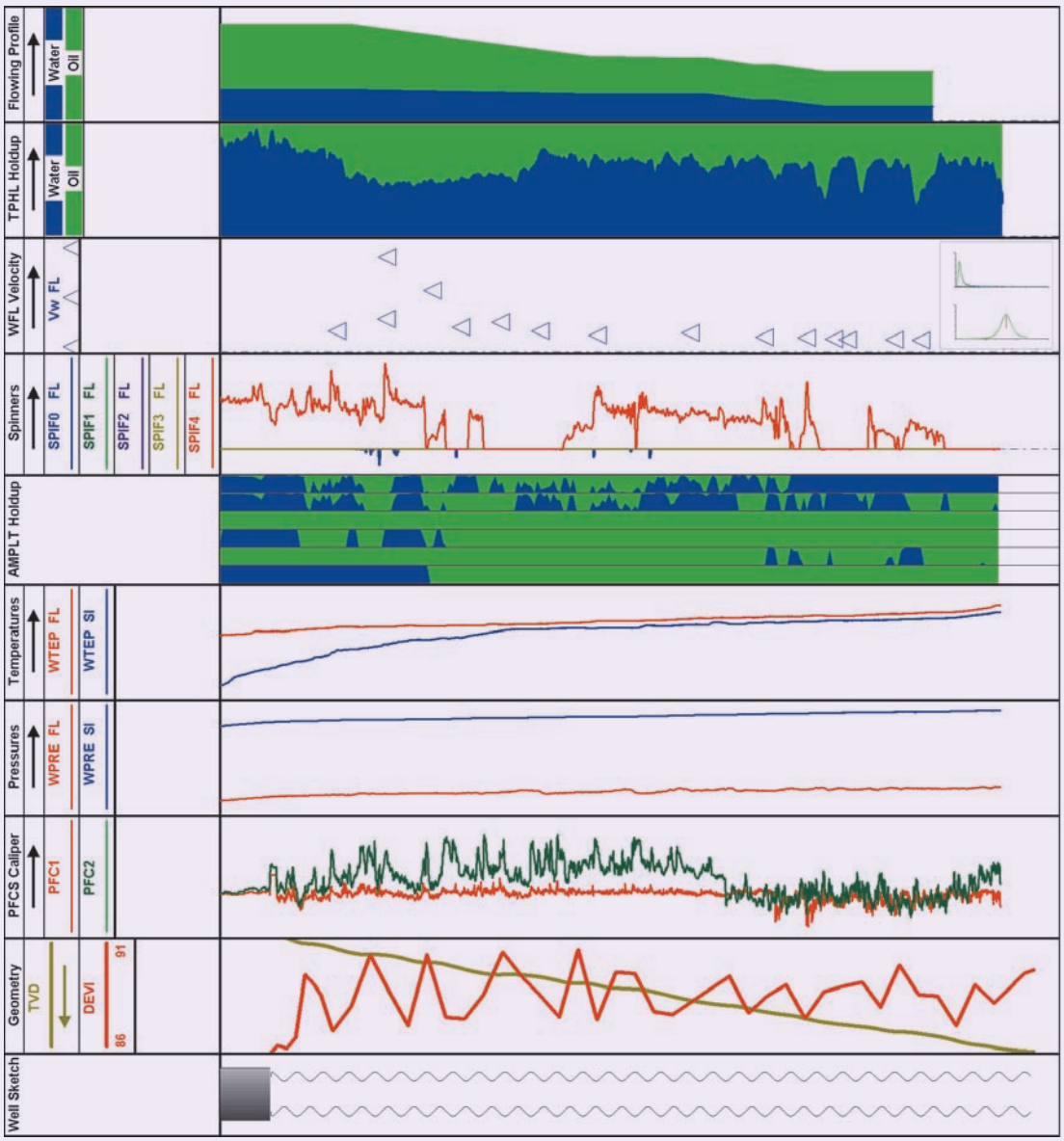

required equipment:

- If debris and scale are expected, get agreement to run the advanced multiphase PLT and PNLT in a single run.
- If debris and scale are not expected, get agreement whether the PNLT is required on-site or not.

2. Verify the reliability of the surface rate measurement, and that it shows a sufficient water rate that can be detected by the tool.
3. Collect relevant well information to ensure effective data acquisition, such as well history, completion detail, open hole and cased hole data — logs and images — and deviation data.
4. Perform conveyance simulation modeling to determine the conveyance method and limitation at the depth reached.
5. Take extra measures if high temperature, hydrogen sulfide, or carbon dioxide is present in the wellbore.
6. Prepare a logging plan if the well is dead or stops flowing.

Sticky Material Mapping

Scale deposition during the production of crude oil is costly and troublesome. Scale can be deposited in any area of an oil production facility, but most damage occurs in the near wellbore area and inside the ESP. In addition, collecting samples of different materials has always been preferred prior to the acquisition.

Fig. 11 *Well-B: The advanced multiphase PLT and PNLT acquired data from a high flow rate survey.*

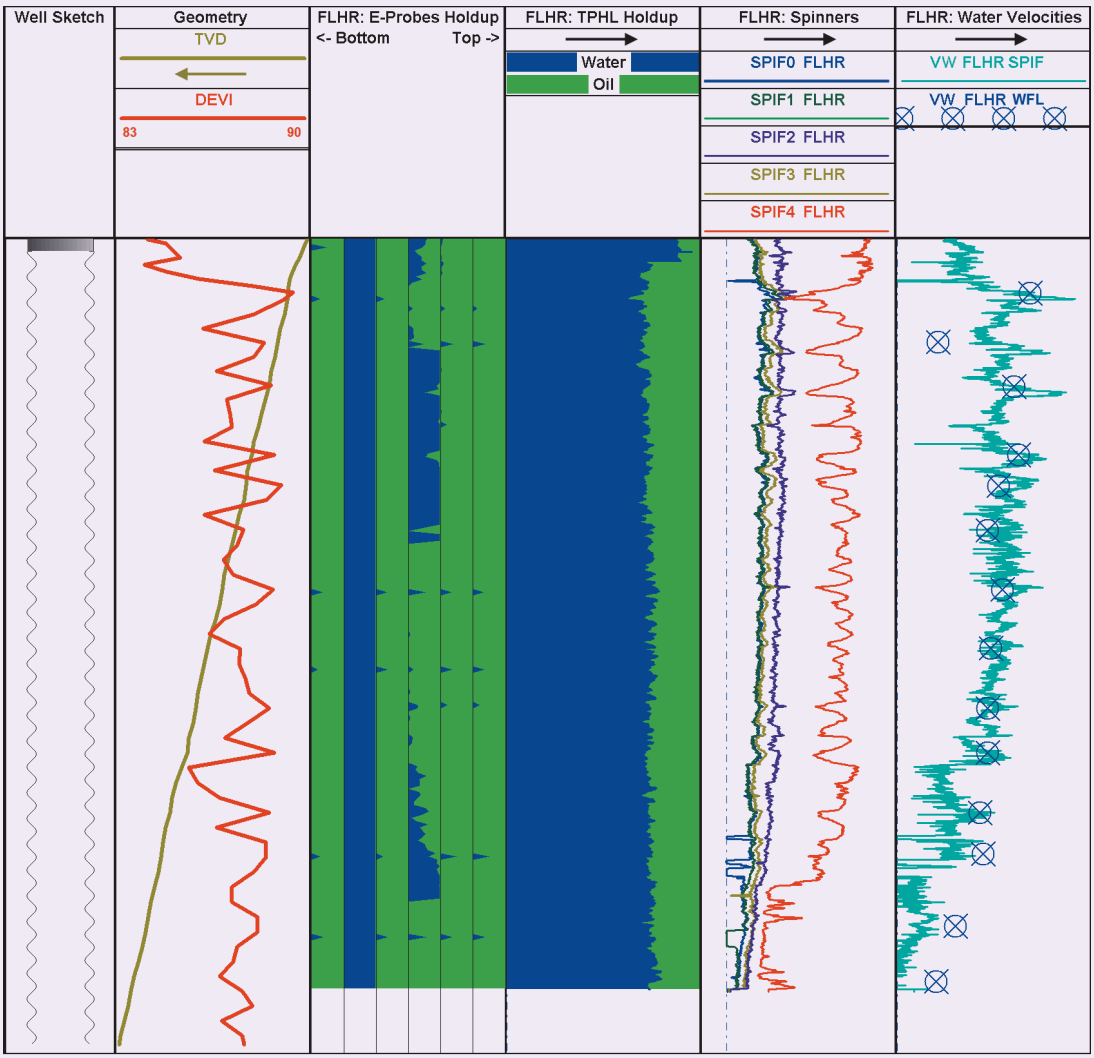

A successful mapping inspection is the result of the combination of a high probability of sticky material present with the confidence that the full area of interest has been totally covered. The existence of such data will guide the operators to clean up the wells properly before running in the hole. This will improve the logging resolution and will reduce the logging tool sensitivity to the presence of debris.

Laboratory Analysis

In production systems, changes in temperature, the decline of the reservoir pressure, or the change in chemical composition of the crude oil by the addition of miscible solvents combined with the streaming potential effects in the well tubing affects the asphaltene solubility. Laboratory investigation is necessary to develop an inhibitor for preventing the precipitation of scales in oil reservoirs and production equipment.

Data Analysis — Advanced Multiphase PLT and PNLT

In advanced multiphase PLT analysis, data processing of acquired data and interpretation are conducted to determine water entries and flow rate computations. The PNLT interpretation involves calculating the water velocity from the PNLT water flow log stations while the water, oil, and gas holdups are obtained from the three-phase holdup log. The integrated advanced multiphase PLT and the PNLT interpretation involves calculating the total flow rate from the advanced multiphase PLT spinners and incorporating the PNLT three-phase holdup log and water flow log to compute the oil and water rates.

Case Studies — Data Acquisition and Results

The four logging examples discussed in this article are in the same field. Well-X did not show downhole

Fig. 12 *Well-B: The advanced multiphase PLT and PNLT acquired data from a low flow rate survey.*

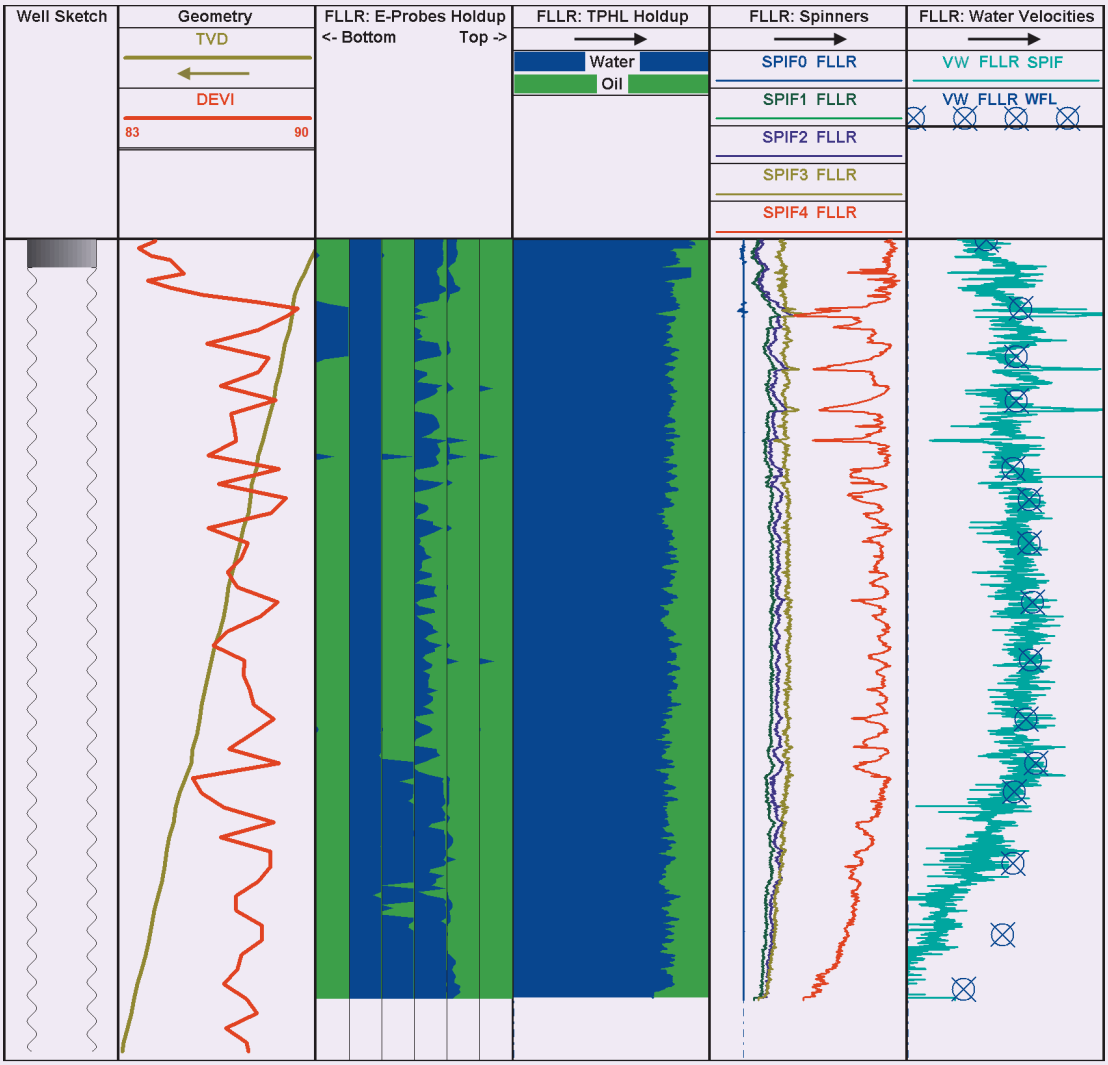

scale or debris deposits, and it serves as an example of conventional production logging acquisition in horizontal wells. Applications for the unconventional integrated production logging solution are demonstrated through the field examples of Well-A, Well-B, and Well-C. Washing with solvent to remove the deposits of scales was not done in Well-A. In contrast, Well-B and Well-C were logged after cleaning the wells of the sticky material. The wells were completed with a Y-block assembly to facilitate reservoir access.

As part of reservoir management logging requirements, the logs will be used to evaluate the well flow profile and determine the water entry zones and intervals. Also, the logging data will be cross-checked with the surface meter flow rate readings.

Example Well-X

Logging Job

The advanced multiphase PLT was conveyed using 1¾" CT with 99% coverage of the completed interval. The data shown in Fig. 8 is the log result of Well-X. The flowing survey (one choke setting) was performed prior to the shut-in survey. The well stabilized during the flowing passes. The comparison of flowing and shut-in passes showed pressure variation of up to 14 psi. The spinners and holdups reflected the inflow zones and the change in well deviation. The spinners at the top of the vertical axis (SPIF3 and SPIF4) read much faster rates than the bottom spinners (SPIF0 and SPIF1), clearly representing lighter fluid/oil and heavier fluid/water, respectively — at a deviation of 89.5°. The optical probes did not show any presence of gas.

Summary of Results

Based on the interpretation of all holdup, spinner, and

Fig. 13 *Well-B: The advanced multiphase PLT and PNLT acquired data from the shut-in survey.*

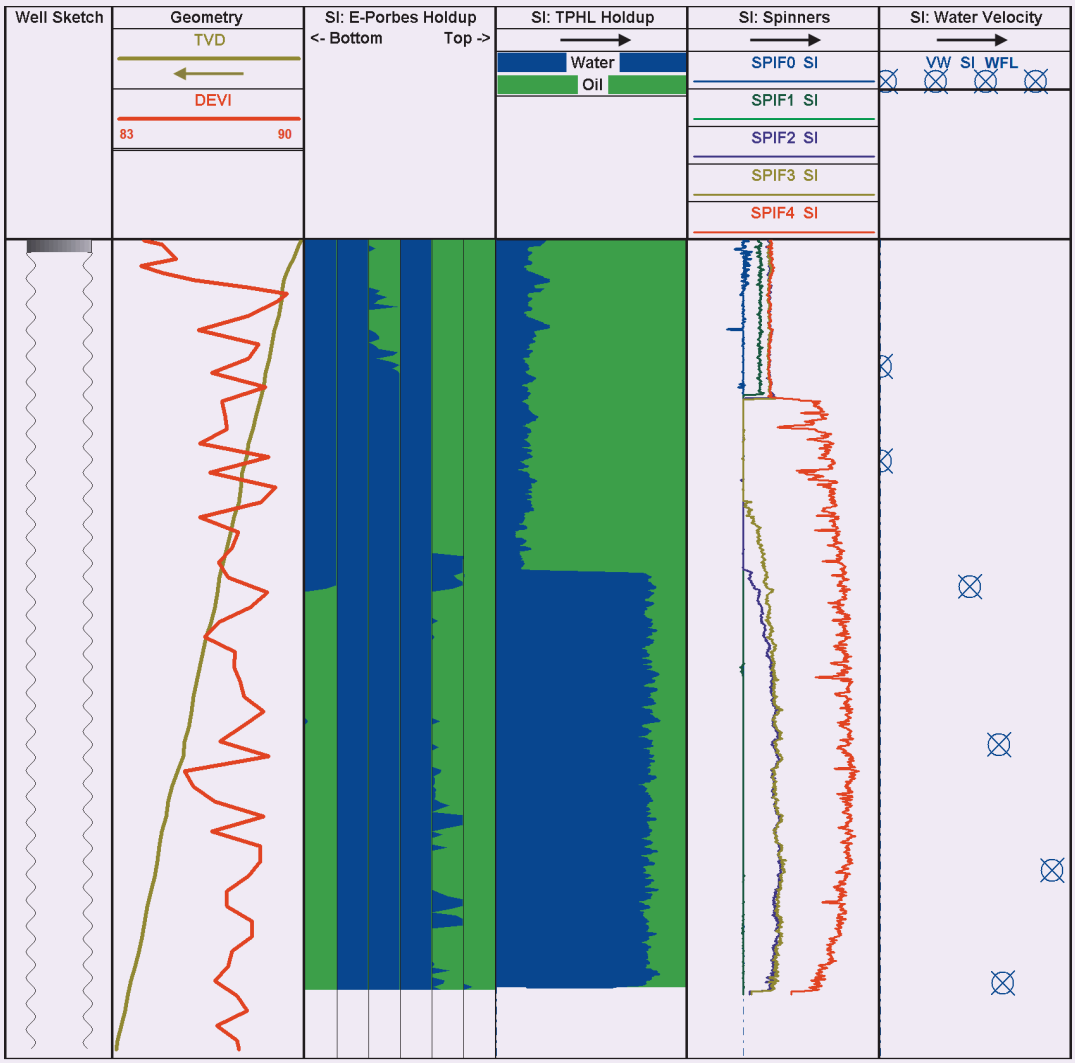

caliper data, the flow profile was generated. All the water and oil production are from the bottom logged interval. The temperature behavior showed that there was a fracture entry signature or superpermeability feature at this interval. Crossflow was not detected during the shut-in or flowing surveys. The flow profile cross sections displayed in Fig. 8 support the fluid interpretation.

Remedial Actions

Special considerations were made for the production logging results to isolate the water production interval. The workover operation was successfully completed to install the inflow control device (ICD) completion and the ESP system. ICDs with open hole packers were deployed to control the drawdown in each section of the horizontal well and to delay the accelerated water production. The measured surface rates showed that the ICD dramatically reduced the water cut.

Example Well-A

Logging Job

A preventive well clean out was not completed before the logging operation. The tool was conveyed using a 1¾" CT with 96% coverage of the completed interval. The shut-in survey was logged prior to the flowing survey. At shut-in logging, the spinner's responses indicated the accumulation of debris downhole. The spinners stopped rotating gradually — from bottom to top — in the horizontal section while logging the first shut-in down pass, Fig. 9. During the flowing survey, the well was relatively stable, and no choking effects were observed. The comparison between flowing pressures in the down and up passes showed maximum pressure variation up to 8 psi.

The two-arm caliper tool detected a possible washout interval in the open hole segment. Spinners 0, 1, 2, and 3 were sticky during flowing passes due to the

Fig. 14 *Well-B: The advanced multiphase production logging and pulsed neutron logging integrated answer.*

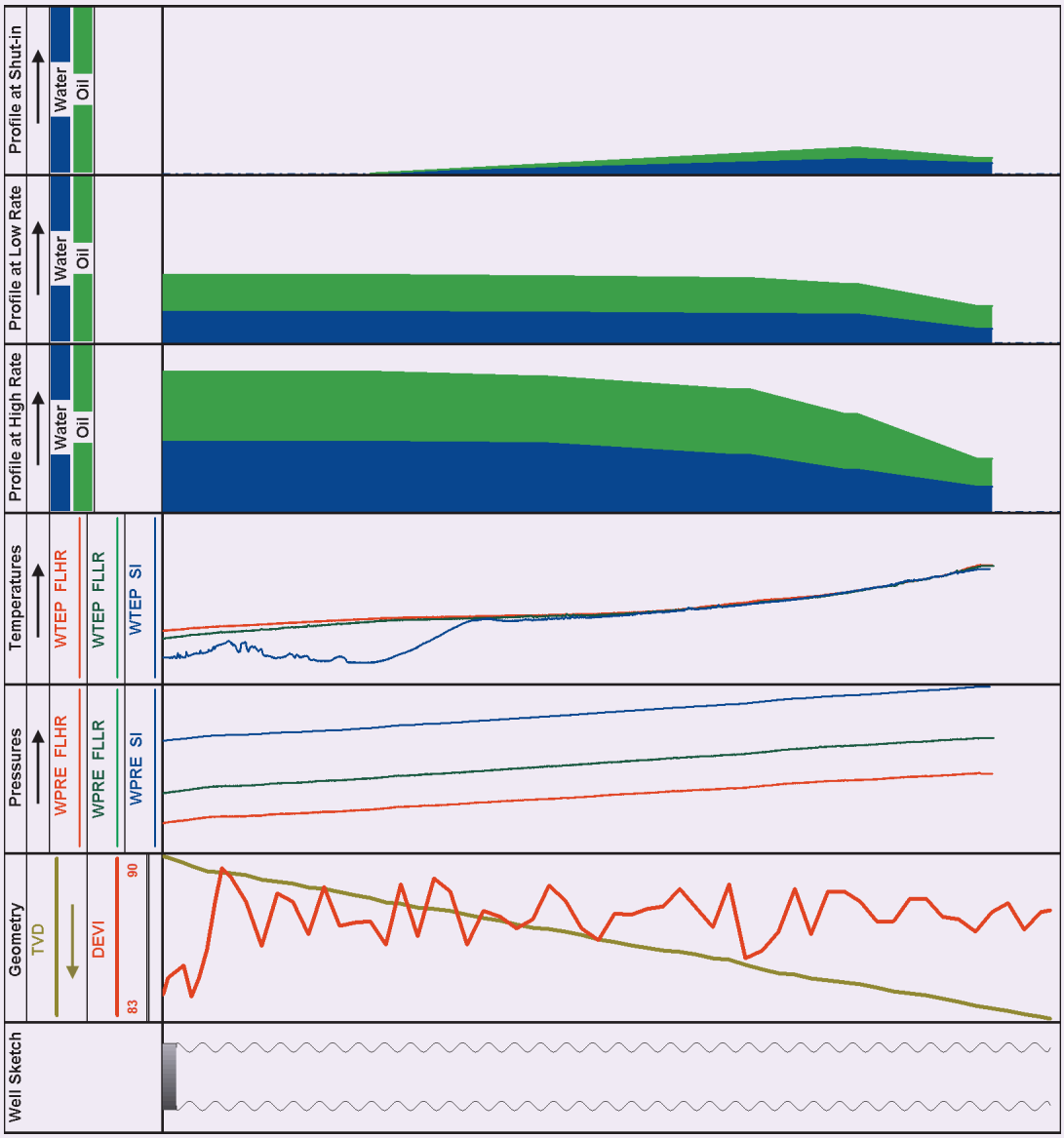

downhole condition. No spinner stationary measurement was recorded because the priority was given to acquire continuous down and up passes, and to get the spinners functioning.

The advanced multiphase PLT e-probes were blinded and not able to detect actual water holdup across the logged interval. Run_1 started with the advanced multiphase PLT. Then, the pulsed neutron logging data was logged after (Run_2) to complete the advanced multiphase PLT response, which was affected by debris and waxy material.

Summary of Results

During the shut-in survey, no crossflow was detected. Surface rates fluctuated during the job. During the flowing surveys, the combination between the advanced multiphase PLT and pulsed neutron logging data provided accurate quantification of water-oil zonal contributions. The main water and oil production zone was identified from the interval below the maximum logging depth reached. This was supported by the comparison between the flowing and shut-in temperature measurements, Fig. 10.

Example Well-B

Logging Job

A job to clean sticky material was successfully completed using 2" CT. The production logging acquisition tool was conveyed using a 2" CT with 93% coverage of the completed interval. The advanced multiphase PLT and PNLT were integrated into one tool string.

Fig. 15 *Well-C: The advanced multiphase PLT and PNLT acquired data from a high flow rate survey.*

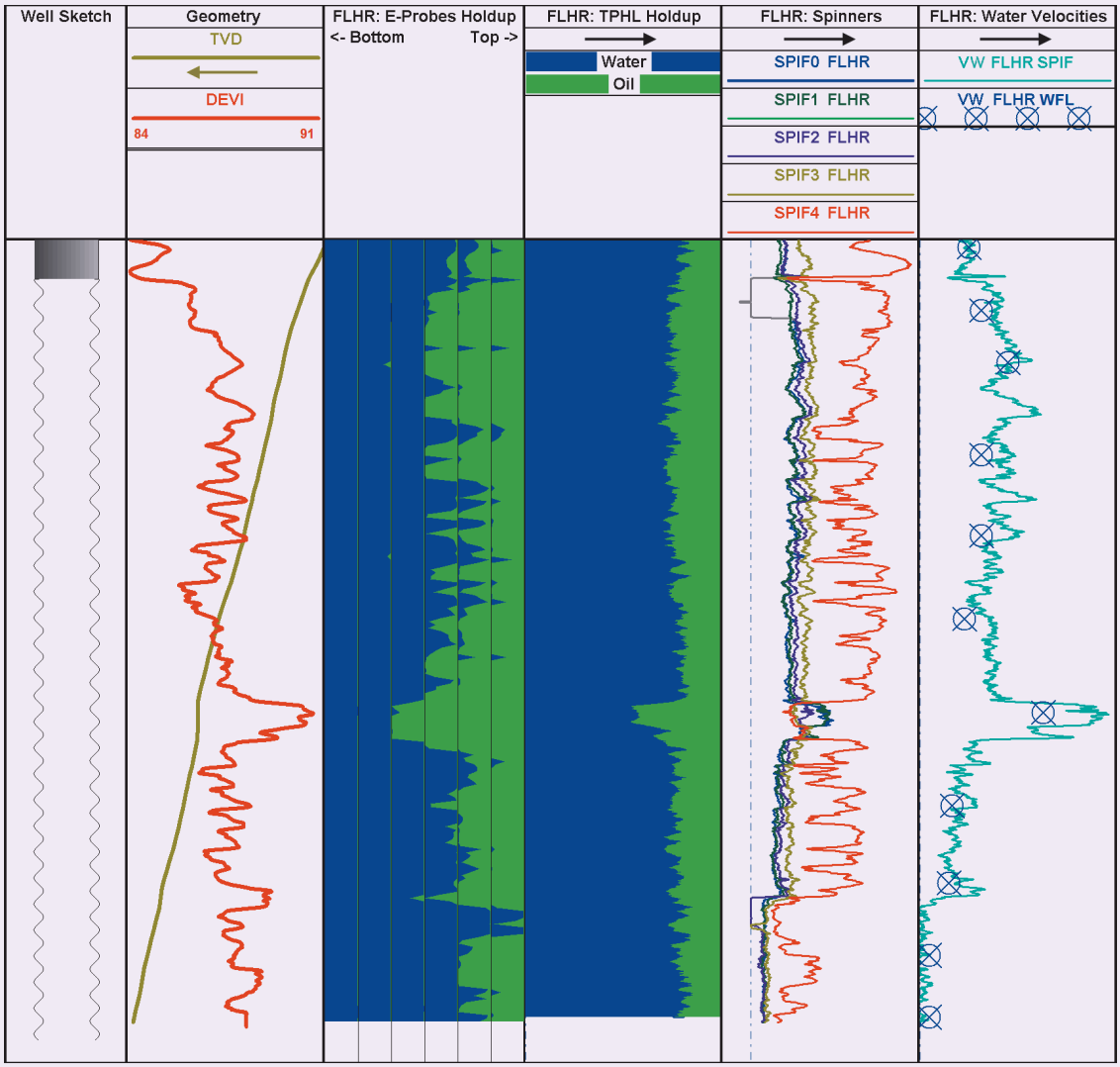

The well was logged at two flowing rates, high choke, Fig. 11, and low choke, Fig. 12. Figure 13 shows the data acquired from the shut-in survey.

The well was considered stable from the high rate, low rate, and shut-in surveys. In general, the down pass spinners' data were good and interpretable, whereas the up pass spinners' data were affected by downhole conditions. The calculated spinner and water flow log measured water velocities are compared in the sixth track, and they show a good match. The holdup from the e-probes did not match the three-phase holdup log. Spinner 4 was immersed in oil during all the surveys. The PNLT and water flow log three-phase holdup log data were acquired to complement the advanced multiphase PLT data in the three surveys.

Summary of Results

An upward crossflow of water and oil was observed during the shut-in survey. The water movement at shut-in was detected by the water flow log, because it was insignificant and below the minimum velocity required to rotate the spinners. For both the flowing choke settings, the downhole flow profile was considered as nonuniform because not all of the production interval was contributing to the total flow, and some zones were dominating the total production. The main intervals contributing water and oil were detected at both high and low flow rates, Fig. 14.

Example Well-C

Logging Job

Acid stimulation was successfully completed using 2" CT to remove suspected formation damage. The production logging acquisition tool was conveyed using a 2" CT with 99% coverage of the completed interval. The advanced multiphase PLT and PNLT were integrated in one tool string. The well flowed at

Fig. 16 *Well-C: The advanced multiphase PLT and PNLT acquired data from a low flow rate survey.*

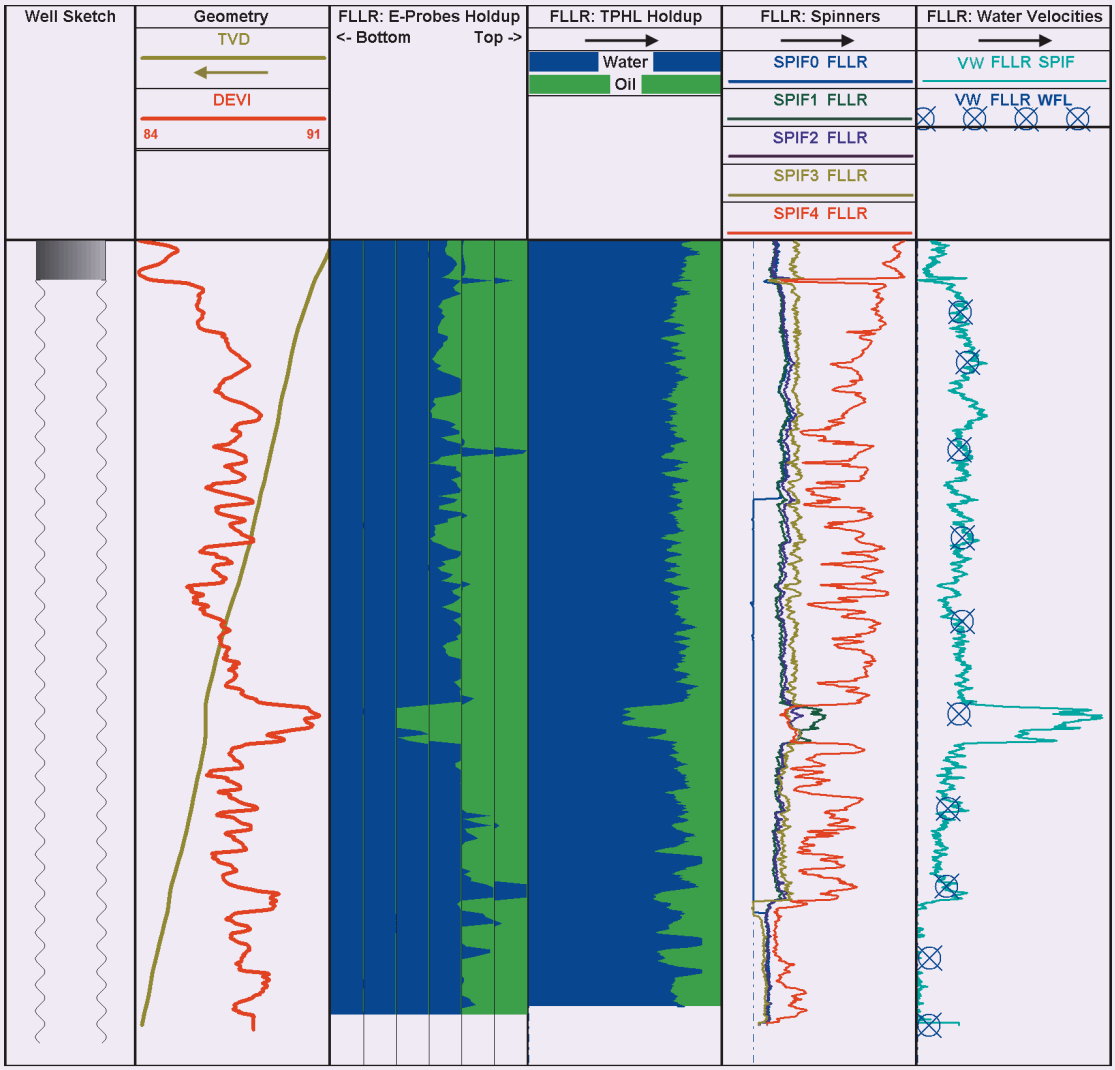

two different flow rates, Fig. 15 and Fig. 16, followed by a shut-in period, Fig. 17. During these surveys, the well was considered stable.

The advanced multiphase production logging and the pulsed neutron logging data were found comparable. Holdup from the e-probes matched the holdup from the three-phase holdup log. In general, both the down pass and up pass spinner data were good and interpretable. The analysis was performed based on the integration of the acquired measurements from the advanced multiphase PLT and the PNLT.

Summary of Results

The upward crossflow of water and oil was observed during the shut-in survey. The water movement at shut-in was detected by the water flow log and the spinners. For both flowing choke settings, the downhole flow profile was considered as nonuniform since not all the production interval was contributing to the total flow and some zones were dominating the total production. The main intervals contributing water were detected at both high and low flow rates, Fig. 18. The major fluid entry was supported by the temperature log, which showed a sharp deflection at the entry interval.

Conclusions

1. In this article, field cases of horizontal wells were discussed with the goal of understanding the production behavior and water breakthrough contrasts within a fractured carbonate reservoir.
2. The introduction of the proactive solution and the unconventional logging technique significantly broadens the range of logging interventions that can be performed. It also enables accessing reservoir data that in some cases, have been inaccessible and which can be key to the optimization of production management of entire fields.

Fig. 17 *Well-C: The advanced multiphase PLT and PNLT acquired data from the shut-in survey.*

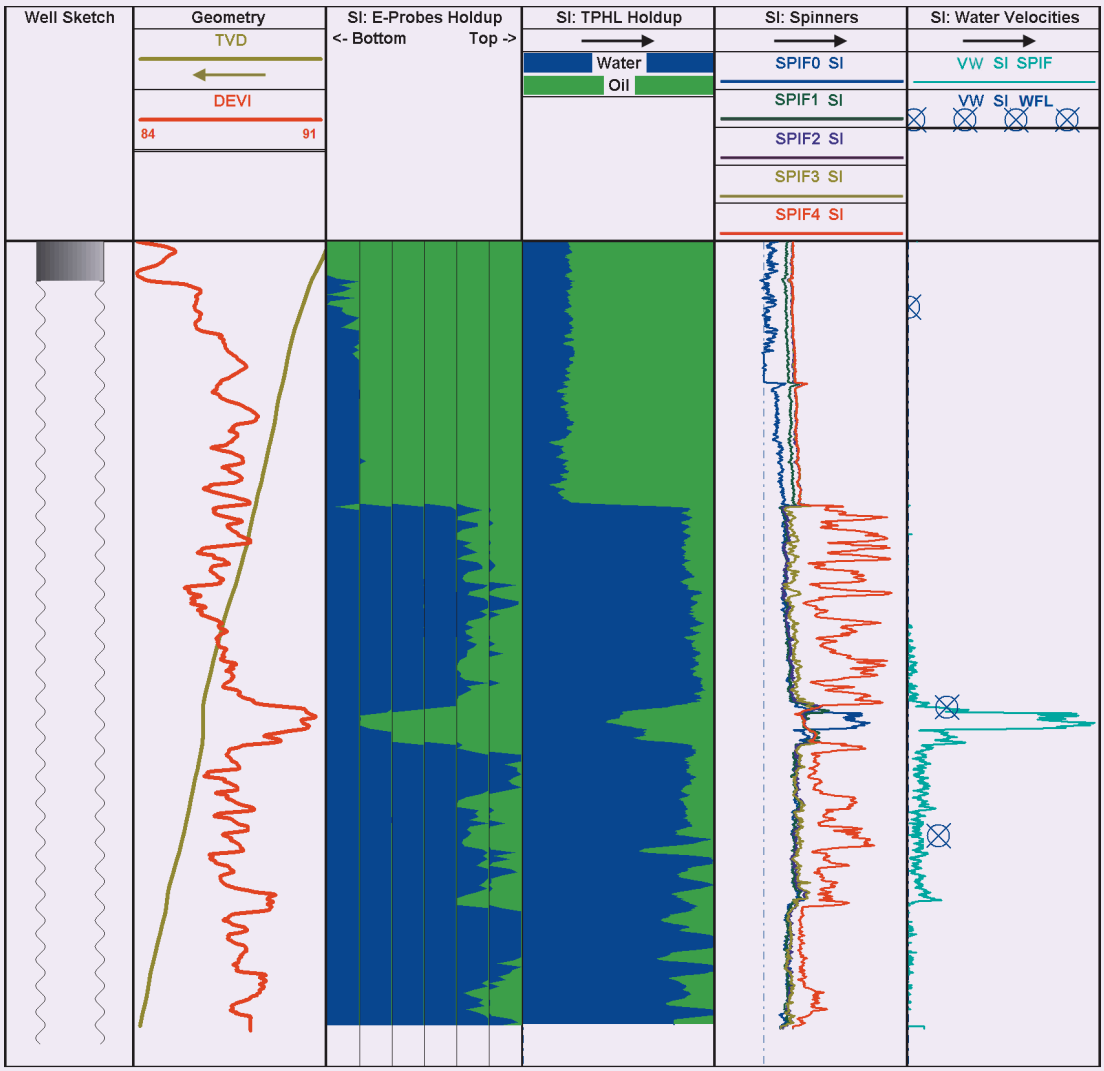

3. Production logging is pivotal in the enhanced oil recovery subject. The integration between advanced multiphase PLT and water flow log three-phase holdup log measurements through PNLT has been validated as an effective technique to obtain the water and oil rates.
4. Pumping/washing with solvent has a positive effect on removing scale deposits. The advantages of the clean out process are shown in the acquired data and results from Well-B and Well-C.

Recommendations

1. The preventive clean out with solvent has been fundamental to a successful deployment of the acquisition tool string in highly deviated profile wells, and the presence of high scale content.
2. Well conditions must be suitable; sufficient flow, stable flow, and clean fluids are required. All production aspects must be evaluated to choose the best technology, operational planning and logging sequence to support the quality logging acquisition, gather sufficient data, and promote well integrity.
3. Spinners should be checked for proper operation on the surface, and the tool string should be run centralized. Multiple passes, both up and down should be made, and stationary readings should also be taken. Also, repeat runs are desirable to confirm stable flow conditions.
4. Shut-in passes must be carefully evaluated to recognize possible communication/crossflow across the open hole horizontal section.
5. The phase velocity log is another PLT used in conjunction with the PNLT to measure the velocity of two separate phases — water and oil. The marker used is nonradioactive (gadolinium) and can be mixed in oil or water. This chemical marker with a high thermal neutron absorption cross section

Fig. 18 *Well-C: The advanced multiphase production logging and pulsed neutron logging integrated answer.*

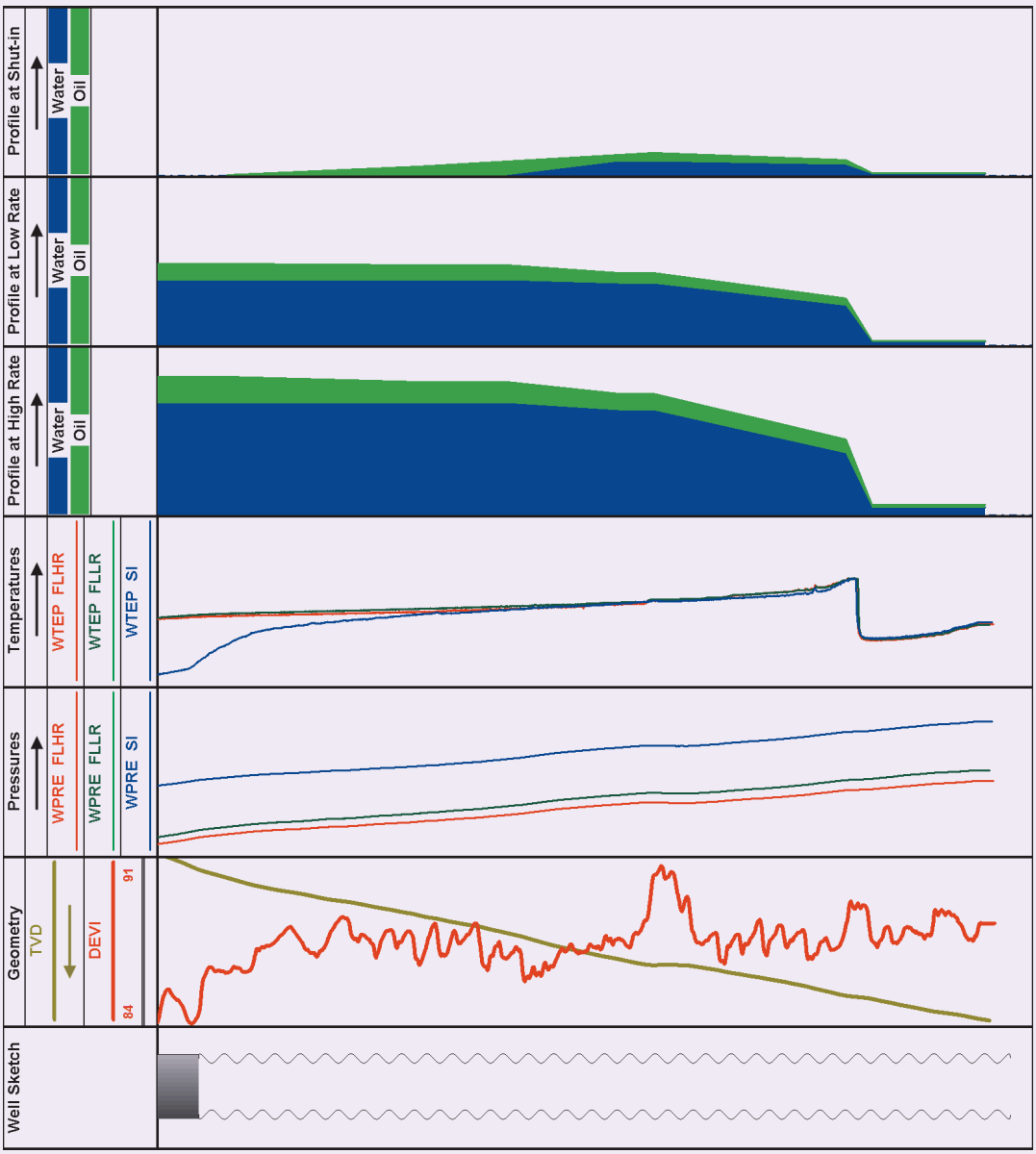

(sigma) that is miscible only with the phase of interest is injected into the borehole. The passage of the marker downstream is detected by the borehole sigma measurement of the PNLT.

Acknowledgments

The authors would like to thank the management of Saudi Aramco and Schlumberger for their support and permission to publish this article. The authors would also like to thank Saudi Aramco's Production Engineering, Reservoir Description, and Reservoir Management Divisions; and Schlumberger Software Integrated Solutions (Data Services Production Division) and Wireline Segment, and their team for the support provided during the logging operations.

This article was presented at the Asia Pacific Oil and Gas Conference and Exhibition, Bali, Indonesia, October 29-31, 2019.

References

1. Al-Mulhim, W.A., Al-Ajmi, F.A., Al-Shehab, M.A. and Pham, T.R.: "Best Practices in Khurais Complex Development," SPE paper 136950, presented at the SPE/DGS Annual Technical Symposium and Exhibition, al-Khobar, Saudi Arabia, April 4-7, 2010.

2. Al Zahrani, A.R., Kalu-Ulu, T.C., Al Nasser, A.N. and Al Yami, S.F.: "Successful Logging Operations through Y-Tool; Challenges and Lessons Learned on Restricted Completions," SPE paper 192362, presented at the SPE

Kingdom of Saudi Arabia Annual Technical Symposium and Exhibition, Dammam, Saudi Arabia, April 23-26, 2018.

3. Mukerji, P.: "Defining Production Logging: Principles of Production Logging," *Oilfield Review*, Vol. 25, Issue 3, Autumn 2013, pp. 63-64.

4. Baldauff, J., Runge, T., Cadenhead, J., Faur, M., et al.: "Profiling and Quantifying Complex Multiphase Flow," *Oilfield Review*, Vol. 16, Issue 3, September 2004, pp. 62-68.

5. Bawazir, M.A., Ahmad, N., Zeybek, M. and Malik, S.: "Pinpointing Water Entries in Dead Horizontal Wells," IPTC paper 15375, presented at the International Petroleum Technology Conference, Bangkok, Thailand, November 15-17, 2011.

6. Ahmad, N., Musharfi, N.M., Zaouali, Z., Bawazir, M.A., et al.: "Integrated Solution for Emulsion Diagnosis in Horizontal Production Logs," SPE paper 166532, presented at the SPE Annual Technical Conference and Exhibition, New Orleans, Louisiana, September 30-October 2, 2013.

7. Roscoe, B.A.: "Field Test Results of a Three-Phase Holdup Measurement in Horizontal Wells with a Pulsed Neutron Source," *SPE Reservoir Evaluation & Engineering*, Vol. 1, Issue 5, October 1998, pp. 449-456.

8. McKeon, D.C., Scott, E., Patton, G.L. and Howard, J.J.: "Interpretation of Oxygen Activation Logs for Detecting Water Flow in Producing and Injection Wells," paper presented at the Society of Petrophysicists and Well Log Analysts 32nd Annual Logging Symposium, Midland, Texas, June 16-19, 1991.

9. Al-Mulhim, A., Al-Thwaiqib, I., Bogari, A., Bawazir, M., et al.: "Integrated Production Logging Approach for Successful Leak Detection between Two Formations: A Case Study," SPE paper 174835, presented at the SPE Annual Technical Conference and Exhibition, Houston, Texas, September 28-30, 2015.

About the Authors

Khaled J. Alsunnary

B.S. in Petroleum and Natural Gas Engineering, West Virginia University

Khaled J. Alsunnary began his career with Saudi Aramco as a Production Engineer working in the Khurais Engineering Division. Currently, he is working as a Reservoir Engineer in the Southern Area Reservoir Management Department.

Khaled's work in the Khurais field for six years has provided extensive experience with intelligent field and electric submersible pumps, as Khurais is considered the largest intelligent field in the Middle East.

He also has experience with gas production and completion, which has a great impact on his development in fracturing operations.

Khaled received his B.S. degree in Petroleum and Natural Gas Engineering from West Virginia University, Morgantown, WV.

Mohammed S. Almuslem

M.S. in Petroleum Engineering, University of Southern California

Mohammed S. Almuslem is a Petroleum Engineer currently working in the Khurais Production Engineering Unit of Saudi Aramco's Southern Area Production Engineering Department. Prior to that, he worked as a Petrophysicist and Well Log Analyst in the Reservoir Description and Simulation Department, where he managed a portfolio of over 100 wells per year, applying the latest well logging technologies in open hole and cased hole oil and gas fields.

Mohammed received his B.S. degree in Petroleum Engineering from the University of Manchester, and an M.S. degree in Petroleum Engineering with Smart Oil Field Technologies Certification from the University of Southern California, Los Angeles, CA.

Yousif A. Al-Abdulmohsin

B.S. in Petroleum Engineering, King Fahd University of Petroleum and Minerals

Yousif A. Al-Abdulmohsin is a Production Engineer working in the Khurais Production Engineering Unit of Saudi Aramco's Southern Area Production Engineering Department.

He has more than 13 years of experience in the oil and gas industry (two years of experience with reservoir engineering and 11 years of experience with production engineering).

Yousif's extensive experience includes well surveillance, artificial lift, well integrity, well stimulation, well completion, and enhanced oil recovery projects.

In 2005, he received his B.S. degree in Petroleum Engineering from King Fahd University of Petroleum and Minerals (KFUPM), Dhahran, Saudi Arabia.

Mustafa A. Bawazir

B.S. in Petroleum Engineering, King Fahd University of Petroleum and Minerals

Mustafa A. Bawazir is a Borehole Production Engineering Team Lead with Schlumberger in the Software Integrated Solutions (SIS) segment, based in Saudi Arabia. He has been with the company since 2007. Mustafa works on technical support in Production Domain for the KSA GeoMarket. He also assists the organization in the marketing and support of integrated solutions.

In addition to his production and well integrity engineering duties, Mustafa worked as the Schlumberger Coordinator for the Saudi Aramco Upstream Professional Development Center (UPDC). In 2011, he assumed the position of Quality Steering Committee (QSC) Team Leader. During Mustafa's tenure as QSC Leader, he developed a quality culture in SIS, which has brought impressive benefits to the segment, resulting in improved operational performance. Between 2009 and 2011, Mustafa worked as the iLearn Front-Line Support where he was involved in supporting and launching Schlumberger's latest training system.

Mustafa has received several awards recognizing his projects and culture of excellence, winning several President's Awards and Bronze Medallions. Mustafa has been recognized by Saudi Aramco's UPDC for coordinating and conducting collaborative learning events and sharing knowledge with Saudi Aramco's next generation employees.

Mustafa has published and presented several technical papers as well as numerous in-house technical reports and articles. He has been a member of the Society of Petroleum Engineers (SPE) since 2005.

Mustafa received his B.S. degree (with Honors) in Petroleum Engineering from King Fahd University of Petroleum and Minerals (KFUPM), Dhahran, Saudi Arabia.

Zouhir Zaouali

M.S. in Reservoir Geosciences and Engineering, French Institute of Petroleum

Zouhir Zaouali works in the field of production and perforation, and has spent his career with Schlumberger covering various position in wireline and data processing centers in France, Algeria, Libya, Congo, the North Sea, and Saudi Arabia for the past 17 years.

He has contributed to enhancing production logging and reservoir saturation interpretation, perforation optimization techniques, surveillance in brown fields, water control in gas wells, and underbalanced perforations.

In 2001, Zouhir received his M.S. degree in Reservoir Geosciences and Engineering from the French Institute of Petroleum (IFP), Rueil-Malmaison, France.

He is member of the Society of Petroleum Engineers (SPE).

Surface Complexation Model of Alkaline SmartWater Electrokinetic Interactions in Carbonates

Dr. Moataz O. Abu-Al-Saud, Amani O. Alghamdi, Dr. Subhash C. Ayirala, and Dr. Mohammed B. Al-Otaibi

Abstract /

Understanding the effect of injection water chemistry is becoming crucial, as it has recently been shown to have a major impact on oil recovery processes in carbonate formations. Various studies have concluded that surface charge alteration is the primary mechanism behind the observed change of wettability toward water-wet due to SmartWater injection in carbonates. Therefore, understanding the surface charges at calcite/brine and crude oil/brine interfaces becomes essential to optimize the injection water compositions for enhanced oil recovery (EOR) in carbonate formations.

In this work, the physicochemical interactions of different brine recipes with and without alkali in carbonates are evaluated using the Surface Complexation Model (SCM). First, the zeta (ζ) potential of calcite/brine and crude oil/brine interfaces are determined for SmartWater, sodium chloride, and sodium sulfate (Na_2SO_4) brines at a fixed salinity. The high salinity seawater is also included to provide the baseline for comparison. Then, two types of alkali (sodium hydroxide (NaOH) and sodium carbonate (Na_2CO_3)) are added at 0.1 wt% concentration to the different brine recipes to verify their effects on the computed ζ-potential values in the SCM framework. The SCM results are compared with experimental data of the ζ-potentials obtained with calcite in brine and crude oil in brine suspensions using the same brines and the two alkali concentrations.

The SCM results follow the same trends observed in experimental data to reasonably match the ζ-potential values at the calcite/brine interface. Generally, the addition of alkaline drives the ζ-potentials toward more negative values. This trend toward negative ζ-potential is confirmed for the SmartWater recipe with the impact being more pronounced for Na_2CO_3 due to the presence of a divalent anion carbonate $(CO_3)^{-2}$. Some discrepancy in the ζ-potential magnitude between the SCM results and experiments are observed at the crude oil/brine interface with the addition of alkali. This discrepancy can be attributed to neglecting the reaction of carboxylic acid groups in the crude oil with a strong alkali, i.e., NaOH and Na_2CO_3.

The novelty of this work is that it clearly validates the SCM results with experimental ζ-potential data to determine the physicochemical interaction of alkaline chemicals with SmartWater in carbonates. These modeling results provide new insights on defining optimal SmartWater compositions to synergize with alkaline chemicals to further improve oil recovery in carbonate reservoirs.

Introduction

The ionic water composition in the waterflooding process plays a crucial role in oil recovery for carbonate formations[1]. The chemistry of injected water strongly affects the reservoir wettability, which has been proven and observed, in numerous laboratory and field studies for both carbonates and sandstones[2-4]. Modifying the water chemistry to alter the rock wettability is known as SmartWater or low salinity[5]. The root causes of this wettability alteration effect, which takes place at the pore level, remain poorly understood, especially for carbonates[6].

This lack of fundamental understanding of the root causes of wettability alteration has resulted in conflicting studies, where some studies have observed an increase in oil recovery while other cases have not shown an increment in oil recovery[7]. Various pore scale mechanisms have been proposed to delineate the wettability alteration process in carbonates. Some of these plausible mechanisms include an electric double layer[4], in situ soap generation (saponification effect)[8], and multiple ion exchange[9]. The surface charges of carbonate/brine and crude oil/brine are altered in such pore-scale processes, which affects the zeta (ζ) potential measurements used in understanding rock wettability[10, 11].

Recently, the synergy between tailored water salinity and enhanced oil recovery (EOR) has gained a lot of attention[12]. For polymer EOR, it has been shown that the use of low salinity (SmartWater) reduces the polymer consumption used to increase the injected water viscosity[13]. For surfactant-based EOR, it has been observed that decreasing the water salinity increases the effect of surfactant on crude oil/brine through efficiently reducing the interfacial tension (IFT)[14].

It is well-known that surfactants are adsorbed on carbonate rock surfaces. Therefore, a large amount of

chemical surfactant is consumed before the chemical reaches the crude oil/brine interface. To minimize surfactant adsorption on carbonate rock surfaces, alkaline is added to the injected water[15]. The alkaline chemical reacts with both crude oil/brine and calcite/brine interfaces. The reaction of alkali and naphthenic acid in crude oil generates in situ soap that locally reduces the IFT of the crude oil/brine interface. For the calcite surface, the adsorption of alkali changes the electric charges balance on the calcite/brine interface, which alters the carbonate wettability toward a more water-wet state[15]. Therefore, understanding the electrokinetics of brine with alkaline chemicals in carbonates is crucial to define the optimal water compositions for improving oil recovery.

There are several electrokinetic studies involving ζ-potentials that have reported the synergy effect of water salinity, crude oil, and alkaline in carbonates for crude oil/brine[16, 17] and calcite/brine interfaces[15, 18]. To the best of our knowledge, the role of individual ions in different brine compositions in the presence of alkaline chemicals for both the calcite/brine and crude oil/brine interfaces has not been previously studied using a surface chemistry model and lab measurements. In this work, we study the electrokinetics with various brine recipes interacting with crude oil and calcite, with and without alkali chemicals using a Surface Complexation Model (SCM). We validate the modeling results with ζ-potentials of calcite/brine and crude oil/brine interfaces measured in the lab.

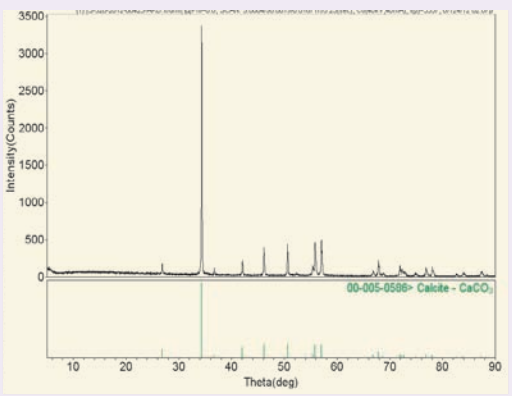

Fig. 1 *XRD diffractograms of calcite ($CaCO_3$) disk with reference patterns of pure calcite compound. The X-ray wavelength is 1.54 Å.*

Materials and Methods

Experiment

Rock sample. Pure calcium carbonate ($CaCO_3$) is used to represent the calcite rock sample. The purity of the calcite disk sample is measured using X-ray diffraction (XRD), which is composed of 99 wt% of $CaCO_3$, Fig. 1. The calcite purity confirms that there are no mineral impurities interfering with the ion adsorption on the calcite surface. The calcite disk is grounded manually using a granite mill for 30 minutes at atmospheric conditions far from contaminants to avoid surface impurities.

Brine and crude oil properties. Synthetic brine ionic compositions are prepared by adding different salts to deionized water. Table 1 lists the ionic composition of the considered brine samples used. Table 2 lists the crude oil properties.

Alkaline chemicals. Two types of alkali (sodium hydroxide (NaOH) and sodium carbonate (Na_2CO_3)) are added at 0.1 wt% concentration (1,000 ppm) relevant to each brine recipe. Typically, alkali chemicals increase the brine pH level, which causes calcium and magnesium ions to precipitate as calcium hydroxide and magnesium hydroxide, respectively. Therefore, the addition of alkali to seawater is not considered to avoid precipitation, as seawater contains a high ionic concentration of hardness ions such as Mg^{2+} and Ca^{2+}.

Table 1 *The ionic composition of different synthetic brines used in this study.*

	Brine Samples (Concentration mg/L)			
Ions	**Seawater**	**SmartWater**	**NaCl**	**Na_2SO_4**
Na^+	18,300	1,824	2,266	1,865
Cl^-	32,200	3,220	3,495	—
Ca^{2+}	650	65	—	—
Mg^{2+}	2,110	211	—	—
SO_4^{-2}	4,290	429	—	3,896
HCO3-	120	—	—	—
Total Dissolved Solids (ppm)	57,670	5,761	5,761	5,761
pH	7.45	7.4	6.3	6.11

Table 2 *Crude oil properties.*

API	27.1
Acid Number mg KOH/g	0.47
Base Number mg KOH/g	0.04
Saturates (%)	50.6
Asphaltenes (%)	1.6
Resins (%)	20.7
Aromatics (%)	27.1

Table 3 lists the equilibrium pH level of different brines, including alkali chemicals. The brine pH is measured after reaching equilibrium with alkaline and calcite suspensions without manually adjusting the pH level.

ζ-potential measurement. The measurement of the ζ-potential is conducted by using a phase analysis light scattering technique (ζ PALS) applied to the calcite in the brine and crude oil emulsion in the brine samples. A total of 0.2 g of pure calcite particles (ground) were thoroughly mixed with 50 cm^3 of different brines for a minimum of 48 hours to ensure suspension and equilibrium are achieved. The ratio of solid-liquid and liquid-liquid is fixed throughout the experiment to guarantee consistency in the reported values. The brine pH level is not manually adjusted. The oil droplets and calcite particle size distribution in different brines is determined using optical microscopy, similar to the approach by Alotaibi and Yousef (2017)[19].

The average calcite particle size distribution is estimated to be around 10 µm, while the average oil droplet size is between 14 µm to 35 µm. Sonification is used to avoid calcite particle aggregation or crude oil coalescence in brine suspensions. The ζ-potential values are determined using Smoluchowski approximation based on the electrophoretic mobility of brine suspensions. Each ζ-potential measurement is repeated three times to ensure consistent results. The measurement variation for each reported ζ-potential value is within 3 mV.

Additional details on the sample preparation and experimental ζ-potential measurement procedures can be found in Alotaibi and Yousef (2017)[19].

SCM

The SCM describes the equilibrium state of ion adsorption based on specified surface reactions. The surface reactions of ions give rise to surface electric charges. For the calcite/brine/crude oil system, the adsorption of ions on crude oil/brine and calcite/brine interfaces determine the surface charges and the corresponding ζ-potentials. The SCM has been employed to gain insight on the effect of electrokinetics on wettability in the context of brine chemistry in carbonates[20-23].

Brady et al. (2012)[21] used SCM based on surface reactions proposed in Van Cappellen et al. (1993)[24] and Pokrovsky et al. (1999)[25] to predict ζ-potentials for both rock-brine and crude oil/brine interfaces in sandstone and carbonate rocks. Subsequently, the SCM has not been validated with experimental ζ-potential measurements. Mahani et al. (2017)[22] studied the electrokinetics of carbonate-based rocks with different water salinities using the SCM. The SCM results were qualitatively validated with different carbonate-brine ζ-potential measurements.

Song et al. (2017)[23] applied SCM and reported quantitative agreement with experimental ζ-potential measurements of synthetic calcite and multiple brine recipes. The SCM surface reactions are based on the model proposed in Heberling et al. (2011)[26], which includes different SCM reactions compared to the models in Brady et al. (2012)[21] and Mahani et al. (2017)[22]. The SCM work of Song et al. (2017)[23] has been recently extended to include surface reactions of organic and inorganic impurities occurring in natural carbonates[27].

In this work, we use SCM with surface reactions similar to the approach in Song et al. (2017)[23] to predict ζ-potentials for pure calcite and different brine recipes with and without alkali chemicals. In addition, we determine crude oil/brine ζ-potentials by modeling SCM reactions at the crude oil/brine interface. Tables 4 and 5 list the surface reactions and the corresponding equilibrium constants for both calcite and crude oil surfaces, respectively.

The non-integer surface charge values of $> CaOH^{-0.75}$ and $> CO_3H^{+0.75}$ hydrated calcite sites is due to the structure of calcite crystal. The ionic bonding between Ca and O atoms from $(CO_3)^{-2}$ gives an effective charge

Table 3 *Equilibrium pH values of calcite suspension in different electrolytes containing alkali.*

Type of Electrolyte	pH ($CaCO_3$)	pH $CaCO_3$ (NaOH 0.1 wt.%)	pH $CaCO_3$ (Na_2CO_3 0.1 wt.%)
Na_2SO_4	9.8	12.0	10.0
NaCl	9.4	11.3	10.0
SmartWater	8.6	11.7	10.0
Seawater	7.4	—	—

Table 4 *Surface complexation reactions and parameters for the calcite surface.*

Calcite Surface Reaction	Equilibrium Constant (log_{10} K_{int})
$> CaOH^{-0.75} + H^{+} \leftrightarrow > CaOH_2^{+0.25}$	0.4
$> CO_3H^{(+0.75)} + OH^{-} \leftrightarrow > CO_3^{-0.25} + H_2O$	0.5
$> CaOH^{-0.75} + Ca^{2+} \leftrightarrow > CaOH..Ca^{+1.25}$	1.53
$> CaOH^{-0.75} + Mg^{2+} \leftrightarrow > CaOH..Mg^{+1.25}$	1.15
$> CO_3H^{+0.75} + SO4^{2-} \leftrightarrow > CO_3H..SO_4^{-1.25}$	1.5
$> CO_3H^{+0.75} + CO_3^{2-} \leftrightarrow > CO_3H..CO_3^{-1.25}$	2.23
$> CO_3H^{+0.75} + HCO_3^{-} \leftrightarrow > CO_3H..HCO_3^{-0.25}$	0.09
$> CaOH^{-0.75} + Na^{+} \leftrightarrow > CaOH..Na^{+0.25}$	0.22
$> CO_3H^{+0.75} + Cl^{-} \leftrightarrow > CO_3H..Cl^{-0.25}$	0.65

Table 5 *Surface complexation reactions and parameters for the crude oil surface.*

Crude Oil Surface Reaction	Equilibrium Constant (log_{10} K_{int})
$-COOH \leftrightarrow -COO^{-} + H^{+}$	6.0
$-N + H^{+} \leftrightarrow -NH^{+}$	4.0
$-COOH + Ca^{+2} \leftrightarrow -COOCa^{+} + H^{+}$	-4.0
$-COOH + Mg^{+2} \leftrightarrow -COOMg^{+} + H^{+}$	-4.3
$-COOH + Na^{+2} \leftrightarrow -COONa + H^{+}$	-4.0

of +⅓ for Ca atoms[26]. In this model, a charge of +¼ is assumed for Ca atoms, following the approach in Song et al. (2017)[23] and Heberling et al. (2011)[26]. The crude oil surface reactions are similar to the models used in Xie et al. (2018)[20], Brady et al. (2012)[21], and Takeya et al. (2019)[28].

The SCM equations are solved using PHREEQC software[29], whereby the double layer model is specified. In the model, the concentration of adsorbed surface complexes (adsorbed ions) determines the total surface charge as follows:

$$\sigma = \frac{F}{SA}\Sigma z_i c_i, \qquad 1$$

where σ is the surface charge density (C/m^2), F is the Faraday constant (96493.5 C/mol), S is the surface material mass (g), A is the specific surface area (m^2/g), z_i is the ionic electric charge, and c_i is the adsorbed ion concentration (mol). The surface charge and the surface potential are related through the Gouy-Chapman model[29]:

$$\sigma = (8000\epsilon_o\epsilon_w RTI)^{1/2} \sinh\left(\frac{\nu F\Psi.}{2RT}\right), \qquad 2$$

where ϵ_o is the vacuum permittivity $\left(\frac{C^2}{mJ}\right)$, ϵ_o is the water relative permittivity Ψ is the surface potential (V), R is the gas constant $\left(\frac{J}{mol\,K}\right)$, T is the temperature (K), I is the brine ionic strength (mol/l), and ν is the electrolyte ionic charge, which is assumed to be unity in PHREEQC[29]. The bulk concentration of ions interacts with the adsorbed ions at the surface due to coulombic forces. Therefore, the apparent equilibrium constants are considered to include the effect of the bulk concentration of the ions. The apparent and intrinsic equilibrium constants (listed in Tables 4 and 5) are described through the Boltzmann distribution[29]:

$$K_{app} = K_{int} \exp\left(\frac{Z_c F\Psi.}{RT}\right), \qquad 3$$

where Z_c is the net change of the surface charge at the surface due to surface reaction. The ζ-potential can be approximated from the surface potential based on the linearized Debye-Huckel theory[23], which is valid for $|\Psi| \leq 25$ mV[30]:

$$\zeta = \psi \exp(-\kappa d_s), \qquad 4$$

where κ is the inverse Debye length-scale, and d_s is the slipping plane distance from the outer Helmholtz plane. For brines with an ionic strength of 0.1 mol/l (the considered brine recipes except for seawater), the d_s is 0.33 nm[23, 26], while the Debye length κ^{-1} is 0.97 nm. For the seawater case (ionic strength of 1.1 mol/l), d_s is 0.1 nm ($d_s = 0.1/c^{0.5}$)[26], while κ_{sw}^{-1} is 0.29 nm.

The site density for the calcite surface is 4.95 sites/nm^2 [26, 27], while the crude oil surface has a site density of 0.47 sites/nm^2 [28]. The calcite specific surface area is 1 m^2/g[26], while the crude oil specific area is 0.5 m^2/g[28]. Additional details of these SCM equations are elaborated in Parkhurst and Appelo (2013)[29] and Dzombak and Morel (1990)[31].

Results and Discussion

Figures 2 to 7 compare the SCM and experimental measurements of the ζ-potential values for different brine recipes with and without alkali. First, the ζ-potentials for the calcite/brine interface are analyzed, Figs. 2 to 4, followed by the crude oil/brine interface, Figs. 5 to 7. The intrinsic equilibrium constants are varied in the SCM to match the measured ζ-potentials. The number of fitting parameters is equal to the number of surface reaction equations — nine equations for the calcite/brine interface, and five equations for the crude oil/brine interface. The site density and specific surface area of the considered surfaces are fixed.

For the calcite/brine interface, the SCM results follow the trends observed in the experimental data, and quantitatively agree with the lab's ζ-potential measurements, especially for sodium chloride, SmartWater, and sodium sulfate (Na_2SO_4) brines. For the seawater case without alkali, the SCM underestimates the ζ-potential as can been seen in Fig. 2. When NaOH alkaline is added to the brine recipes, the change in ζ-potential values of the calcite/brine interface is almost negligible and in agreement with the experimental ζ-potential measurements, Fig. 3 (within a 2.5 mV difference). The addition of $(OH)^-$ ions increases the negative charge, and decreases the adsorption of H^+ protons while adding Na^+ ions increase the charge positivity resulting in an insignificant total change in the surface charge.

For the Na_2CO_3 alkaline, the SCM calcite/brine

Fig. 2 *The experimental and SCM ζ-potential values at the calcite/brine interface.*

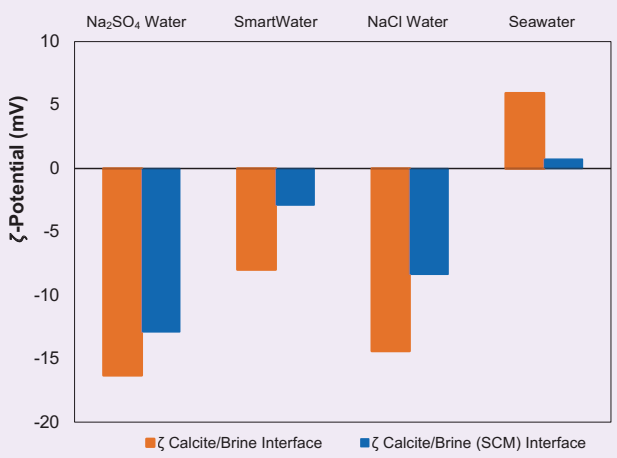

Fig. 3 *The experimental and SCM ζ-potential values at the calcite/brine interface. The brine contains 0.1 wt% NaOH.*

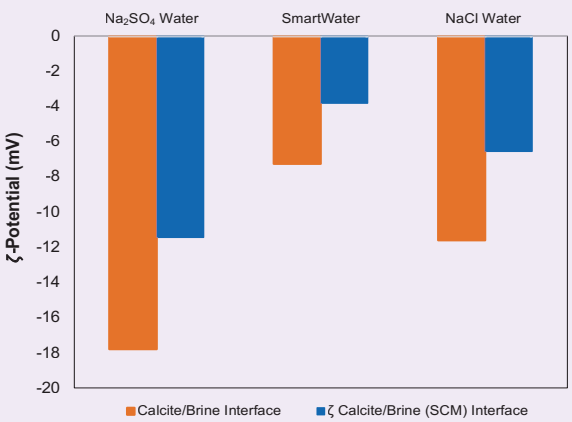

Fig. 4 *The experimental and SCM ζ-potential values at the calcite/brine interface. The brine contains 0.1 wt% Na_2CO_3.*

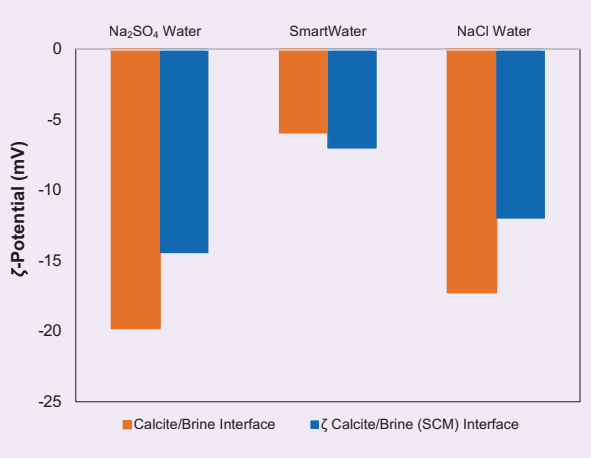

Fig. 5 *The experimental and SCM ζ-potential values at the crude oil/brine interface.*

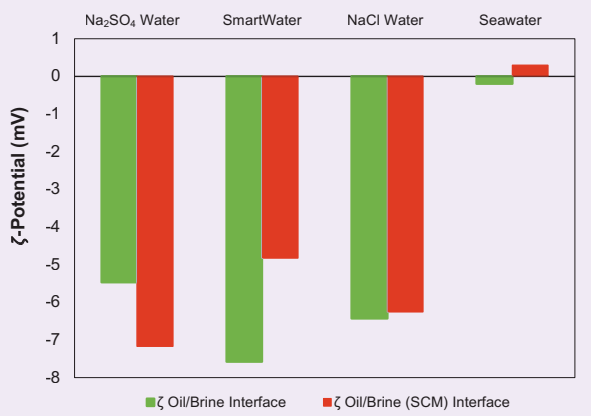

Fig. 6 *The experimental and SCM ζ-potential values at the crude oil/brine interface. The brine contains 0.1 wt% NaOH.*

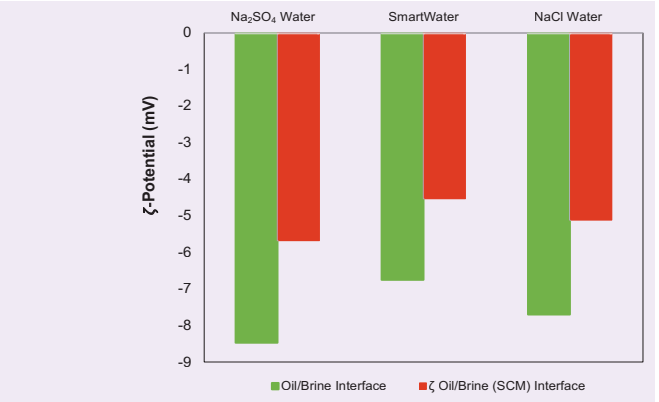

Fig. 7 *The experimental and SCM ζ-potential values at the crude oil/brine interface. The brine contains 0.1 wt% Na_2CO_3.*

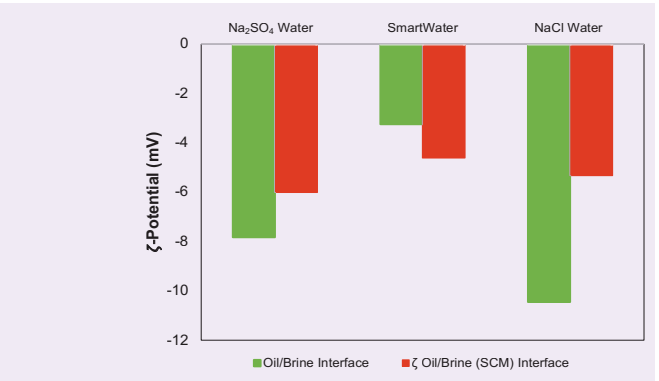

ζ-potentials decrease for the considered brine recipes, Fig. 4. This decrease in ζ-potential values is mainly due to the presence of divalent anion carbonate $(CO_3)^{-2}$, which forms a surface complex on the calcite surface with a -1.25 charge as illustrated in reaction 6 in Table 3. Calcite precipitation/dissolution was not been considered in the SCM, which is likely to contribute to the slight discrepancy observed in the SmartWater recipe case in Fig. 4.

The intrinsic equilibrium constants (fitting parameters) in Table 4 are in agreement with the work of Song et al. (2017)[23] except for the Cl^- ion, which has the largest discrepancy. The SCM confirms that the total surface charge and ζ-potential of calcite/brine interface strongly depend on the divalent ions — Ca^{2+}, Mg^{2+}, CO_3^{2-}, and SO_4^{2-} — due to large intrinsic equilibrium constants compared to the other ions. The SCM predicts that the most effective ion in pushing the calcite surface charge to a negative value is the divalent anion carbonate $(CO_3)^{-2}$, which has the largest equilibrium constant.

For the crude oil/brine interface cases, the SCM ζ-potential results qualitatively match the experimental observations. The predicted ζ-potentials are in general negatively charged, Fig. 5, which agree with the experimental results. The equilibrium constants in Table 5 agree with the values reported in the literature[21, 28] (the discrepancy in the equilibrium constants are within a value of one for each reaction). At pH > 7 (greater than the isoelectric point for the crude oil/brine interface with a similar acid number[32]), the carboxylic acids in crude oil are not completely protonated (reaction 1 in Table 5). Also, the protonation of nitrogen bases (reaction 2 in Table 5) is not sufficient to switch the crude oil surface to a positive charge.

When alkali is added to the brine recipe, Figs. 6 and 7, the variation in the SCM ζ-potentials is less than 2 mV. The ζ-potentials slightly increase on the positive side, especially for the NaOH alkaline. This slight increase is not expected as the protonation activity decreases with the increase of the brine pH level. Subsequently, the reactions in the SCM predict that the adsorption of Mg^{2+} and Ca^{2+} (reactions 3 and 4) slightly compensates for the decrease in H^+, which results in a small increase in the ζ-potential. Based on the model predictions of calcite/brine and crude oil/brine ζ-potentials, the Na_2SO_4 brine with Na_2CO_3 alkaline provides the largest interface negative charges, Figs. 4 and 7.

The modeling results support the conclusion drawn from the experiments that the Na_2SO_4 brine with Na_2CO_3 alkaline is the preferable brine recipe to synergize with anionic surfactants due to its large negative ζ-potential. This large negative ζ-potential increases the water wetness toward the carbonate reservoir[18] and reduces the anionic surfactant retention[15]. Further improvement and refinement in the SCM will be considered, as this is a starting point for ongoing research in electrokinetic modeling.

Such improvements include using an SCM triple layer model, nonlinear diffuse double layer model to infer the ζ-potential from the surface potential, and adding dissolution/precipitation reactions for the calcite/brine interface. In addition, including the crude oil chemistry (acid/base numbers) to be part of the surface site density[33] of the nitrogen base and carboxylate groups will improve the SCM for the crude oil/brine interface.

Conclusions

This work explores the electrokinetic interactions of different brine recipes with and without alkali in carbonates using SCM. Various SCM calculations of calcite/brine and crude oil/brine ζ-potentials were conducted to evaluate the synergy between different brine recipes and alkali chemicals. The proposed SCM predicts the ζ-potential results that are consistent with the experimental measurements for choosing the Na_2SO_4 brine with Na_2CO_3 alkaline to be the most suitable alkaline-based recipe due to its large negative ζ-potentials.

In the alkaline/surfactant EOR process, the negative

electrokinetic calcite charge repels the anionic surfactant causing a reduction in surfactant retention. The modeling of ζ-potential results quantitatively agree with the experiments for the calcite/brine interface. For the crude oil/brine interface, the SCM ζ-potential results reasonably match the experimental measurements. Further correlation of the carboxylic acid group and nitrogen base crude oil active surface sites with the acid/base number is required[33] to quantitatively predict accurate ζ-potentials and gain additional insights on the electrokinetics of crude oil surfaces.

Acknowledgments

The authors would like to thank the management of Saudi Aramco for their support and permission to publish this article. The authors would also like to thank Hussain Saleem and Dong Kyu Cha for their help with ζ-potential measurements.

References

1. Austad, T., Strand, S., Høgnesen, E.J. and Zhang, P.: "Seawater as IOR Fluid in Fractured Chalk," SPE paper 93000, presented at the SPE International Symposium on Oil Field Chemistry, The Woodlands, Texas, February 2-4, 2005.

2. Yousef, A.A., Al-Saleh, S.H., Al-Kaabi, A. and Al-Jawfi, M.S.: "Laboratory Investigation of the Impact of Injection-Water Salinity and Ionic Content on Oil Recovery from Carbonate Reservoirs," *SPE Reservoir Evaluation & Engineering*, Vol. 14, Issue 5, October 2011, pp. 578-593.

3. Yousef, A.A., Liu, J.S., Blanchard, G.W., Al-Saleh, S., et al.: "Smart Waterflooding: Industry," SPE paper 159526, presented at the SPE Annual Technical Conference and Exhibition, San Antonio, Texas, October 8-10, 2012.

4. Ligthelm, D.J., Gronsveld, J., Hofman, J., Brussee, N., et al.: "Novel Waterflooding Strategy by Manipulation of Injection Brine Composition," SPE paper 119835, presented at the EUROPEC/EAGE Conference and Exhibition, Amsterdam, the Netherlands, June 8-11, 2009.

5. Morrow, N. and Buckley, J.: "Improved Oil Recovery by Low Salinity Waterflooding," *Journal of Petroleum Technology*, Vol. 63, Issue 5, May 2011, pp. 106-112.

6. Mahani, H., Keya, A.L., Berg, S., Bartels, W., et al.: "Insights into the Mechanism of Wettability Alteration by Low Salinity Flooding (LSF) in Carbonates," *Energy & Fuels*, Vol. 29, Issue 3, March 2015, pp. 1352-1367.

7. Jackson, M.D., Al-Mahrouqi, D. and Vinogradov, J.: "Zeta Potential in Oil-Water-Carbonate Systems and its Impact on Oil Recovery during Controlled Salinity Water Flooding," *Scientific Reports*, Vol. 6, November 2016.

8. McGuire, P.L., Chatham, J.R., Paskvan, F.K., Sommer, D., et al.: "Low Salinity Oil Recovery: An Exciting New EOR Opportunity for Alaska's North Slope," SPE paper 93903, presented at the SPE Western Regional Meeting, Irvine, California, March 30-April 1, 2005.

9. Lager, A., Webb, K.J., Black, C.J.J., Singleton, M., et al.: "Low Salinity Oil Recovery — An Experimental Investigation," *Petrophysics*, Vol. 49, Issue 1, February 2008, pp. 28-35.

10. Al-Mahrouqi, D., Vinogradov, J. and Jackson, M.D.: "Zeta Potential of Artificial and Natural Calcite in Aqueous Solution," *Advances in Colloid and Interface Science*, Vol. 240, February 2017, pp. 60-76.

11. Jackson, M.D., Vinogradov, J., Hamon, G. and Chamerois, M.: "Evidence, Mechanisms and Improved Understanding of Controlled Salinity Waterflooding Part 1: Sandstones," *Fuel*, Vol. 185, December 2016, pp. 772-793.

12. Ayirala, S. and Yousef, A.: "A State-of-the-Art Review to Develop Injection-Water-Chemistry Requirement Guidelines for IOR/EOR Projects," *SPE Production & Operations*, Vol. 30, Issue 1, February 2015, pp. 26-42.

13. Ayirala, S.C., Uehara-Nagamine, E., Matzakos, A.N., Chin, R.W., et al.: "A Designer Water Process for Offshore Low Salinity and Polymer Flooding Applications," SPE paper 129926, presented at the SPE Improved Oil Recovery Symposium, Tulsa, Oklahoma, April 24-28, 2010.

14. Alameri, W., Teklu, T.W., Graves, R., Kazemi, H., et al.: "Low Salinity Water-Alternate-Surfactant in Low Permeability Carbonate Reservoirs," paper presented at the 18th European Symposium on Improved Oil Recovery, Dresden, Germany, April 14, 2015.

15. Hirasaki, G., Miller, C.A. and Puerto, M.: "Recent Advances in Surfactant EOR," *SPE Journal*, Vol. 16, Issue 4, December 2011, pp. 889-907.

16. Liu, Q., Dong, M., Yue, X. and Hou, J.: "Synergy of Alkali and Surfactant in Emulsification of Heavy Oil in Brine," *Colloids and Surfaces A: Physicochemical and Engineering Aspects*, Vol. 273, Issue 1-3, February 2006, pp. 219-228.

17. Chan, K.S. and Shah, D.O.: "The Physico-Chemical Conditions Necessary to Produce Ultralow Interfacial Tension at the Oil/Brine Interface," in *Surface Phenomena in Enhanced Oil Recovery*, Shah, D.O. (ed.), Springer: Boston, MA, 1981, pp. 53-72.

18. Hirasaki, G. and Zhang, D.L.: "Surface Chemistry of Oil Recovery from Fractured, Oil-Wet, Carbonate Formations," *SPE Journal*, Vol. 9, Issue 2, June 2004, pp. 151-162.

19. Alotaibi, M.B. and Yousef, A.: "The Role of Individual and Combined Ions in Waterflooding Carbonate Reservoirs: Electrokinetic Study," *SPE Reservoir Evaluation & Engineering*, Vol. 20, Issue 1, February 2017, pp. 77-86.

20. Xie, Q., Sari, A., Pu, W., Chen, Y., et al.: "pH Effect on Wettability of Oil/Brine/Carbonate System: Implications for Low Salinity Water Flooding," *Journal of Petroleum Science and Engineering*, Vol. 168, September 2018, pp. 419-425.

21. Brady, P.V., Krumhansl, J.L. and Mariner, P.E.: "Surface Complexation Modeling for Improved Oil Recovery," SPE paper 153744, presented at the SPE Improved Oil Recovery Symposium, Tulsa, Oklahoma, April 14-18, 2012.

22. Mahani, H., Keya, A.L., Berg, S. and Nasralla, R.: "Electrokinetics of Carbonate/Brine Interface in Low Salinity Waterflooding: Effect of Brine Salinity, Composition, Rock Type, and pH on ζ-Potential and a Surface Complexation Model," *SPE Journal*, Vol. 22, Issue 1, February 2017, pp. 53-68.

23. Song, J., Zeng, Y., Wang, L., Duan, X., et al.: "Surface Complexation Modeling of Calcite Zeta Potential Measurements in Brines with Mixed Potential Determining Ions (Ca^{2+}, CO_3^{2-}, Mg^{2+}, SO_4^{2-}) for Characterizing Carbonate Wettability," *Journal of Colloid and Interface Science*, Vol. 506, November 2017, pp. 169-179.

24. Van Cappellen, P., Charlet, L., Stumm, W. and Wersin, P.: "A Surface Complexation Model of the Carbonate Mineral Aqueous Solution Interface," *Geochimica et Cosmochimica*

Acta, Vol. 57, Issue 15, August 1993, pp. 3505-3518.

25. Pokrovsky, O.S., Schott, J. and Thomas, F.: "Dolomite Surface Speciation and Reactivity in Aquatic Systems," *Geochimica et Cosmochimica Acta*, Vol. 63, Issues 19-20, October 1999, pp. 3133-3143.

26. Heberling, F., Trainor, T.P., Lützenkirchen, J., Eng, P., et al.: "Structure and Reactivity of the Calcite Water Interface," *Journal of Colloid and Interface Science*, Vol. 354, Issue 2, February 2011, pp. 843-857.

27. Song, J., Rezaee, S., Zhang, L., Zhang, Z., et al.: "Characterizing the Influence of Organic Carboxylic Acids and Inorganic Silica Impurities on the Surface Charge of Natural Carbonates Using an Extended Surface Complexation Model," *Energy & Fuels*, Vol. 33, Issue 2, January 2019, pp. 957-967.

28. Takeya, M., Shimokawara, M., Elakneswaran, Y., Nawa, T., et al.: "Predicting the Electrokinetic Properties of the Crude Oil/Brine Interface for Enhanced Oil Recovery in Low Salinity Water Flooding," *Fuel*, Vol. 235, January 2019, pp. 822-831.

29. Parkhurst, D.L. and Appelo, T.: "Description of Input and Examples for PHREEQC Version 3 — A Computer Program for Speciation, Batch-Reaction, One-Dimensional Transport, and Inverse Geochemical Calculations," *U.S. Geological Survey Techniques and Methods*, Book 6, Chapter A43, January 2013, 497 p.

30. Israelachvili, J.N.: *Intermolecular and Surface Forces*, 3rd edition, Academic Press, 2011, 704 p.

31. Dzombak, D.A. and Morel, F.M.M.: *Surface Complexation Modeling: Hydrous Ferric Oxide*, John Wiley & Sons, March 1990, 416 p.

32. Buckley, J.S., Takamura, K. and Morrow, N.R.: "Influence of Electrical Surface Charges on the Wetting Properties of Crude Oils," *SPE Reservoir Engineering*, Vol. 4, Issue 3, August 1989, pp. 332-340.

33. Bonto, M., Eftekhari, A.A. and Nick, H.M.: "An Overview of the Oil-Brine Interfacial Behavior and a New Surface Complexation Model," *Scientific Reports*, Vol. 9, Issue 1, April 2019.

About the Authors

Dr. Moataz O. Abu-Al-Saud

Ph.D. in Energy Resources Engineering, Stanford University

Dr. Moataz O. Abu-Al-Saud joined Saudi Aramco in 2004. Currently, he works as a Research Engineer with the Reservoir Engineering SmartWater Team in the Exploration and Petroleum Engineering Center – Advanced Research Center (EXPEC ARC).

Moataz's research interests focus on the fundamental understanding of multiphase flow inside carbonates from the nanoscale to the reservoir scale, as well as digital rock physics.

He has published several conference papers and peer-reviewed journal papers.

Moataz received two B.S. degrees, one in Mechanical Engineering and one in Mathematics from Rice University, Houston, TX, in 2009. He received an M.S. degree in Mechanical Engineering from King Abdullah University of Science and Technology (KAUST), Thuwal, Saudi Arabia, and a Ph.D. degree in Energy Resources Engineering from Stanford University, Stanford, CA.

Amani O. Alghamdi

M.S. in Chemistry, King Abdulaziz University

Amani O. Alghamdi is a Petroleum Scientist at Saudi Aramco, who is currently in out-of-Kingdom training. Prior to this, she conducted work using the density functional theory to study the interactions of ions in SmartWater with calcite and oil at an atomic scale. Amani also applied periodic molecular modeling codes to study catalytic reactions of hydrocarbons.

Her current research interest includes molecular and electrokinetic studies for wettability alteration in carbonates.

Amani has authored and coauthored several technical and peer-reviewed journal papers.

She received her M.S. degree in Chemistry from King Abdulaziz University, Jiddah, Saudi Arabia.

Dr. Subhash C. Ayirala

Ph.D. in Petroleum Engineering, Louisiana State University

Dr. Subhash C. Ayirala is a Petroleum Engineering Specialist and currently the Champion of the SmartWater Flooding Focus Area in Saudi Aramco's Exploration and Petroleum Engineering Center – Advanced Research Center (EXPEC ARC), He has about 15 years of experience in reservoir engineering in the oil industry. Previously, Subhash worked as a Reservoir Engineer in Shell E&P in Houston.

His research interests are in improved/enhanced oil recovery (EOR), including advanced waterflooding, chemical EOR, and miscible carbon dioxide gas injection.

Subhash has authored or coauthored 60 technical papers, more than 35 journal publications, and holds nine U.S. patents, with several pending patent applications.

He is an active member of the Society of Petroleum Engineers (SPE), and serves as an Associate Editor for the *SPE Reservoir Evaluation & Engineering Journal*.

Subhash also serves as one of the Executive Editors for the *Journal of Petroleum Science and Engineering* (JPSE), an Elsevier international journal. He served on the technical program committees of the 2016 SPE Tulsa IOR conference, the 2019 International Petroleum Technology Conference (Beijing), and the 2020 SPE Tulsa IOR conference.

Subhash received the SPE Outstanding Technical Editor recognition in 2008, 2013, 2016, 2017, 2018, and 2019, and is the recipient of the 2017 SPE "A Peer Apart Award." He has also been selected to receive the 2019 SPE Middle East and North Africa Regional Service Award.

Subhash received both his M.S. degree and Ph.D. degree in Petroleum Engineering from Louisiana State University, Baton Rouge, LA.

Dr. Mohammed B. Alotaibi

Ph.D. in Petroleum Engineering, Texas A&M University

Dr. Mohammed B. Alotaibi joined Saudi Aramco in 2001, and is a Petroleum Engineering Specialist working in the Exploration and Petroleum Engineering Center – Advanced Research Center (EXPEC ARC). His research interests are in the areas of reservoir management, SmartWater flooding, dilute surfactant injection, enhanced oil recovery, fluids electrokinetic, rock wettability, drilling fluids, well stimulation, and formation damage.

Mohammed has published several patents and more than 70 technical papers at international conferences and in refereed journals. He is an active member of the Society of Petroleum Engineers (SPE), and a technical editor of several of SPE's journals. In addition, Mohammed received the SPE award for Outstanding Technical Editor (SPEREE) in 2018.

He received his B.S. degree in Chemical Engineering from King Fahd University of Petroleum and Minerals (KFUPM), Dhahran, Saudi Arabia. Mohammed received his M.S. and Ph.D. degrees in Petroleum Engineering from Texas A&M University, College Station, TX.

He also holds a Business Management Certificate from Texas A&M University, and is a Certified SPE Petroleum Engineer.

Material Overview for Electric Submersible Pumps: Part II — Polymeric and Other Materials

Dr. Jinjiang Xiao, Rafael A. Lastra, Brian A. Roth, and Dr. Woon Lee

Abstract / The electric submersible pump (ESP) is a key artificial lift technology in the petroleum industry. Worldwide installations of ESPs in oil wells are in the range of 130,000 units, contributing to about 60% of the total oil production in the world. An ESP is made up of hundreds of components integrated together to perform the lifting function. Materials in these components belong to several categories, including metals, ceramics, polymers, and others. A good understanding of these materials and vigilant selection for a specific application are critical to the reliability and run life of an ESP system. This series of articles provides an overview of all major classes of materials used in ESP systems. It is intended to serve as a reference for ESP field application engineers who are responsible for design, equipment longevity, and production optimization. This article focuses on polymeric and other materials.

The information compiled in this article is the result of extensive literature review. It covers materials used in the motor, protector, pump, and cable (the sensor, packer, Y-tool, diverter valve, surface components of variable speed drives and transformer are not included). For each class of materials, it identifies relevant material properties and discusses suitable application conditions.

Introduction

An electric submersible pump (ESP) is a complex electromechanical system that requires each and every component to perform its intended function to achieve the system's artificial lift purpose. The proper function and reliability of each component depend not only on the design, but more importantly on the specific material chosen. These materials can be grouped into several major categories, Table 1. Metallic and ceramic materials were covered in a previous publication[1]. This article contains a review of polymeric and other materials.

Information of ESP material specifications is scattered in many published articles, industrial standards, ESP manuals, textbooks, and on the internet. A compressive summary of such an important subject cannot be found in the ESP industry. This series of articles intends to fill the gap. It provides a handy reference and a guidance for ESP application engineers. Accurate information on ESP materials is essential for application engineers to properly specify materials and understand ESP failure mechanisms to improve system reliability. Material science is a vast area requiring special expertise and experience. This article is not intended as a substitute for expert advice, but to provide a starting point for higher level discussions.

Every effort is made to avoid the use of material trade names in the article, however, trade names do frequently appear in ESP publications, and it becomes necessary for application engineers to become familiar with them in the literature. Therefore, some trade names are included in the article where it is unavoidable. There is no intention to promote any specific types of materials or companies in this article.

Table 1 *Major categories of materials used in ESPs.*

	Metallic Materials	Ceramic Materials	Polymeric Materials	Others
General Description	Solid-state material of an element, compound or alloy with good thermal and electrical conductivity.	Solid-state material of compounds with high hardness and brittleness.	Solid-state material with molecules made up of a large number of repeating chemical units and having heavy average molecular weight.	Liquids, carbon nano-tube, composite, etc.

Polymeric Materials

Polymeric materials exhibit various unique properties, including high strength, lightweight, elasticity, dielectric, resistance to corrosion. They are utilized in a variety of industrial applications. In the ESP industry, polymers are used for pressure sealing, fluids isolation, expansion, contraction and containment, electric insulation and surface coatings for friction reduction or corrosion resistance.

Polymer classification is a complex topic and common terminologies in use can be very confusing. Methods to classify polymers can be based on origins (natural or synthetic), structures (linear, branched, or cross-linked), applications, and other ways. For example, based on applications, polymers can be classified into elastomers, plastics, and fibers, Fig. 1.

Elastomers have a higher elasticity and are the main elastic material. Forces such as bending, squeezing, stretching, and twisting can deform elastomers. Upon release of the force, they have much better abilities to recover their original dimensions. In contrast, plastics on the other hand are more rigid, and less elastic or flexible in nature. Fibers have a lower elasticity than elastomers and plastics, but a much higher tensile strength. Rubber is another term commonly used in the industry, and it is almost an interchangeable term for elastomer.

As indicated in Fig. 1, according to physical properties, polymers can be categorized as either thermoplastic or thermosetting. Thermoplastic polymers have a glass transition temperature, above which they become soft and can be reformed, and a melting point temperature, above which they become viscous liquids. Thermoplastic polymers can generally be repeatedly heated and reformed. Thermosetting polymers, on the other hand, cannot be remelted and reshaped. Once a thermosetting polymer is cured, an irreversible chemical reaction takes place. It becomes permanently hard, tough, non-swelling, and brittle — especially at low temperatures.

Fig. 1 *Polymer classification.*

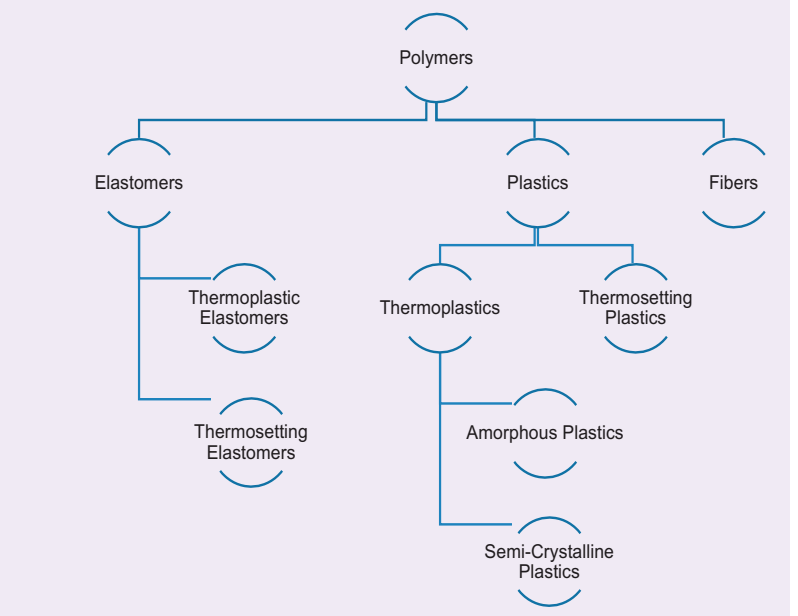

Heating a thermosetting polymer again can cause the polymer to break down or decompose. In general, thermoplastic polymers have chain molecules, whereas thermosetting polymers have three-dimensional (3D) networks of cross-linked molecular chains. Cross-linking individual polymer chains is achieved through irreversible chemical processes. Vulcanization is a type of cross-linking processes during which polymers are combined with sulfur and its derivatives under heat and pressure.

Resin is also a term frequently appearing in the ESP literature. While polymer has a large molecular weight and longer chains, resin has a small molecular weight and shorter chain. Polymers can be formed by the polymerization of resins.

Polymers applied in ESP systems are subjected to very challenging downhole oil field environments: high-pressure, high temperature, a broad range of fluid mediums (hydrogen sulfide (H_2S), carbon dioxide (CO_2), hydrocarbon, water, chloride, diesel, kill fluid, acid, and other well treatment fluids) and solids. Mechanisms for polymer performance degradation and failure are multiple and often interrelated. Common causes include gas permeation, swelling, explosive decompression and others. The potential consequences of an elastomer failure in an ESP system can be weakening or loss of electrical insulation, motor burn, dynamic instability, and fluid recirculation.

Polymeric materials commonly used in the ESP industry are discussed next. Note that the identifications of these materials are customarily made by a combination of chemical names, American Society for Testing and Materials (ASTM) designated abbreviations or trade names.

Elastomers

As previously shown in Fig. 1, elastomers can be classified into thermoplastic elastomers — will soften and melt when heated — and thermosetting elastomer — will not melt when heated. Thermoplastic elastomers have processing advantages, but they are poor in chemical and heat resistance, and can have high compression set at elevated temperatures. Thermosetting elastomers have 3D cross-linked molecular structures allowing them to offer superior performances related to high temperature, chemical attack, and sustained stress. Thermosetting elastomers are the preferred materials in ESP applications.

Ethylene propylene diene monomer (EPDM) is a synthetic thermoset rubber with a wide range of applications. In the ESP industry, EPDM is used as an insulation and jacket material for the main power supply cable and motor lead extension (MLE) cable[2-4]. EPDM has proven to have the best electrical and

mechanical stability at temperatures of -20 °F to 350 °F, and typical downhole pressures. Like other insulation materials, EPDM is permeable to H_2S.

To prevent gas permeation, a metallic layer, such as lead, is often used outside the rubber insulation. The disadvantage of lead is that it does not have sufficient mechanical strength and it also adds weight to the cable. EPDM can swell in oil — mineral oil, solvents, petroleum-based products, and aromatic hydrocarbons — and to a less degree in water. For this reason, in ESP applications it is a common practice to use inhibited brine in the annulus above the ESP packer, not inhibited diesel, to protect the ESP cable from swelling and potential explosive decompression damage.

Fluorocarbon rubber (ASTM designation **FKM**, also known as **FPM** in Europe) is a class of thermosetting elastomers with the molecular structure having the carbon-fluorine bonds. Changes in fluorine content provide variations of rubbers with different properties. ESP applications use O-rings or seal bags made from fluorocarbon rubbers. **Viton** is one of the best-known brand names of fluorocarbon rubbers by DuPont. It is stable in high temperature, tolerant to thermo-cycle, and has chemical and fuel resistance. One limitation of Viton is that the material is not recommended for exposure to amine-based — corrosion inhibitors — well treatment fluids[5] and high pH completion fluids[6]. In applications with H_2S, Viton O-rings had to be upgraded to the Aflas type[7]. **Fluorel™** by Dyneon™ is another fluorocarbon rubber that was tested for ESP applications[8].

Neoprene is a homopolymer of chloroprene, a synthetic rubber by DuPont. Neoprene has found applications in ESP systems[9] as O-rings or cable jacket material. In more demanding applications, as an upgrade, neoprene O-rings were replaced with the Aflas type[10]. Field performance data as well as laboratory testing showed that neoprene can be incompatible with some produced crude[8].

Nitrile butadiene rubber (NBR) and hydrogenated nitrile-butadiene rubber (HNBR) also known as highly saturated nitrile (HSN) are two very common thermoset elastomers used in ESP applications. These two types of rubbers share the same feature in that both their molecules have a repeating structure of one nitrogen atom connected to one carbon atom by a triple covalent bond. NBR is a copolymer of acrylonitrile (ACN) and butadiene. Increasing the content of ACN makes the rubber more resistant to hydrocarbon oil. NBR is used as a cable jacket and seal bag material for low reservoir temperature applications — limited to 200 °F in the presence of H_2S. Bags with NBR will harden when the operating temperatures are too high. When nitrile jacketing is used in the cable, the limiting factor of the cable is nitrile rubber, due to its age-harden tendency[3]. Also, NBR offers minimum resistance to chemical attacks from H_2S, amine inhibitors, or high pH completion fluids[6, 11]. Nevertheless, NBR bags work well with xylene-based asphaltene treatment fluids.

HNBR is the product of NBR's butadiene copolymer reacting and combining with hydrogen (hydrogenation). It has an improved chemical resistance and a higher service temperature over NBR. In particular, it can tolerate a slightly higher content of H_2S in the well fluids and corrosion inhibitors than the NBR. One issue with HNBR is that it can swell in the presence of aromatic oil. In a harsh environment, seal bags with HNBR can harden, deform, swell, and crack due to the attack of the produced fluids — crude oil and water. This can lead to system failures and a short run life[8], forcing design engineers to completely replace bag seals with labyrinth seals to enhance the run life. In other cases, a short motor run life was experienced due to well fluid damage to the HSN bags and mechanical seal bellows. HSN elastomers had to be changed to Aflas[12]. Carboxylated NBR (XNBR) is nitrile with a carboxyl added to the formulation. It is yet another variation of nitrile used in the ESP industry to provide better oil and abrasion resistance, and elastic resilience.

Perfluoroelastomers (ASTM designation **FFKM**) is similar to FKM, but with its polymer backbone fully fluorinated. Due to the increased content of fluorine, FFKM possess superior performance of chemical resistance at harsh environments, including hot amine, steam, solvent, H_2S, CO_2, and hydrocarbon, as well as resistance to rapid gas decompression. FFKM used in ESP applications includes **Kalrez®** (by DuPont) and **Chemraz®** (by Greene Tweed) O-rings[8] for high temperature steam assisted gravity drainage ESP applications.

Silicone rubber represents a group of thermosetting elastomers that possess an excellent resistance to extreme temperature. Silicone rubber gels were used for motor stator potting in the past.

Tetrafluoroethylene-propylene (**TFE/P**, ASTM designation **FEPM**), commonly referred as **Aflas** (trademark of Asahi Glass Co. Ltd., Japan), is a copolymer of tetrafluoroethylene and propylene, with a fluorine content of about 54%. This thermosetting rubber possesses excellent properties of resistance to acid, brine, oil, and H_2S at temperatures up to 400 °F. A possible weakness is low temperature performance in aromatic oil, with only a limited resistance to mineral oil. Aflas is affected by heat, but contrary to HNBR, the thermal effect is recoverable once the heat is removed. Aflas elastomers are used in the following ESP components: protector bags, O-rings (flange seals, pothead connection, and compliant radial bearing system for vibration damping) and mechanical seal bellows[13-15].

Despite numerous advantages with Aflas, there are a few cautions to be noted. Aflas O-rings can lose elasticity and break if the ambient temperature drops below -10 °C[16]. Long-term exposure to diesel can cause Aflas components to swell, and its mechanical property to degrade[15]. Not all Aflas is the same. Suppliers can use different fillers or additives to achieve certain desired properties, and some blending can cause unexpected consequences.

For example, in some Aflas formulations, EPDM was added to enhance the molding process, but this

resulted in a shorter run life because chemicals released from the EPDM can attack Aflas and cause it to harden[17]. Some Aflas can absorb produced crude, causing excessive elastomer swelling and loss of mechanical properties (hardness), leading to failures with the seal bag and mechanical seal bellow[18]. It is important to conduct fluid compatibility tests with any new elastomer material. Aflas can also have an issue with explosive decompression in a CO_2 environment.

In terms of extrusion resistance, Aflas in general is not as good as HNBR. Packers designed for the H_2S environment use Aflas elements[11]. Typically, the Aflas elements are used as the center seal elements and HNBR as the outside elements to completely contain the Aflas elastomer. Without HNBR backup elements, Aflas can extrude, leading to packer sealing failures.

The selection of elastomers for any given application is to match the specific field conditions — temperature, pressure, physical load and characteristics, production, completion type, treatment fluids, and solid content — with the performance characteristics of an elastomer in combination with cost considerations. For example, elastomers such as Aflas, Viton, and Kalrez, can provide exceptional properties as O-rings, seal bags, and bellows, but are costly for use in ESP cables.

General application guidelines on various elastomers can be found in several published sources[3, 6, 8, 19]. Major service companies have their own reference data sheets. These guidelines may not always provide consistent recommendations, partly due to variations in chemical compositions for the same brand named elastomer. Adequate lab testing and field trials are the only way to verify elastomer applicability.

Thermoplastics

As previously shown in Fig. 1, thermoplastics can be further divided into amorphous plastics and semi-crystalline plastics, depending on whether their molecular chains are randomly arranged or highly organized and packed. Amorphous plastics are in general prone to stress cracking, fatigue, and chemical attacks. Semi-crystalline plastics offers better performances and are the exclusive plastics used in ESP applications, due to the demanding downhole conditions.

Ethylene tetrafluoroethylene (ETFE) is a thermoplastic material belonging to the group known as fluoropolymers. **Tefzel™** (trade name by DuPont) is a type of ETFE material used as barrier tapes in ESP power cables[20].

High-density polyethylene (HDPE) is a low cost, commodity thermoplastic. Its use is limited to low temperatures up to 170 °F as a jacket material for the ESP cable. Under high temperatures this material can melt[21].

Polyamides (PA) a thermoplastic material composed of polymers that contains the amide group. PA possess a high tensile strength. **Nylon** is one example of PA materials. It offers good resistance to chemicals and high voltages. **Rilsan®** (trade name by Arkema S.A.) is a nylon-type of material, which can be considered in cable design uses. Nylon film can be used as an insulation material for motor lead extension cables[22], however, nylon is susceptible to hydrolyze by hot water[23]. Its use in cable is not recommended for miscible flood ESP applications[24].

Polyamide-imide (PAI) is a high performance thermoplastic with excellent dielectric property and dimensional stability at high temperatures. Brand name **Torlon** (trademark by Solvay Specialty Polymers) is a PAI-based material used as motor interconnector insulators[25].

Polyether ether ketone (PEEK) is a semi-crystalline high performance thermoplastic material. PEEK possess a few unique properties, including resistance to chemical, wear, hydrolysis, and stability at high temperatures — up to 570 °F. These properties make PEEK an important polymer for many industries. ESP systems use PEEK as an insulation material for motor magnet wires and electrical connectors, and also as a bearing material.

Traditionally, a motor's copper wires are insulated with Kapton tape (a polyimide film, developed by DuPont) and finished with a varnish coating to prevent winding vibration and water/moisture ingress during operations. For high temperature applications, one of the design improvements is to replace the standard, varnished Kapton winding with high strength PEEK insulated winding[16] to enhance the motor's run life. The PEEK insulation system does not need varnish. In addition, PEEK insulation can provide stabilization/protection for winding and end-turn, reducing possible electrical short circuit failures that often occurred at the end-turn[10].

Another area that uses PEEK to improve reliability is the insulation of the MLE or the flat cable. Conventionally, the MLE conductors are insulated with Kapton, and covered with a jacket (usually lead for H_2S applications), which acts as a barrier against gas permeation, and then protected with an interlocking metal armor to provide mechanical strength against damage during installation and retrieval. This type of design had significant reliability issues for high H_2S and high temperature applications. An improved MLE design is to use PEEK to insulate the individual MLE conductor. The system is then covered with a lead sheath[26], or for more superior performances, encapsulated within Monel or Inconel tubes[27].

PEEK has also been used as an exceptional insulating material in electrical connectors. Cross-lined PEEK[28] can provide enhanced creep, extrusion, chemical, and electrical resistance to improve electric connector reliability under high voltage and high temperature applications.

Some ESP systems also use PEEK as a coating material for the tilting pads in high load thrust bearing designs, due to its excellent wear and abrasion resistance[29]. In such applications, the coating material is a PEEK composite with polytetrafluoroethylene (PTFE)[10] or carbon fiber as fillers or additives. This type of design can withstand higher axial load than Babbitt bearings.

In addition, polymer coating reduces startup friction and pad crowning so that a more uniform pressure distribution over the pad can be achieved.

Polypropylene (PP) is a common thermoplastic found used in the ESP industry as an insulation material for low temperature applications[2, 30] — up to 200 °F. Direct contact of PP with copper can result in accelerated aging of the insulation. This is prevented with the use of stabilizers in the insulation or a tin coating of the copper. Also, PP is highly susceptible to softening and creeping by crude oil in direct contact. In some rigless alternative deployment technologies, the deployment cable is designed with an external jacket made with PP. The smooth surface facilitates sealing with well control equipment. The reliability of this material for long-term use is being accessed by the industry. Andrew and Augustine (1992)[31] have shown that PP, when used as an insulation material, resulted in cable failures when it was exposed to either an extreme cold temperature of -40 °F or a high temperature of 230 °F.

Polyphenylene sulfide (PPS) is another high performance thermoplastic material used in ESP applications. Standard corrosion resistant (Ni-resist) impellers can experience corrosion damage due to a high water cut and high chloride content in the water. Impellers made from lightweight PPS (**Ryton**, trade name by Solvay Specialty Polymers) was used to replace Ni-resist impellers[10, 32]. Even though this material has lower mechanical strength, it offers corrosion resistance with thermal and dimensional stability. Ryton can be applied as a coating for ESP stages to provide corrosion and scale resistance.

Polytetrafluoroethylene (PTFE), fluorinated ethylene propylene (FEP) and **perfluoroalkoxy (PFA)** are all high performance thermoplastics. They are all fluoropolymers with different molecular structures but exhibiting similar nonstick properties. FEP is softer than PTFE, and transparent. PFA has improved flow and creep resistance and thermal stability. One brand name of PTFE-based material is **Teflon**, initially manufactured by DuPont.

A barrier created with Teflon extrusion is often used as protection for cable insulation against oil and chemicals. Another application of Teflon is to coat pump stages to prevent scale build up and improve pump performance[5, 33]. Pump impellers and diffusers are made by sand casting and have a rough surface, leading to higher friction and scale build up. **Xylan** (trade name by Metal Coatings Corp.) is a family of fluoropolymer coatings having PTFE, FEP, or PFA as key ingredients. Application of xylan as a thin film in ESP stages provides similar functions as Teflon. Another use of PTFE is to coat the shaft coupling to prevent galling — also known as "adhesive wear" when two surfaces, the shaft and coupling, in contact, seize up as a result of cold welding.

PTFE tapes can be used as an extra insulation barrier over the lead barrier in the MLE for high salinity and corrosion applications[34]. FEP is chemically inert and has good dielectric properties and heat resistance. It can be a candidate material as an external sheath to encapsulate the cable in a rigless alternative ESP deployment. FEP film can be used as the slot liner material for motor stators[7]. PFA offers similar properties to FEP, but is more preferred for services in hostile environments involving chemical attacks, thermal, and mechanical stress. Some MLE cable designs uses PFA as an insulation material.

Polyvinylidene difluoride (PVDF) is a high performance thermoplastic fluoropolymer. PVDF offers excellent resistance to solvents, acids, and bases. In some cable design, this material is used as a gas barrier over EPDM insulation[35]. Brand name **Kynar** (trade name by Pennwalt) is a PVDF-based family of materials.

Polyvinyl fluoride (PVF) is a fluorinated thermoplastic material composed of chemically linked fluorine monomer units. **Tedlar®** (trade name by DuPont) is a PVF material used as barrier tapes in ESP power cables[20].

Thermosetting Plastics

Epoxy resin is a class of materials whose molecular structures contain the highly reactive epoxide groups. Curing as a result of either reaction with resins themselves through catalysts, or with hardeners forms thermosetting polymers with desirable mechanical, thermal properties, and chemical resistance capability. There are many different formulations of epoxy. Epoxy has found applications in several components of an ESP system.

Typical ESP motor designs have unfilled space and open in the stator slots after winding. This allows dielectric motor oil to circulate and cool the motor through convective heat transfer. Some designs have the motor winding 100% vacuum potted with thermally conductive epoxy[5, 36]. Epoxy's chemical resistance and good adhesion properties provide additional electrical insulation to the magnet wires. Moreover, the encapsulated windings allows heat transfer to be enhanced via conduction. This makes the motor run cooler and results in a longer run life. If the stator is long, complete potting can be difficult. Partial potting can leave air voids in the slots, resulting in localized hot spots and potential partial discharge. Some motor designs use epoxy to restrain the stator's end coils to prevent them from movement and damage during shipping and operation. For high temperature applications such as steam assisted gravity drainage[37], epoxy degradation can result in motor failures as the primary failed component.

Downhole ESP sensors oftentimes use epoxy resin as a conformal coating material. The thin film fits into the contours of printed circuit boards to protect the electronic components against moisture and chemicals in the harsh environments.

Pump impellers and diffusers are typically manufactured by sand casting and with a rough surface finish. Stages can be coated with epoxy to improve hydraulic performance[38]. Epoxy coating is also used

to combat ESP housing corrosion. This is usually done as a second step in a two-step coating process. First, a flame-sprayed metalized (Monel or 316 stainless) coating is applied. Then epoxy coating is used to fill porous voids[39]. A cautionary note is that epoxy coating can be damaged as results of chipping or scratching, and for a motor housing, a thicker coating can be detrimental to proper motor cooling.

Epoxy is widely used as a sealing material for electric connectors. Conventional MLE cable connections with the motor is through the pothead, which is filled with epoxy. This is done in the factory. The pothead termination is submerged in water and tested for 50 psi to 100 psi for up to 1 hour. This is an electrically weak termination, especially for high H_2S applications. A sealing defect or damage can lead to H_2S attacks on the copper. Epoxy voids inside the pothead can cause pothead burns. These are common causes of electric failures with MLE/pothead connections[40]. Similarly, epoxy has been used as a sealing material for packer penetrators, specifically for sealing the splicing between the MLE and packer feedthrough cable. Field experiences show repeatedly that an epoxy-based solution can slow down H_2S ingress, rather than prevent it entirely. More reliable designs are needed to prevent electric connection failures[27].

Phenolic is a thermosetting polymeric material commonly used in ESP applications. The material can be hard and strong, but brittle. Floater pump stages often use upthrust and downthrust washers made of laminated phenolic to handle the axial thrust[41].

Polyimide (PI) is a polymer of imide monomers. PI can be made in two forms: thermosetting and thermoplastic. Kapton is an example of a thermosetting PI. It is widely used as an insulation material in ESP systems. The copper wire typically has a PI coating as a primary barrier. In aggressive H_2S environments, magnet wires for motor windings can be insulated with double Kapton layers[42]. Lamination slots can be lined with PI sheets. MLE primary insulation can be Kapton with EPDM as a secondary insulation. **Apical** (trade name by Allied Chemical) is another PI sometimes used in place of Kapton as a primary insulation material. As a cautionary note, hydrolysis can occur with PI materials[26].

Other Materials

Motor oil: ESP motors and protectors use highly refined mineral oils for effective motor cooling and sufficient lubrication of all the radial and thrust bearings. These oils are specially formulated with optimal dielectric strength (> 28 kVDC), good thermal conductivity, and viscosity at high temperatures. Motor oil never gets replaced during the life of an ESP system.

Over time, its dielectric properties and lubricity can deteriorate due to contamination of fine particles generated from the rotating components, or from the well fluids. The contaminants can weaken the motor's electrical integrity, cause motor overheating, or scrape bearing contact surfaces. All of these can lead to motor failures. Some system designs use a filter at the bottom of the protector/seal section to prevent solids from getting into the motor section.

Electric motors do not always have to be filled with dielectric mineral oil. In one subsea application, the motor is filled with water-based liquid — 70% mono ethylene glycol in water. The motor stator is fully encapsulated to prevent any catastrophic electrical failures[43].

Barrier fluids: In some ESP installations, water immiscible heavy barrier fluids with a specific gravity as high as 1.9, have been used to block well fluids' invasion into the motor section. In a conventional ESP configuration, this is applied in the top seal section. In situations where the produced crude is lighter than the motor oil (typically with a specific gravity of 0.85), a labyrinth seal section, which operates based on gravity segregation will not be able to prevent produced crude from entering into the seal section and contaminating the motor oil. One solution was to use a barrier chamber filled with heavy fluids[8]. Rigless deployed ESP systems typically have an inverted configuration with the motor on top to facilitate electric connection with the power cable. This connection is usually made within a shaftless protector in which a barrier fluid is used to provide pressure equalization, as well as to prevent well fluid invasion.

Diamond and graphite: Steam assisted gravity drainage applications typically involves high temperatures (200 °C to 250 °C), with the presence of abrasives. These demanding conditions require new and more reliable designs for the mechanical shaft seal, thrust bearing, and other components. One improvement uses a diamond coating for the seal faces in the mechanical shaft seal to address the challenges of high temperature, abrasiveness, and possibly dry running condition in case of a possible steam breakout[17]. Graphite, due to its self-lubricating nature, has also been used as a coating material for the mechanical seal face[44].

Composite is a type of material that is formed by combining two or more distinctive types of materials. These constituents work together to give the composite unique and superior properties. Composites have found applications in ESP systems. **Cermet** is a composite material consisting of ceramic (cer) and metallic (met) materials. It possesses excellent abrasive resistance properties and has been used to make bearings for downhole pumps[45]. A composite of carbon fiber and PEEK has been used to make coiled tubing and flow line jumpers, which are of a lightweight, high tensile strength, and is corrosion resistant. This type of composite can be a potential material used to make power cables for ESPs in alternative cable deployments.

R&D in the area of carbon nanotube (CNT) and CNT-copper composite is being actively carried out in the industry. These composite materials may in the future become economical materials as conductors, as well as load carrying members to deploy ESPs riglessly.

Discussions

Table 2 provides a list of polymeric materials and their

Table 2 *Commonly used polymeric materials in ESPs.*

Elastomers	
EPDM	Cable jacket and insulation material
FKM/FPM: Viton/Fluorel	O-ring and seal bag material
Neoprene	O-ring material
NBR and HNBR or HSN	Cable jacket and seal bag materials
FFKM: Kalrez/Chemraz	O-ring material
Silicone Rubber	Motor stator potting material
TFE/P/FEPM: Aflas	O-ring and seal bag material
Thermoplastics	
HDPE	Cable jacket material
PA: Nylon/Rilsan	Cable insulation material
PEEK	Insulation material for motor winding and electrical connectors; coating material for thrust bearing tilting pads
PP	Cable insulation material
PPS: Ryton	Pump stage coating material
PTFE, FEP and PFA: Teflon/Xylan	Pump stage coating material; shaft coupling coating material
PVDF: Kynar	Cable jacket material
Thermosetting Plastics	
Epoxy	Motor stator potting, pothead potting, cable splice sealing, stage coating
Phenolic	Pump stage thrust washer
PI: Kapton	Motor winding insulation or coating

associated ESP components discussed in this article. The philosophy of material selection for any particular application is a balancing act and optimization process with several factors taken into consideration: material cost, functionality, and manufacturability.

Correct material specification depends on a good understanding of material property and limitation, and the requirement and conditions of the intended application in terms of pressure, temperature, physical load, fluid composition, and solid content. Material selection, quality, product design, fabrication, testing, and installation are all crucial steps for any applications to be successful.

Conclusions

This article reviews and discusses polymeric and other materials commonly in use in the ESP industry. Relevant properties and suitable application areas are briefly highlighted. The article is intended to be a high-level guide to help engineers develop some basic understanding on ESP materials. This knowledge is required to correctly specify materials and to understand failure causes so that ESP run life can be improved.

For any particular application, defining material specifications is often an evolving process and always involves consideration of factors such as material cost, functionality, and manufacturability. In addition, ESP run life depends not only on materials, but also equally on design, quality fabrication, assembly, testing, installation, and operation.

Acknowledgments

The authors would like to thank the management of Saudi Aramco for their support and permission to publish this article.

References

1. Xiao, J.J., Lastra, R.A., Roth, B.A. and Lee, W.: "Material Overview for Electric Submersible Pumps: Part I — Metallic and Ceramic Materials," *SPE Production & Operations*, (in publication), July 2019.

2. Wargin, R.V.: "Material Approach to the Development of Oil Well Cables," *Society of Petroleum Engineers Journal*, Vol. 20, Issue 6, December 1980, pp. 591-597.

3. Guzy, R. and Vandervier, J.: "Technical Advancements in Submersible Pump Power Cable for Harsh Environments," *SPE Production Engineering*, Vol. 2, Issue 2, May 1987, pp. 119-123.

4. Al-Kady, A.A., Al-Mulhim, A.A., Al-Subaie, F.M.,

Cumings, M., et al.: "Implementing Technical Improvements of ESP Application in Water Supply Wells for Extending Lifetime and Operation Efficiency," SPE paper 181341, presented at the SPE Annual Technical Conference and Exhibition, Dubai, UAE, September 26-28, 2016.

5. Limanowka, W.A., Degen, S. and Benwell, G.: "Preventive Maintenance of Electric Submersible Pumps and its Relationship to Root Cause of Failure Analysis," SPE paper 68789, presented at the SPE Western Regional Meeting, Bakersfield, California, March 26-30, 2001.

6. Petrowiki: https://petrowiki.org/Elastomers

7. Wilson, B.L. and Comeau, T.P.: "Increasing the Run Life of ESPs in High H_2S Wells," SPE paper 28527, presented at the SPE Annual Technical Conference and Exhibition, New Orleans, Louisiana, September 25-28, 1994.

8. Young, J., Kappelhoff, G.H. and Watson, A.: "ESP Run Life Improvement in Harsh Elastomer Environments, the Moomba Field," SPE paper 80526, presented at the SPE Asia Pacific Oil and Gas Conference and Exhibition, Jakarta, Indonesia, April 9-11, 2003.

9. Iskam, M.: "Use of Electrical Submersible Pumps (ESPs) in Oil and Gas Production Facilities — A Brief Review," paper presented at the NACE International/CORROSION 2005 Conference and Exhibition, Houston, Texas, April 3-7, 2005.

10. Miwa, M., Yamada, Y. and Kobayashi, O.: "ESP Performance in Mubarraz Field," SPE paper 87257, presented at the Abu Dhabi International Petroleum Exhibition and Conference, Abu Dhabi, UAE, October 13-15, 2000.

11. Alquwizani, S.A., Shepler, R.A., Zoraia, G.H. and Khamis, M.N.: "Managing Tubing-Casing-Annulus in ESP Completions for Enhanced Wellbore Integrity and Improved ESP Runlife," SPE paper 173702, presented at the SPE Middle East Artificial Lift Conference and Exhibition, Manama, Kingdom of Bahrain, November 26-27, 2014.

12. Al-Zahrani, A.R., Al-Nasser, R.H., Collen, T.W. and Khade, S.: "Case Study: First Successful Offshore ESP Project in Saudi Arabia," SPE paper 126066, presented at the SPE Saudi Arabia Section Technical Symposium, al-Khobar, Saudi Arabia, May 9-11, 2009.

13. Gallegos, M., Ordonez, E.F., Milne, A.W. and Robles, M.: "Stimulation in Wells with Electric Submersible Pumps Increases Production and Save Costs without Damaging Pumps," SPE paper 152320, presented at the SPE Latin America and Caribbean Petroleum Engineering Conference, Mexico City, Mexico, April 16-18, 2012.

14. Al-Khalifa, M.A., Shepler, R.A., Cox, R.L. and Alquwizani, S.A.: "ESP Reliability Lessons Learned from Three H_2S Saudi Arabian Fields," SPE paper 184176, presented at the SPE Middle East Artificial Lift Conference and Exhibition, Manama, Kingdom of Bahrain, November 30-December 1, 2016.

15. Pujol, D., Moraglia, F., Torrealba, F., Echarki, A., et al.: "Dual Boosting ESPs Completion: Design Philosophy and Experience Gained in Tempa Rossa," paper presented at the Offshore Mediterranean Conference and Exhibition, Ravenna, Italy, March 29-31, 2017.

16. Marzona, M., Aguila, A., Oyarzun, R. and Teves, R.: "ESP Motor Reinstall Criteria to Maintain Reliability in Cerro Dragon Field," SPE paper 185148, presented at the SPE Electric Submersible Pump Symposium, The Woodlands, Texas, April 24-28, 2017.

17. Merrill, D. and Dwiggins, J.: "Understanding Seal Section and the Phantom Failures," SPE paper 185133, presented at the SPE Electric Submersible Pump Symposium, The Woodlands, Texas, April 24-28, 2017.

18. Sarkis, N., Guerra, W., Moreno, L.F., Cuellar, H., et al.: "Implementation of New Seal Design to Improve ESP Performance in Corcel Field," SPE paper 165024, presented at the SPE Artificial Lift Conference-Americas, Cartagena, Colombia, May 21-22, 2013.

19. James, B.: "Sour Service Sealing," paper submitted at the Energy Rubber Group Fall Education Symposium, Houston, Texas, September 21, 1994.

20. API: "Recommended Practice for the Application of Electric Submersible Cable Systems," API RP 11S5, American Petroleum Institute, October 2013.

21. Ribeiro, M.P., da Silva Oliveira, P., de Matos, J.S. and da Silva, J.E.: "Field Applications of Subsea Electrical Submersible Pumps in Brazil," OTC paper 17415, presented at the Offshore Technology Conference, Houston, Texas, May 2-5, 2005.

22. Cohen, D.J.: "Captain Field Electric Submersible Pump, Condition Monitoring and Completion Systems," OTC paper 8510, presented at the Offshore Technology Conference, Houston, Texas, May 5-8, 1997.

23. Neuroth, D.H.: "Design Features of Improved Electric Submersible Pump (ESP) Cable to Withstand Installation and Service Conditions," OTC paper 4980, presented at the Offshore Technology Conference, Houston, Texas, May 6-9, 1985.

24. Durham, M.O. and Miller, G.: "Enhancing Performance of Submersibles Operating in Miscible Flood Conditions," SPE paper 25446, presented at the SPE Production Operations Symposium, Oklahoma City, Oklahoma, March 21-23, 1993.

25. Blanksby, J.M., Hicking, S. and Milne, W.H.: "Deployment of High Horsepower ESPs to Extend Brent Field Life," SPE paper 96797, presented at the Offshore Europe Conference, Aberdeen, Scotland, U.K., September 6-9, 2005.

26. Pastre, L.F. and Fastovets, A.: "The Evolution of ESP Technology in the North Sea: A Reliability Study based on Historical Data and Survival Analysis," SPE paper 187735, presented at the SPE Russian Petroleum Technology Conference, Moscow, Russia, October 16-18, 2017.

27. Xiao, J., Shepler, R., Windiarto, Y., Parkinson, S., et al.: "Development and Field Test of an Electric Submersible Pump Reliable Power Delivery System," *SPE Production & Operations*, Vol. 33, Issue 3, August 2018, pp. 449-458.

28. Atkinson, S.: "Collaboration Improves Reliability of High-Voltage ESPs," *Sealing Technology*, Vol. 2018, Issue 5, May 2018, p. 7.

29. Pastre, L. and Carolini, A.: "Power Study and Tailored Solution for High H_2S Environment Extends ESP Run Life in Douglas Field in the Irish Sea," SPE paper 189269, presented at the SPE Symposium: Production Enhancement and Cost Optimization, Kuala Lumpur, Malaysia, November 7-8, 2017.

30. Schultz, R.E., MacKenzie, B.T. and Marefat, K.: "ESP Cable Insulation: Selection for Performance," SPE paper 14690, presented at the SPE Production Technology Symposium, Lubbock, Texas, November 11-12, 1985.

31. Andrew, J.H. and Augustine, B.G.: "Initial Experience with ESPs on the Alaskan North Slope," OTC paper

7062, presented at the Offshore Technology Conference, Houston, Texas, May 4-7, 1992.

32. Shimokata, N. and Yamada, Y.: "Troubles, Problems, and Improvements of ESP," SPE paper 137337, presented at the Abu Dhabi International Petroleum Exhibition and Conference, Abu Dhabi, UAE, November 1-4, 2010.
33. Colodette, G., Pereira, C.A.G., Siqueira, C.A.M., Ribeiro, G.A.S., et al.: "Flow Assurance and Artificial Lift Innovations for Jubarte Heavy Oil in Brazil," *SPE Projects, Facilities & Construction*, Vol. 3, Issue 1, March 2008, pp. 1-8.
34. Brahmi, H.: "Recommended Solutions for ESP Installed in Very High Salinity Reservoirs and Severe Corrosive Media," SPE paper 184181, presented at the SPE Middle East Artificial Lift Conference and Exhibition, Manama, Kingdom of Bahrain, November 30-December 1, 2016.
35. Xiao, J., Roth, B., Lastra, R., Sarawaq, Y., et al.: "Cable Concept Evaluation for ESP Rigless Deployment," SPE paper 184193, presented at the SPE Middle East Artificial Lift Conference and Exhibition, Manama, Kingdom of Bahrain, November 30-December 1, 2016.
36. Garcia, E.L., Gonzalez, J.S., Banos Torales, F.L., Campos, I.M., et al.: "Electric Submersible Pumping, First Application in a Mature Field in Mexico, Using the Unconventional Technology with Synchronous Permanent Magnet Motor (PMM) + 'Power Save' Pump," SPE paper 173966, presented at the SPE Artificial Lift Conference — Latin America and Caribbean, Salvador, Bahia, Brazil, May 27-28, 2015.
37. Graham, J., Coates, B., Montilla, C. and Padilla, O.: "Evaluating the Performance of Advanced ESP Motor Technology in a Steam Assisted Gravity Drainage SAGD Field in Canada," SPE paper 183882, presented at the SPE Middle East Oil & Gas Show and Conference, Manama, Kingdom of Bahrain, March 6-9, 2017.
38. Vidrianto, M., Noviansyah, M., Rajain, A.K. and Wang, F.M.: "Increasing ESP Run Life Using a Combination of Reliable Abrasion-Resistant Pumps and 24/7 Real-Time Surveillance," SPE paper 184183, presented at the SPE Middle East Artificial Lift Conference and Exhibition, Manama, Kingdom of Bahrain, November 30-December 1, 2016.
39. Wilson, B.L.: "Materials for ESPs in Corrosive Environments," paper presented at the Electrical Submersible Pump Workshop, Houston, Texas, April 8-9, 1986.
40. Britvar, J. and Williams, S.: "Improving ESP Application for Unconventional Wells in the Bakken," SPE paper 185150, presented at the SPE Electric Submersible Pump Symposium, The Woodlands, Texas, April 24-28, 2017.
41. Wilson, B.L.: "The Effects of Abrasives on Electrical Submersible Pumps," *SPE Drilling Engineering*, Vol. 5, Issue 2, June 1990, pp. 171-175.
42. Komova, T., Faila, M., Osipova, I., Cuadros, E., et al.: "Optimizing ESP Performance in the Kharyaga Field," SPE paper 166891, presented at the SPE Arctic and Extreme Environments Technical Conference and Exhibition, Moscow, Russia, October 15-17, 2013.
43. Cunha, L.S., Felix, T., Meuter, P., Bourne, M., et al.: "Development and Qualification of a High Differential Pressure Subsea Pump," OTC paper 24401, presented at the Offshore Technology Conference, Rio de Janeiro, Brazil, October 29-31, 2013.
44. Dewidar, M.: *Electric Submersible Pumps, Chapter 4, Protector (Seal)*, 2013.
45. Harden, W.G. and Downie, A.A.: "Field Trial and Subsequent Large-Scale Deployment of a Novel Multiphase Hydraulic Submersible Pump in the Captain Field," OTC paper 13197, presented at the Offshore Technology Conference, Houston, Texas, April 30-May 3, 2001.

About the Authors

Dr. Jinjiang Xiao

Ph.D. in Petroleum Engineering, University of Tulsa

Dr. Jinjiang Xiao is a Senior Petroleum Engineering Consultant working in Saudi Aramco's Exploration and Petroleum Engineering Center – Advanced Research Center (EXPEC ARC). His current focus is artificial lift research and development.

Prior to joining Saudi Aramco in 2003, Jinjiang spent 10 years with Amoco and later BP-Amoco, working on multiphase flow, flow assurance and deep-water production engineering.

He received both his M.S. and Ph.D. degrees in Petroleum Engineering from the University of Tulsa, Tulsa, OK.

Rafael A. Lastra

M.S. in Management of Information Systems, Texas A&M University

Rafael A. Lastra is a Petroleum Engineering Consultant working with the Production Technology Division of Saudi Aramco's Exploration and Petroleum Engineering Center – Advanced Research Center (EXPEC ARC). He provides internal consultation related to artificial lift technologies, especially in the area of electric submersible pumps.

Rafael has more than 25 years of extensive and versatile oil industry experience obtained through a variety of international engineering and management positions, including research and development, management of artificial lift operations, project control, and business development.

He received his B.S. degree in Electrical Engineering from the Universidad del Valle, Cali, Valle del Cauca, Colombia, and his M.S. degree in Management of Information Systems from Texas A&M University, College Station, TX.

Brian A. Roth

Masters of Business Administration, Texas A&M University

Brian A. Roth is a Petroleum Engineering Consultant in the Production Technology Division of Saudi Aramco's Exploration and Petroleum Engineering Center – Advanced Research Center (EXPEC ARC). His focus is on R&D efforts with an emphasis on artificial lift technologies. Before joining Saudi Aramco in 2012, Brian spent over 25 years in engineering and leadership roles in large oil and gas service companies.

He has over 24 applied and granted patents, and has authored or coauthored several technical and journal papers.

Brian received his B.S. degree in Mechanical Engineering from the University of Texas at Austin, Austin, TX, and an MBA degree from Texas A&M University, College Station, TX.

Dr. Woon Lee

Ph.D. in Mechanical Engineering, Rice University

Dr. Woon Lee is the R&D Manager of Alkhorayef Petroleum Company, Dammam, Saudi Arabia, which is a supplier of electric submersible pump (ESP) equipment.

Prior to joining Alkhorayef in 2008, he spent 18 years with Reda, a Schlumberger company, and later with Weatherford ESP, working on designs of pumps, gas separators, and gas handling pumps.

Woon received both his M.S. and Ph.D. degrees in Mechanical Engineering from Rice University, Houston, TX.

Notes

Got an article you would like to publish? Here are our guidelines.

These guidelines are designed to simplify and help standardize submissions. They need not be followed rigorously. If you have any questions, please call us.

Length

Average of 2,500-4,000 words, plus illustrations/photos and captions. Maximum length should be 5,000 words. Articles in excess will be shortened.

What to send

Send text in Microsoft Word format via email plus one hard copy. Send illustrations/photos and captions separately but concurrently, both as email and as hard-copy (see file format section for more information).

Procedure

Notification of acceptance is usually within three weeks after the submission deadline. The article will be edited for style and clarity and returned to the author for review. All articles are subject to the company's normal review. No paper can be published without a signature at the manager level or above.

Format

No single article need include all of the following parts. The type of article and subject covered will determine which parts to include.

Working Title
Lorem Ipsum here.

Abstract
Usually 150-300 words to summarize the main points.

Introduction
Different from the abstract in that it sets the stage for the content of the article, rather than telling the reader what it is about.

Main body
May incorporate subtitles, artwork, photos, etc.

Conclusion/Summary
Assessment of results or restatement of points in introduction.

Endnotes/References/Bibliography
Use only when essential. Use author/date citation method in the main body. Numbered footnotes or endnotes will be converted. Include complete publication information. Standard is *The Associated Press Stylebook*, 52nd ed. and *Wesbter's New World College Dictionary*, 5th ed.

Acknowledgments
Use to thank those who helped make the article possible.

Illustration/Tables/Photos and explanatory text

Submit these separately. Do not place in text. Positioning in the text may be indicated with placeholders. Initial submission may include copies of originals; however, publication will require the originals. When possible, submit both electronic versions and printouts. Color is preferable.

File Format

Illustration files with .EPS extensions work best. Other acceptable extensions are .TIFF/.JPEG/.PICT.

Permission(s) to reprint, if appropriate

Previously published articles are acceptable but can be published only with written permission from the copyright holder.

Author(s)/Contibutor(s)

Please include a brief biographical statement.

Submission/Acceptance Procedures

Papers are submitted on a competitive basis and are evaluated by an editorial review board comprised of various department managers and subject matter experts. Following initial selection, authors whose papers have been accepted for publication will be notified by email.

Papers submitted for a particular issue but not accepted for that issue may be carried forward as submissions for subsequent issues, unless the author specifically requests in writing that there be no further consideration.

Submit articles to:

Editor
The Saudi Aramco Journal of Technology
C-11B, Room AN-1080
North Admin Building #175
Dhahran 31311, Saudi Arabia
Tel: +966-013-876-0498
Email: *william.bradshaw.1@aramco.com.sa*

Submission deadlines

Issue	Paper submission deadline	Release date
Summer 2020	February 11, 2020	June 30, 2020
Fall 2020	May 12, 2020	September 30, 2020
Winter 2020	August 13, 2020	December 31, 2020
Spring 2021	November 16, 2020	March 31, 2021

There is more.

A Novel Approach to Propagate MHz EM Signals and Map Reservoir Saturation Hundreds of Meters Away from the Wellbore

Jesus M. Felix Servin, Dr. Max Deffenbaugh, Robert W. Adams, and Dr. Val Riachentsev

Abstract / This study describes a novel approach to propagate high frequency (MHz) electromagnetic (EM) signals through the subsurface. Our technique relies on the presence of subsurface transmission lines, in the form of highly resistive evaporite seals bounded by hydrocarbon reservoirs, to achieve greatly increased EM propagation. As the signal propagates through the seal, variations in the fluid saturation of the bounding reservoirs modulates the signal amplitude and velocity, paving the way for improved EM surveys for reservoir characterization.

Development of a Robust and Nondestructive Microscopic Phase Behavior Monitoring Method for Screening High Performance Surfactants

Marwah M. AlSinan, Dr. Hyung T. Kwak, Alhasan B. Fuseni, and Jun Gao

Abstract / Surfactant screening for enhanced oil recovery involves studies of fluid-fluid and fluid-rock interactions to optimize the surfactant formulation for the reservoir of interest. In this article, we present a suite of advanced low field nuclear magnetic resonance (NMR) technologies capable of monitoring the phase behavior microstructure of fluid mixtures developed for high salinity and high temperature conditions. An anionic and nonionic-anionic surfactant mixture were selected since they were developed for high salinity and high temperature reservoirs.

Pushing the Limits of Coiled Tubing to Address the Challenges of Matrix Stimulation in Multilateral Extended Reach Power Water Injectors

Hasan M. Al-Jassem, Naji K. Al-Salman, Rifat Said, Danish Ahmed, and Kaisar Al Hamwi

Abstract / In carbonate reservoirs in the Middle East, power water injector wells are typically completed with long open hole laterals. The reservoir contact provides pressure support and enhances sweep efficiency in the low transmissibility reservoirs. Due to the wells' deviation and length, coiled tubing (CT) interventions are required to successfully enter and identify each lateral, as well as to remove formation damage by pumping the matrix stimulation treatment across entire laterals.

Effective Corrosion Mitigation Exploiting Glass Reinforced Epoxy Lined Tubulars in Offshore Producing and Injection Wells

Laurie S. Duthie, Hamad M. Almarri, Hussain A. Saiood, Ashwani K. Lata, and Gokul Radhakrishnan

Abstract / Corrosion in offshore well completions can lead to serious well integrity problems and costly workover operations. Although carbon steel is an ideal material for most completions, under certain conditions, corrosion can attack and severely damage carbon steel equipment. Corrosion resistant alloys (CRAs) are a good option, but come with the considerable downside of very high cost. A relatively simple and cost-effective approach to protect completion equipment against these corrosive elements is to line carbon steel completion tubulars with a nonmetallic glass reinforced epoxy (GRE). The GRE material properties provide excellent protection against a range of conditions, including highly corrosive fluids, erosive granular materials, hydrogen sulfide (H_2S), carbon dioxide (CO_2), and acid treatments.

To read these articles and others, go to www.saudiaramco.com/jot

أرامكو السعودية
saudi aramco

Aramco
Journal
of Technology

Liked this issue? Sign up. It's free.

To begin receiving the *Aramco Journal of Technology* please complete this form, scan and send by email to ***william.bradshaw.1@aramco.com.***

Got questions?

Just give us a call at +966-013-876-0498 and we'll be happy to help!

Scan the QR code to go straight to your email and attach the form!

Subscription Form

Name

Title

Organization

Address

City

State/Province

Postal code

Country

Email address

Number of copies